

# NOTE TO USERS

This reproduction is the best copy available.

**UMI**<sup>®</sup>



**A NEW DYNAMIC FINITE ELEMENT FORMULATION WITH APPLICATIONS TO  
COMPOSITE AIRCRAFT WINGS**

by

**Stephen R. Borneman  
BEng. Ryerson University 2002**

**A thesis  
presented to Ryerson University**

**in partial fulfillment of the  
requirements for the degree of  
Master of Applied Science  
in the Program of  
Mechanical Engineering**

**Toronto, Ontario, Canada, 2004**

**Stephen R. Borneman 2004 ©**

**PROPERTY OF  
RYERSON UNIVERSITY LIBRARY**

UMI Number: EC52916

### INFORMATION TO USERS

The quality of this reproduction is dependent upon the quality of the copy submitted. Broken or indistinct print, colored or poor quality illustrations and photographs, print bleed-through, substandard margins, and improper alignment can adversely affect reproduction.

In the unlikely event that the author did not send a complete manuscript and there are missing pages, these will be noted. Also, if unauthorized copyright material had to be removed, a note will indicate the deletion.

**UMI**®

---

UMI Microform EC52916

Copyright 2008 by ProQuest LLC.

All rights reserved. This microform edition is protected against unauthorized copying under Title 17, United States Code.

ProQuest LLC  
789 E. Eisenhower Parkway  
PO Box 1346  
Ann Arbor, MI 48106-1346

**Borrower's Page**

A NEW DYNAMIC FINITE ELEMENT FORMULATION WITH APPLICATIONS TO COMPOSITE  
AIRCRAFT WINGS

Master of Applied Science  
in the Program of  
Mechanical Engineering

2004

STEPHEN ROBERT BORNEMAN

School of Graduate Studies

Ryerson University

Abstract

This thesis presents a new dynamic finite element (DFE) formulation for the free vibration of composite wings modeled as beam assemblies. Implementing Euler-Bernoulli beam theory, the initially assumed uniform beam is modeled in a progressive manner to produce a complex tapered composite thin-walled wing. The DFE employs dynamic trigonometric shape functions (DTSF's) to produce a single dynamic stiffness matrix containing both mass and stiffness properties. Then, the Wittrick-William root counting algorithm is used to solve the resulting non-linear eigenvalue problem. The effective stiffness of a flat fibrous composite beam is modeled using classical laminate theory. The effective stiffness of a thin-walled wing-box is achieved by employing a circumferentially asymmetric stiffness (CAS) configuration. The convergence of the DFE is significantly better as compared to other existing methods, the Finite Element Method (FEM) and the Dynamic Stiffness Matrix (DSM), particularly for complex elements and higher modes of free coupled vibration.

## Acknowledgements

First, I wish to thank my advisor, Professor Seyed Mohammad Hashemi, for his patience and guidance. He gave me the chance, with enthusiasm and structure to complete this thesis. It was with his great expectations and helpful discussions that lead to the successful completion of this research as well as his extensive knowledge of the Dynamic Finite Elements.

I wish to thank my parents and family for their love and support.

I wish to thank Janelle Gallo, Braden Evans, Noah Armenta, Sorin Costicov and Andrew Roach for the countless discussions that opened my mind to new possibilities.

I would also like to thank National Science and Engineering Research Council of Canada (NSERC) and Ryerson University for the financial support provided.

## Dedication

I dedicate this thesis paper to my Mother and Father.

## Table of Contents

<b>CHAPTER 1 INTRODUCTION.....</b>	<b>1</b>
1.1    GENERAL INTRODUCTION .....	1
1.2    PRE-PROCESSING.....	5
1.3    THESIS ORGANIZATION AND MODELING CONSIDERATIONS .....	6
<b>CHAPTER 2 SOLUTION METHODOLOGY.....</b>	<b>9</b>
2.1    INTRODUCTION.....	9
2.2    FREE VIBRATION ANALYSIS BASED ON DISCRETE MODELS: LINEAR EIGENPROBLEMS.....	9
2.3    ANALYTICAL FORMULATION BASED ON CONTINUOUS MODELS: NON-LINEAR EIGENPROBLEMS .....	10
2.4    FIXED SHAPE FUNCTIONS AND LINEAR EIGENPROBLEM SOLUTION .....	11
2.5    DYNAMIC TRIGONOMETRIC SHAPE FUNCTIONS AND NON-LINEAR EIGENPROBLEM SOLUTION.....	11
2.6    EXTRACTING THE MODES .....	13
2.7    CONCLUSION.....	14
<b>CHAPTER 3 COMPOSITE RIGIDITIES.....</b>	<b>16</b>
3.1    INTRODUCTION .....	16
3.2    ASSUMPTIONS .....	16
3.3    EFFECTIVE RIGIDITIES FOR A SOLID CROSS-SECTION .....	17
3.4    EFFECTIVE RIGIDITIES FOR A THIN-WALLED BOX-BEAM SECTION.....	22
<b>CHAPTER 4 UNIFORM LAMINATED COMPOSITE WING MODEL.....</b>	<b>25</b>
4.1    INTRODUCTION .....	25
4.2    WING MODEL.....	25
4.3    ASSUMPTIONS .....	26
4.4    DFE FORMULATION.....	26
4.4.1 <i>Frequency dependent trigonometric shape functions.</i> .....	30
4.5    NUMERICAL RESULTS .....	36
4.5.1 <i>Free vibration of a uniform beam.</i> .....	36
4.5.2 <i>Numerical example for a step beam</i> .....	43
4.6    CONCLUSIONS.....	44
<b>CHAPTER 5 TAPERED WING MODEL.....</b>	<b>46</b>
5.1    INTRODUCTION .....	46
5.2    WING MODEL.....	46
5.3    ASSUMPTIONS .....	47
5.4    DFE FORMULATION.....	48
5.4.1 <i>Application of deviators.</i> .....	52
5.5    APPLICATION OF THE THEORY AND EXAMPLES OF LINEARLY TAPERED WINGS .....	54
5.5.1 <i>Numerical tests for a linearly tapered beam.</i> .....	54
5.5.2 <i>Limitations on dynamic finite element deviators.</i> .....	64
5.5.3 <i>A dually tapered wing model.</i> .....	66
5.6    CONCLUSION.....	71
<b>CHAPTER 6 GEOMETRIC AND MATERIAL COUPLED WING MODEL.....</b>	<b>72</b>
6.1    INTRODUCTION .....	72
6.2    MODEL, HYPOTHESES AND SIMPLIFYING ASSUMPTIONS.....	72
6.3    THEORY .....	74
6.4    NUMERICAL TESTS.....	80
6.4.1 <i>Example of a quadratic tapered wing.</i> .....	80
6.4.2 <i>Cubic tapered wing.</i> .....	84

6.6	CONCLUSION.....	90
<b>CHAPTER 7 CONCLUSION .....</b>		<b>91</b>
7.1	CONCLUDING REMARKS.....	91
7.2	FUTURE WORK.....	94
<b>APPENDIX A: MATLAB<sup>®</sup> DYNAMIC FINITE ELEMENT WING ANALYSIS. ....</b>		<b>95</b>
A.1	INTRODUCTION.....	95
A.2	DFE UNIFORM/TAPERED COMPOSITE BEAM PROGRAM .....	96
A.3	DFE WING ANALYSIS FOR COMPOSITE WING-BOX SECTIONS.....	99
<b>APPENDIX B: FLOW CHARTS.....</b>		<b>103</b>
<b>REFERENCES .....</b>		<b>118</b>
<b>NOMENCLATURE .....</b>		<b>XIII</b>

## List of Tables

TABLE 4-1: MATERIAL PROPERTIES OF A GLASS/EPOXY LAMINATE.....	37
TABLE 4-2: NUMERICAL VALUES OF THE FIRST FIVE NATURAL FREQUENCIES (HZ) USING VARIOUS METHODS ARE PRESENTED. 'B' DENOTES A PREDOMINANT BENDING MODE AND 'T' DENOTES A PREDOMINANT TORSION MODE. ....	40
TABLE 5-1 MATERIAL PROPERTIES OF A GLASS/ EPOXY COMPOSITE LAMINATE.....	55
TABLE 5-2: THE FIRST FIVE NATURAL FREQUENCIES (HZ) OF A LINEARLY TAPERED WING COMPOSED OF GLASS/EPOXY COMPOSITE MATERIAL, WITH A TAPER COEFFICIENT OF $C=-1$ .....	55
TABLE 5-3: COMPARISON STUDY BASED ON SMALL TAPER ANGLES. THE NATURAL FREQUENCIES ARE FOR A 1 DEGREE TAPERED COMPOSITE GLASS/EPOXY WING. ....	61
TABLE 5-4 MATERIAL PROPERTIES OF CYTEK 5445-T800 CARBON FIBRE/EPOXY.....	66
TABLE 5-5 WING DIMENSIONS AND CONFIGURATION. ....	66
TABLE 5-6: THE FUNDAMENTAL NATURAL FREQUENCIES (Hz) OF A CARBON FIBRE/EPOXY WING WITH A -0.75 TAPER COEFFICIENT .....	70
TABLE 6-1: MATERIAL PROPERTIES OF A GRAPHITE/EPOXY COMPOSITE LAMINATE.....	81
TABLE 6-2: FUNDAMENTAL FREQUENCIES IN HZ FOR A GRAPHITE/EPOXY QUADRATIC TAPERED COMPOSITE WING.....	84
TABLE 6-3: NATURAL FREQUENCIES FOR A DUALY CUBIC TAPERED GRAPHITE/EPOXY COMPOSITE WING. ...	87

## List of Figures

FIGURE 3-1: UNIDIRECTIONAL FIBRES SURROUNDED BY A MATRIX .....	17
FIGURE 3-2: COORDINATE TRANSFORMATION FROM PRINCIPAL DIRECTIONS TO GLOBAL (X,Y,Z) DIRECTION. WHERE $E_L$ AND $E_T$ AND THE LONGITUDINAL AND TRANSVERSE ELASTIC MODULAE .....	17
FIGURE 3-3: COMPOSITE LAMINATE BEAM CONSISTING OF MULTIPLE PLYS, WHERE $h_k$ IS THE DISTANCE FROM THE MID-PLANE OF THE COMPOSITE. ....	20
FIGURE 3-4: GENERAL CARTESIAN COORDINATE SYSTEM .....	22
FIGURE 3-5: BOX BEAM WITH RECTANGULAR CROSS-SECTION (BOX-SECTION) .....	23
FIGURE 4-1: COMPOSITE BEAM ON A RIGHT HANDED COORDINATE SYSTEM.....	26
FIGURE 4-2: A 2-NODE 6-DOF BEAM ELEMENT.....	28
FIGURE 4-3: FIRST FLEXURAL SHAPE FUNCTION PLOTTED FOR THE FIRST 4 NATURAL FREQUENCIES OF A UNIFORM BEAM.....	34
FIGURE 4-4: SECOND FLEXURAL SHAPE FUNCTION PLOTTED FOR THE FIRST 4 NATURAL FREQUENCIES OF A UNIFORM BEAM.....	34
FIGURE 4-5: THIRD FLEXURAL SHAPE FUNCTION PLOTTED FOR THE FIRST 4 NATURAL FREQUENCIES OF A UNIFORM BEAM.....	34
FIGURE 4-6: FOURTH FLEXURAL SHAPE FUNCTION PLOTTED FOR THE FIRST 4 NATURAL FREQUENCIES OF A UNIFORM BEAM.....	34
FIGURE 4-7: FIRST TORSIONAL SHAPE FUNCTION PLOTTED FOR THE FIRST 4 NATURAL FREQUENCIES OF A UNIFORM BEAM.....	35
FIGURE 4-8: SECOND TORSIONAL SHAPE FUNCTION PLOTTED FOR THE FIRST 4 NATURAL FREQUENCIES OF A UNIFORM BEAM.....	35
FIGURE 4-9: PLOT OF RIGIDITIES VS PLY ANGLE FOR A GLASS/EPOXY COMPOSITE.....	37
FIGURE 4-10: CONVERGENCE OF DFE AND FEM FOR THE FIRST FOUR NATURAL FREQUENCIES OF A UNIFORM COMPOSITE WING. PERCENT ERROR IS RELATIVE TO THE EXACT VALUES OBTAINED FROM THE DSM (BANERJEE AND WILLIAMS, 1995). ....	38
FIGURE 4-11: NATURAL MODES OF FREE VIBRATION FOR A COUPLED BENDING-TORSION UNIFORM COMPOSITE BEAM. (A) FIRST NATURAL MODE; (B) 2 <sup>ND</sup> NATURAL MODE; (C) 3 <sup>RD</sup> NATURAL MODE;. EACH 2D MODE DISPLACEMENT DUE TO TORSION IS REPRESENTED BY A DASHED (--) LINE AND BENDING IS REPRESENTED BY A SOLID (-) LINE. ....	39
FIGURE 4-12: NATURAL MODES OF FREE VIBRATION FOR A COUPLED BENDING-TORSION UNIFORM COMPOSITE BEAM. (D) 4 <sup>TH</sup> NATURAL MODE. EACH 2D MODE DISPLACEMENT DUE TO TORSION IS REPRESENTED BY A DASHED (--) LINE AND BENDING IS REPRESENTED BY A SOLID (-) LINE. ....	40
FIGURE 4-13: VARIATIONS IN THE FIRST NATURAL FREQUENCY FOR DIFFERENT PLY ORIENTATIONS.....	41
FIGURE 4-14: VARIATIONS IN THE SECOND NATURAL FREQUENCY FOR DIFFERENT PLY ORIENTATIONS.....	41
FIGURE 4-15: VARIATIONS IN THE THIRD NATURAL FREQUENCY FOR DIFFERENT PLY ORIENTATIONS.....	42
FIGURE 4-16: VARIATIONS IN THE FOURTH NATURAL FREQUENCY FOR DIFFERENT PLY ORIENTATIONS.....	42
FIGURE 4-17: VARIATIONS IN THE FIFTH NATURAL FREQUENCY FOR DIFFERENT PLY ORIENTATIONS .....	42
FIGURE 4-18: CONVERGENCE FOR A STEP BEAM FORMED FROM THREE STEPS USING THE FEM AND DFE FOR THE FIRST 4 NATURAL FREQUENCIES. 'NF' REPRESENTS NATURAL FREQUENCY. ....	43
FIGURE 4-19: CONVERGENCE FOR A STEP BEAM FORMED FROM THREE STEPS USING THE FEM AND DFE FOR THE 5 <sup>TH</sup> , 6 <sup>TH</sup> , 7 <sup>TH</sup> NATURAL FREQUENCIES. ....	44
FIGURE 5-1: (A) TAPERED BEAM IN GLOBAL (X, Y, Z) COORDINATE SYSTEM. (B) SIDE VIEW IN (X, Z) PLANE. (C) BEAM CROSS-SECTION. ....	47
FIGURE 5-2 SIGN CONVENTION, WHERE S DENOTES THE TRANSVERSE FORCE, M DENOTES THE BENDING MOMENT AND T DENOTES THE TORQUE .....	50
FIGURE 5-3: COMPARATIVE STUDY BETWEEN DFE CONVERGENCE RATES FOR THE FIRST FIVE NATURAL FREQUENCIES OF A LINEARLY TAPERED COMPOSITE WING ( $c=-1$ ) INCORPERATING DIFFERENT DEVIATORY TERMS: (A) THE FIRST; (B) THE SECOND; (C) THE THRID; (D) THE FOURTH. 'EIDDEV', REPRESENTS THE BENDING RIGIDITY DEVIATOR; 'GJDEV', REPRESENTS THE TORSION RIGIDITY DEVIATOR; 'KDEV' REPRESENTS THE COUPLED BENDING-TORSION RIGIDITY DEVIATOR, 'MDEV'	

REPRESENTS THE MASS DEVIATOR; 'IALFDEV', REPRESENTS THE MASS MOMENT OF INERTIA DEVIATOR. ....	56
FIGURE 5-4: COMPARATIVE STUDY BETWEEN DFE CONVERGENCE RATES FOR THE FIRST FIVE NATURAL FREQUENCIES OF A LINEARLY TAPERED COMPOSITE WING ( $C=-1$ ) INCORPORATING DIFFERENT DEVIATORY TERMS: (E) THE FIFTH NATURAL FREQUENCIES. 'EIDEV', REPRESENTS THE BENDING RIGIDITY DEVIATOR; 'GJDEV', REPRESENTS THE TORSION RIGIDITY DEVIATOR; 'KDEV' REPRESENTS THE COUPLED BENDING-TORSION RIGIDITY DEVIATOR, 'MDEV' REPRESENTS THE MASS DEVIATOR; 'IALFDEV', REPRESENTS THE MASS MOMENT OF INERTIA DEVIATOR. ....	57
FIGURE 5-5: 1 <sup>ST</sup> NORMALIZED NATURAL MODE OF A TAPERED COMPOSITE WING. A SOLID LINE (-) REPRESENTS BENDING DISPLACEMENT AND DASHED LINE (--) REPRESENTS TORSION DISPLACEMENT. .	58
FIGURE 5-6: 2 <sup>ND</sup> NORMALIZED NATURAL MODE OF A TAPERED COMPOSITE WING. A SOLID LINE (-) REPRESENTS BENDING DISPLACEMENT AND DASHED LINE (--) REPRESENTS TORSION DISPLACEMENT. .	58
FIGURE 5-7: 3 <sup>RD</sup> NORMALIZED NATURAL MODE OF A TAPERED COMPOSITE WING. A SOLID LINE (-) REPRESENTS BENDING DISPLACEMENT AND DASHED LINE (--) REPRESENTS TORSION DISPLACEMENT. .	58
FIGURE 5-8: 4 <sup>TH</sup> NORMALIZED NATURAL MODE OF A TAPERED COMPOSITE WING. A SOLID LINE (-) REPRESENTS BENDING DISPLACEMENT AND DASHED LINE (--) REPRESENTS TORSION DISPLACEMENT. .	58
FIGURE 5-9: 5 <sup>TH</sup> NORMALIZED NATURAL MODE OF A TAPERED COMPOSITE WING. A SOLID LINE (-) REPRESENTS BENDING DISPLACEMENT AND DASHED LINE (--) REPRESENTS TORSION DISPLACEMENT. .	59
FIGURE 5-10: CONVERGENCE OF DFE, FEM, DSM AND DFE +DEVs FOR THE FIRST NATURAL FREQUENCY. ....	59
FIGURE 5-11: CONVERGENCE OF DFE, FEM, DSM AND DFE +DEVs FOR THE SECOND NATURAL FREQUENCY. ....	60
FIGURE 5-12: CONVERGENCE OF DFE, FEM, DSM AND DFE +DEVs FOR THE THIRD NATURAL FREQUENCY. ....	60
FIGURE 5-13: CONVERGENCE FOR THE FIRST NATURAL FREQUENCY FOR A GLASS/EPOXY 1 DEGREE TAPERED BEAM. ....	62
FIGURE 5-14: CONVERGENCE FOR THE SECOND NATURAL FREQUENCY FOR A GLASS/EPOXY 1 DEGREE TAPERED BEAM. ....	62
FIGURE 5-15: CONVERGENCE FOR THE THIRD NATURAL FREQUENCY FOR A GLASS/EPOXY 1 DEGREE TAPERED BEAM. ....	63
FIGURE 5-16: CONVERGENCE OF THE DFE WITH AND WITHOUT DEVIATORS FOR THE FIRST THREE NATURAL FREQUENCIES. ....	63
FIGURE 5-17: ILLUSTRATION OF COMPOSITE WING TAPER ANGLE. ....	65
FIGURE 5-18: DUALY TAPERED CYTEK 5245-T800 CARBON FIBRE/EPOXY WING GEOMETRY. ....	66
FIGURE 5-19: FIRST NATURAL FREQUENCY FOR LAY-UP #1 WITH A $C=-0.5$ . ....	67
FIGURE 5-20: SECOND NATURAL FREQUENCY FOR LAY-UP #1 WITH A $C=-0.5$ . ....	68
FIGURE 5-21: THIRD NATURAL FREQUENCY FOR LAY-UP #1 WITH A $C=-0.5$ . ....	68
FIGURE 5-22: FIRST NATURAL FREQUENCY FOR LAY-UP #2 WHERE $C=-0.75$ . ....	69
FIGURE 5-23: SECOND NATURAL FREQUENCY FOR LAY-UP #2 WHERE $C=-0.75$ . ....	69
FIGURE 5-24: THIRD NATURAL FREQUENCY FOR LAY-UP #2 WHERE $C=-0.75$ . ....	70
FIGURE 5-25: FOURTH NATURAL FREQUENCY FOR LAY-UP #2 WHERE $C=-0.75$ . ....	70
FIGURE 6-1: (A) 3-D DRAWING OF A COMPOSITE WING CROSS-SECTION AIRFOIL, WITH LENGTH = $L$ . ....	73
FIGURE 6-2: (B) CROSS-SECTION OF A WING-BOX, WHERE $C$ IS THE CHORD LENGTH, $M_{box}$ IS THE WING-BOX MASS, $E_s$ AND $G_s$ ARE, RESPECTIVELY, THE GEOMETRIC ELASTIC CENTRE AND MASS CENTRE AXIS. ....	74
FIGURE 6-3: : DUALY TAPERED COMPOSITE WING-BOX. ....	78
FIGURE 6-4: PLOT OF RIGIDITIES VS PLY ANGLE FOR A GRAPHITE/EPOXY COMPOSITE. ....	81
FIGURE 6-5: CONVERGENCE OF DUALY QUADRATIC TAPERED WING-BOX FOR THE FIRST NATURAL FREQUENCY. ....	82
FIGURE 6-6: CONVERGENCE OF DUALY QUADRATIC TAPERED WING-BOX FOR THE SECOND NATURAL FREQUENCY. ....	82
FIGURE 6-7: CONVERGENCE OF DUALY QUADRATIC TAPERED WING-BOX FOR THE THIRD NATURAL FREQUENCY. ....	83
FIGURE 6-8: CONVERGENCE OF DUALY CUBIC TAPERED WING-BOX FOR THE FIRST NATURAL FREQUENCY. ....	84
FIGURE 6-9: CONVERGENCE OF DUALY CUBIC TAPERED WING-BOX FOR THE SECOND NATURAL FREQUENCY. ....	85

FIGURE 6-10: CONVERGENCE OF DUALY CUBIC TAPERED WING-BOX FOR THE THIRD NATURAL FREQUENCY.	85
FIGURE 6-11: CONVERGENCE OF DUALY CUBIC TAPERED WING-BOX FOR THE FOURTH NATURAL FREQUENCY.	86
FIGURE 6-12: CONVERGENCE OF DUALY CUBIC TAPERED WING-BOX FOR THE FIFTH NATURAL FREQUENCY.	86
FIGURE 6-13: FIRST PREDOMINANTLY BENDING MODE OF VIBRATION FOR A COMPOSITE GRAPHITE/EPOXY CUBIC TAPERED WING IN BOTH 2-D AND 3-D PLOTS. FOR THE 2-D PLOT THE BENDING DISPLACENMENT IS REPRESENTED BY A SOLID LINE (-) AND TORSION IS REPRESENTED BY A DASHED LINE (--).	87
FIGURE 6-14: SECOND PREDOMINANTLY BENDING MODE OF VIBRATION FOR A COMPOSITE GRAPHITE/EPOXY CUBIC TAPERED WING IN BOTH 2D AND 3-D PLOTS. FOR THE 2-D PLOT THE BENDING DISPLACENMENT IS REPRESENTED BY A SOLID LINE (-) AND TORSION IS REPRESENTED BY A DASHED LINE (--).	88
FIGURE 6-15: THIRD PREDOMINANTLY TORSION MODE OF VIBRATION FOR A COMPOSITE GRAPHITE/EPOXY CUBIC TAPERED WING IN BOTH 2D AND 3-D PLOTS. FOR THE 2-D PLOT THE BENDING DISPLACENMENT IS REPRESENTED BY A SOLID LINE (-) AND TORSION IS REPRESENTED BY A DASHED LINE (--).	88
FIGURE 6-16: FOURTH BENDING-TORSION MODE OF VIBRATION FOR A COMPOSITE GRAPHITE/EPOXY CUBIC TAPERED WING IN BOTH 2D AND 3-D PLOTS. FOR THE 2-D PLOT THE BENDING DISPLACENMENT IS REPRESENTED BY A SOLID LINE (-) AND TORSION IS REPRESENTED BY A DASHED LINE (--).	89
FIGURE 6-17: FIFTH BENDING-TORSION MODE OF VIBRATION FOR A COMPOSITE GRAPHITE/EPOXY CUBIC TAPERED WING IN BOTH 2D AND 3-D PLOTS. FOR THE 2-D PLOT THE BENDING DISPLACENMENT IS REPRESENTED BY A SOLID LINE (-) AND TORSION IS REPRESENTED BY A DASHED LINE (--).	89

## Nomenclature

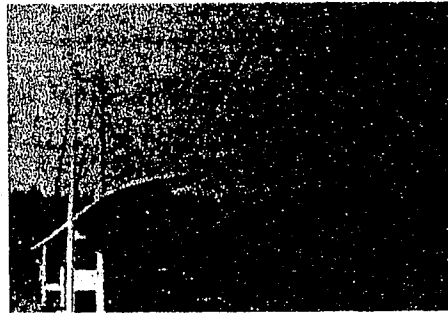
$U$	Eigenvector
$[K]$	Stiffness Matrix
$[M]$	Mass Matrix
$\lambda$	Eigenvalue
$\omega$	Frequency [rads/s]
$J$	Number of total frequencies exceeded by the trial frequency
$J_o$	Total number of clamped-clamped frequencies exceeded by the trial frequency
$\text{sgn}\{K_{DSM}\}$	Sign count of negatives along the leading diagonal of the dynamic stiffness matrix
$[B]$	Stiffness matrix for a simply-supported beam
$J_m$	Number of clamped-clamped frequencies exceeded for each element
$J_b$	Number of clamped-clamped frequencies exceeded for the bending portion
$\text{sgn}\{B\}$	Sign count of negatives along the leading diagonal of the simply supported dynamic stiffness matrix
$J_t$	Number of clamped-clamped frequencies exceeded for the twisting portion
$D_f$	Denominator of to the flexural shape functions
$D_t$	Denominator of to the torsion shape functions
$\alpha$	Coefficient to the governing differential equation of motion for bending
$\gamma$	Coefficient to the governing differential equation of motion for torsion
$\{F\}$	Applied Force Vector
$\bar{\omega}_n$	Perturbation of the natural frequency
$\bar{F}$	Perturbation of the force vector
$Q_{ij}$	Reduced stiffness constants
$E_T$	Transverse elastic modulus
$E_L$	Longitudinal elastic modulus
$G_{LT}$	Principle shear modulus
$\nu$	Poisons ratio
$\bar{Q}_{ij}$	Transformed reduced stiffness constants
$N(x, y)$	Resultant force
$M(x, y)$	Resultant Moment
$A_{ij}$	Extensional stiffness matrix
$B_{ij}$	Coupling stiffness matrix

$D_{ij}$	Bending stiffness matrix
$\theta$	Bending slope
$\psi$	Angle of twist
$EI$ or $H_f$	Bending stiffness
$GJ$ or $H_t$	Torsion stiffness
$K$	Coupled bending-torsion stiffness
$b$	Base
$h$	Wall thickness
$d$	Depth of a box-beam section
$L$	Length of the beam (wing)
$R$	Radius of curvature
$A(s)$	Reduced axial stiffness
$B_t$	Reduced coupling stiffness on the top skin of a box-section
$A_e$	Enclosed area of the box-section
$a$	Width of a box-section
$C_t$	Reduced shear stiffness on the top skin of a box-section
$C_v$	Reduced shear stiffness on the side panels of a box-section
$s$	Circumference of the cross-section
$w$	Bending displacement
$I_\alpha$	Mass moment of Inertia per unit length
$m$	Mass per unit length
$W_{INT}$	Internal Work
$W_{EXT}$	External Work
$l_k$	Element Length
$W_f^k$	Elementary work corresponding to bending
$W_t^k$	Elementary work corresponding to bending
$N_f$ or $N$	Flexural shape functions
$N_t$	Twist shape functions
$\Gamma_r$	Reference variable
$DEV$	Deviator terms
$\Gamma_{ave}$	Average variable
$x_\alpha$	Distance between mass axis and geometric elastic axis
$c$	Chord length
$M_{box}$	Mass of wing box
$G_s$	Geometric elastic axis
$E_s$	Mass axis

# Chapter 1 Introduction

## 1.1 General Introduction

Mechanical vibrations are exhibited by all structures, the study of these vibrations is important because they can be destructive in a design. A bridge is a good example of a static structure that can undergo mechanical vibrations. If the bridge is forced to vibrate at one of its resonance (i.e. natural) frequencies by an externally applied load, the modes of deformation associated with this resonance can lead to catastrophic failure. For example, the Tacoma bridge as seen in the illustration below is undergoing twisting motion caused by vibrating at a particular natural frequency (see <http://www.ketchum.org>). The vibration analysis of structures is an essential part of the design phase, as unwanted resonance behaviour can result ultimately in failure of the structure. Not only can the modes of deformation cause irreversible plastic deformation, but also fatigue damage caused by oscillating motion can lead to crack propagation and finally failure in design.



It is the vibration response of a system which must be studied to prevent such failures in design. The first step for any vibration analysis is determining the free vibration response (i.e., natural frequencies and modes) of the structure. Once a method is adopted for determining the resonant frequencies and modes of free vibration the design can potentially be optimized for any desired vibration response.

Aircraft control surfaces and wing flutter can lead to detrimental fatigue damage and possible failure. The knowledge of the natural frequencies and modes of free vibration for these systems are essential to their flutter analysis and aero elastic tailoring (Lilico and Butler, 1998; Lilico *et al*, 1997). The free vibration analysis of composite aircraft wings is the main focus of this research. In most optimization processes the reduction in mass for a design means lower costs. The search for lighter materials which satisfy the requirements of aircraft structures is a continuing effort. The requirements on materials

1

have become greater than ever before, to the extent that homogeneous material cannot achieve the multitude of performance needs. Composite materials possessing unidirectional fibres can satisfy most if not all the requirements, for example lighter weight, higher strength, designable stiffness, longer fatigue life and corrosion resistance (see, for example publications by Jones (1998) and Berthelot (1999), etc.).

The stiffness properties of composites, is of particular interest as it leads to possible optimization of composite aircraft wings. By changing the ply orientation and stacking sequence, one can alter the stiffness characteristics of the composite material. The free vibration of aircraft wings is then extended to fibrous composites in which couplings arise from an unbalanced lay-up. For symmetric lay-ups, where stacking sequence and thickness is symmetric with reference to the mid-plane of the laminate, couplings occur between bending and torsion modes of deformation and are observed to be the most predominant factor influencing the natural frequencies and modes of free vibration (Banerjee, 1998; Borneman and Hashemi, 2003; Hashemi and Borneman, 2003; Hashemi and Borneman, 2004).

The coupled free vibration of a laminated composite wing, idealized as beam assemblies have been investigated by Abramovich and Livshits (1994), Teoh and Huang (1997), Teh and Huang, (1980) using different analytical approaches and Chandra, Stemple and Chopra (1990), Wu and Sun (1991), Jaehong and Kim (2002), Teh and Huang (1979), Suresh and Venkatesan (1990), Chen, Liu and Lim (2003), Jung, Nagaraj and Chopra (2001), Volovoi and Hodges (2002) using various numerical models. Numerical models based on Rayleigh-Ritz, Galerkin and Finite Element Method (FEM) use element matrices evaluated from assumed fixed interpolation functions (Cook *et al*, 2001). The Finite Element Method is commonly used as it provides a general systematic approach to formulate the element mass and stiffness matrices for a given structure. Considering the fixed nature of the shape functions, the natural frequencies can be found by solving the resulting linear eigenvalue problem. This approximate method is widely accepted, see for example Chandra *et al* (1990), Wu and Sun (1991), Jaehong and Kim (2002), Teh and Huang (1979), for its monotonic convergence to the exact values, with the appropriate type and number of elements. Commercial software packages such as ANSYS® are used to construct the FEM model of complex structures and to carry

various analyses. Although a wing modeled as an assembly of uniform beam elements is not highly complex, difficulty arises from modeling the composite nature of the beam. Taylor and Butler (1997), Lillico and Butler (1998) have used ANSYS<sup>®</sup> with shell (SHELL91) elements to construct composite type elements. In this research due to the unavailability of a composite module in the Educational version of ANSYS<sup>®</sup>, the FEM was programmed using MATLAB<sup>®</sup>.

An elaborated FEM model takes a very long time to create. For the preliminary design process, one needs a simple and accurate model to calculate the natural frequencies of a system and further detailed design and optimization would be possible using FEM. This has led to the analytical and semi analytical approaches. In addition to the FEM and other weighted residual methods, the Dynamic Stiffness Matrix (DSM) method can alternatively be employed to determine the free vibration response of a structure. The DSM was developed by Kolousek in 1940 for homogeneous (metallic) Euler-Bernoulli beams (Banerjee and Williams, 1985). The DSM has since been refined continuously. In the last decade, Banerjee and his colleagues extended the DSM method to the vibration analysis of many different homogeneous and composite beam models. Banerjee and Williams (1995) developed the DSM for a uniform Euler-Bernoulli beam, Banerjee and Williams (1996) extended that to the Timoshenko beam theory and then later this model was further extended to include an axial force (Banerjee, 1998). The DSM models for composite beams are developed based on the exact member theory (Banerjee and Williams, 1995). Furthermore, the elements of the frequency dependent stiffness matrix are derived in closed form. Were each element of the DSM matrix is evaluated based on algebraic expressions, resulting in faster execution compared to the numerical alternative matrix inversion method.

Using Reduce<sup>®</sup> software extensive manipulation was undertaken in the search for a symbolically inverted element DSM matrix (Banerjee and Williams, 1995). The computational time has been compared between the closed form solution and the numerical solution presented by Banerjee and Williams (1995). Their results revealed significant time reduction using the closed form solution. Given that the general DSM matrix is frequency dependent, a non-linear eigenvalue problem results. The natural frequencies are solved by application of the Wittrick-Williams root counting algorithm

(Wittrick and Williams, 1971; Wittrick and Williams, 1982) in conjunction with a numerical bisection method. For simple uniform beam configurations the DSM method requires only one element to produce the exact solution. For some cases involving more complex geometries the DSM has slower convergence than the FEM (Hashemi, 1998; Hashemi and Borneman, 2003). It is for this reason that a new more flexible method was devised to include the advantages of both the FEM and DSM.

The Dynamic Finite Element (DFE) exploits the advantages of the FEM and DSM. It provides a general systematic procedure (i.e., Integral Formulation based on the Weighted Residual Method (WRM)), which it shares with the FEM formulation and the accuracy and ability to converge on any particular natural frequency adopted from the DSM method. The proposed technique follows the same procedure as the FEM by formulating the element equations discretized to a local domain, then, element stiffness matrices are constructed and assembled into a single global matrix. The generality adopted from the FEM provides easy implementation to elements with higher complexity.

The Dynamic Finite Element (DFE) method was first proposed by Hashemi (1998) and has since been well established for the free vibration analysis of homogeneous beams, blades and beam-like structures ( Hashemi , Richard and Dhatt, 1999; Hashemi and Richard, 1999; Hashemi and Richard, 2000(A); Hashemi and Richard, 2000 (B), Hashemi and Richard, 2001; Hashemi, 2002). It has been shown that the DFE method has higher convergence to the exact values than both the FEM and DSM for complex geometries (i.e. tapered beams). The Dynamic Trigonometric Shape Functions (DTSF's) produce a frequency dependent stiffness matrix similar to the DSM. In fact, the DFE reduces to the DSM matrix for simple cases such as Euler-Bernoulli homogeneous uniform beams (Hashemi, 1998).

The goal of this research is to investigate laminated composite wings and to develop a DFE formulation for the free vibration analysis of such structures. Due to coupling terms found in the governing equations of motion arising from the composite nature of the material, the DSM will not reduce to the same matrix as the DFE as previously described for Euler-Bernoulli beams.

As it will be discussed later in this thesis, when coefficients of the governing differential equation of motion are variable (e.g., a tapered configuration) the DFE can incorporate additional terms to increase the convergence rate of the solution. These additional terms known as deviator terms were first used by Hashemi (1998). Deviator terms are simply refining terms used to replace the initial averaged distribution of variables with the exact distribution. The addition of these deviator terms is the most important factor that differentiates the DFE from the DSM. The DFE, with its frequency dependent stiffness matrix, leads to a non-linear eigenvalue problem similar to the DSM where a dedicated Wittrick-William algorithm is then used to solve the system. It will be shown that the combined advantages of the FEM, DSM and refining deviator terms makes the DFE an accurate, flexible, and systematic method capable to advantageously determine the natural frequencies of free vibration of a beam or wing configuration. The DFE is validated by its higher convergence rate to the natural frequencies compared to other existing methods (Borneman and Hashemi, 2003; Hashemi and Borneman, 2003; Hashemi and Borneman, 2004).

## **1.2 Pre-processing**

Considerable analysis into the composite lay-up and stacking sequence must be accomplished before studying the free vibration of a materially coupled system. Since the rigidities will change with fibre angle, pre-processing must be carried out to determine the effective rigidities of the system for a particular fibre orientation. Solid rectangular cross-sections are among the simplest to analyse. Through a detailed literature survey it was difficult to find the values for effective bending,  $EI$ , torsion,  $GJ$ , and coupled bending-torsion,  $K$ , rigidities of a composite beam. A number of references (Jones, 1998; Berthelot, 1999; Banerjee, 1998) clearly outline a general procedure in calculating the stiffness properties of an assumed solid rectangular beam cross-section. Most authors displayed the principal, transverse and longitudinal elastic modulus, Poison's ratio and principal shear modulus, but did not show the numerical values for the effective rigidities. It is for this reason that additional efforts was required to develop a pre-processor type program in MATLAB<sup>®</sup> to evaluate the effective rigidities of a composite

beam. This program was later altered to calculate the effective rigidities for any fibre angle and stacking sequence.

The calculation of rigidities for a composite box beam is more complex than for the assumed solid cross-section. Reserchers such as Armanios and Badir (1995), Berdichevsky, Armanios and Badir (1992) produced a general formulation to evaluate the rigidities of a composite box-beam section. The box-beam rigidity calculation was essential to accurately describe a composite wing-box geometry. In these references, two types of box-beam configurations are considered, *Circumferentially Asymmetric Stiffness (CAS)* and *Circumferentially Uniform Stiffness (CUS)*. The CAS configuration is the only configuration considered in this thesis as it exhibits the bending-torsion coupling behaviour. The CUS configuration results in extension-twist coupling. Smith and Chopra (1990) described a similar model of a box-beam, where rigidity calculations are based on either a symmetric or anti-symmetric configuration. Similar to the CAS, the symmetric configuration produces a bending-torsion coupling.

### **1.3 Thesis Organization and Modeling Considerations**

In the attempt to construct an accurate and complete wing model a progressive technique is implemented. In, brief, this thesis starts the wing idealization with a very simple uniform solid rectangular cross-section laminated composite beam model. Then, more geometric and material complexities are gradually incorporated in the model leading to stepped, tapered, and dually coupled configuration and finally, ending with a geometric- materially coupled tapered laminated composite wing box model.

The opening Chapter 1 gives a general introduction to the importance of mechanical vibrations and applicability of composite materials. Three of the most attractive vibration analysis techniques, FEM, DSM, and DFE, are outlined and briefly differentiated. The coupled bending-torsion coupling produced by an unbalanced lay-up of composite plies is also described. The purpose of this research is stated and the overall outline of the thesis is presented.

In Chapter 2, a short introduction to mechanical vibrations is first presented. Different categories of structural free vibrations, the associated discrete and continuous models, various types of resulting eigenvalue problems are also investigated. Then the dedicated solution methods to both the linear and non-linear eigenproblems are briefly introduced. The linear eigenvalue problem results from the assumed fixed polynomial shape functions. The is obtained when frequency dependent assumed shape functions are used to express the field variables of the problem. More emphasis is placed on the non-linear frequency dependent eigenvalue problem where implementation of the Wittrick-William root counting algorithm (Wittrick and Williams, 1971) to solve for the natural frequencies is presented. As it is then briefly discussed , the corresponding modes of coupled vibration can be extracted using a simple perturbation technique (Hashemi, 1998).

In Chapter 3, the calculation of effective rigidities for both solid rectangular and thin-walled box beam cross-sections is presented. The calculation of effective rigidities is limited to symmetric or Circumferentially Asymmetric Stiffness (CAS) cross sections as these configurations produce coupled bending-torsion behaviour inherent to the design. The influence of fibre angle and stacking sequence for an unbalanced unidirectional composite will change the effective stiffness the beam or wing model, resulting in significantly different vibration response.

In Chapter 4, the Dynamic Finite Element (DFE) formulation for an Euler-Bernoulli uniform composite beam with a solid rectangular cross section is presented. The bending and torsion Dynamic Trigonometric Shape Functions (DTSF) are developed and used to form the frequency dependent stiffness matrix. The formulation is then applied to uniform and piecewise uniform stepped beams.

General tapered wing geometry is considered in Chapter 5. The DFE formulation is prepared with refining terms known as 'deviator terms' (Hashemi and Richard, 1999; Hashemi, 1998; Hashemi and Borneman, 2003; Borneman and Hashemi, 2003; Hashemi and Borneman 2004; Borneman and Hashemi, 2004) to enhance the tapered model. This

formulation is applied to two different wing configurations: a linearly tapered by chord only (constant wing thickness), and a second wing model linearly tapered by chord and stepped by thickness wing. At the end of Chapter 5, a comparative study is also presented to illustrate the limitations associated with the application of the deviator terms. The importance of these limitations for consideration in further developments is then acknowledged.

Prior to Chapter 6, only material coupling resulting from an unbalanced lay-up in the composite wing is considered. In Chapter 6, not only material coupling terms but also geometric coupling effects are taken into account. The geometrical coupling arises from non-coincident mass and elastic axes in a wing box cross-section. Several dually coupled wing configurations are considered with applications of higher order tapers such as a 2<sup>nd</sup> and 3<sup>rd</sup> degrees. The CAS configuration is used to model the composite stiffness of the assumed thin-walled box-beam cross-section to ensure a bending-torsion coupled response.

Finally, the general conclusions are presented in Chapter 7 where the direction and future of the research are also stated.

## Chapter 2 Solution Methodology

### 2.1 Introduction

In general, the vibration analysis of an engineering system requires: the idealization of the system into a form that can be analyzed, the formulation of the governing equilibrium equations of this idealized system, the solutions of the governing equations, and finally the interpretation of the results. Physical systems may be broadly classified into two categories: discrete systems or continuous systems. Based on laws of physics, an engineering problem is thus represented either by a discrete system, which is characterized by a set of algebraic equations involving a finite number of unknowns or degrees of freedom; or by a continuous system which is very often characterized by a set of partial differential equations with corresponding boundary conditions (Bathe, 1982; Hashemi, 2002).

The exact solution of the differential equations and which satisfies all boundary conditions is only possible for relatively simple systems, and numerical procedures must in general be employed to predict the system response. These procedures, in essence, reduce the continuous system to a discrete idealization that can be analyzed in the same manner as a discrete physical system. The free vibration analysis of a discrete or continuous system leads to a so called *Eigenvalue problem*.

### 2.2 Free Vibration Analysis Based on Discrete Models: Linear Eigenproblems

Critical buckling and undamped free vibration problems are often solved using finite elements to obtain a discrete model with a finite number of degrees of freedom. In vibration problems, an alternative discrete model is often obtained by “lumping” distributed masses at convenient points. Further, these models usually yield linear eigenvalue problems Hashemi (2002) as:

$$[K]\{U\} = \lambda[M]\{U\} = 0; \quad [K(\omega)]\{U\} = [K - \omega^2 M]\{U\} = 0 \quad (0.1)$$

which can be solved by many proven and secure mathematical methods. Here,  $K$  and  $M$  represent stiffness and mass matrices of the system, respectively, and  $K(\omega)$  is the so-called Dynamic Stiffness Matrix (DSM) of the system. For a continuous system, the formulation generally leads to (Bathe (1982)):

$$L_1(u) = \lambda L_2(u) \text{ on a domain } V, \text{ and } \ell_1(u) = \lambda_2(u) \text{ on boundary } S \text{ of } V \quad (0.2)$$

where  $L_1$ ,  $L_2$ ,  $\ell_1$ , and  $\ell_2$  are linear differential operators. In the free vibration analysis of structures, the basic idea is to solve the relevant eigenproblem leading to the eigenvalues,  $\lambda$ , and eigenvectors,  $\{U\}$ , which represent the natural frequencies,  $\omega$ , and the modes of structures, respectively. The characteristics of this model depend on the analysis to be carried out, in essence, *the actual continuous system is reduced to an appropriate discrete system* where the element equilibrium, constitutive relations and element interconnectivity requirements are satisfied (this will be discussed in more details farther in this thesis).

### ***2.3 Analytical Formulation Based on Continuous Models: Non-Linear Eigenproblems***

A practical structure, assembled from elements possessing distributed mass, will have an infinite number of degrees of freedom and an infinite number of natural frequencies. The “Exact” member, or element, equations exist for structures including plane frames, space frames, grids, and many plate and shell problems. For plane frames, the member equations often incorporate the stability functions for buckling problems, and their dynamic equivalents for vibration problems (Wittrick and Williams (1983)). In this thesis, the focus is on the free undamped vibration problems. The exact member equations are then used to assemble the overall dynamic stiffness matrix,  $K(\omega)$ , of the

structure. The natural frequencies, in this case, will be obtainable from a non-linear eigensystem as in equation 2.1.

The elements of the displacement vector  $U$ , to which  $K(\omega)$  corresponds, is the finite set of amplitudes of nodal point displacements, varying sinusoidally with time. The frequency dependent matrices  $[K(\omega)]$  resulting from the Dynamic Stiffness Matrix (DSM) method and Dynamic Finite Element (DFE) approach both lead to non-linear eigenvalue problems. The Finite Element Method (FEM) based on fixed interpolation functions leads to a linear eigenvalue problem. In the following sections, the solution methods for both linear and non-linear eigenproblems are briefly addressed.

## ***2.4 Fixed shape functions and Linear Eigenproblem solution***

In the conventional FEM formulation, the basis functions of the approximation space are generally polynomial expressions. The basis functions are then used to construct the 'Fixed' interpolation functions (i.e. they only vary with element span-wise position  $x$ ). The polynomial shape functions satisfy both completeness and inter-element continuity conditions. The solution of the natural frequencies pertaining to this technique is simple considering this is a linear eigenvalue problem (0.1). For simple systems, setting the determinant to zero leads to a linear algebraic equation from which the natural frequencies can be easily extracted. For more complex systems, with large number of Degrees-Of-Freedom (DOF), one could solve the resulting classical linear eigenproblem using an inverse iteration, subspace or Lanczos method (Bathe ,1982). It is important to notice that due to the approximate nature of the conventional FEM, one could only solve for as many natural frequencies as the total DOF of the system.

## ***2.5 Dynamic trigonometric shape functions and Non-Linear Eigenproblem solution***

As it was stated in previous sections, the DSM and DFE formulations obtained from continuous models are different compared to the FEM considering the stiffness matrix is usually frequency dependent. One of the advantages of using a dynamic stiffness matrix is that natural frequencies are not missed. They lead to a non-linear eigenvalue problem as:

$$[K_{DSM}(\omega)]\{w_n\} = 0 \quad (0.3)$$

There are two possible sets of solutions pertaining to the above equation.

$$\{w_n\} \neq 0 \rightarrow |K_{DSM}(\omega)| = 0 \quad (0.4)$$

$$\{w_n\} = 0 \rightarrow |K_{DSM}(\omega)| = \infty \quad (0.5)$$

Then, the method frequently used for determining the natural frequencies of the system is the Wittrick-Williams algorithm presented in different occasions by Wittrick and Williams (1971), Wittrick and Williams (1982), Wittrick and Williams (1983). The method is based on the Sturm sequence properties of the frequency dependent stiffness matrix of the system and involves the input of a trial frequency. The number of natural frequencies exceeded by this trial frequency is then calculated as follows:

$$J = J_o + \text{sgn}\{K_{DSM}\} \quad (0.6)$$

where  $J$  represents the total number of natural frequencies of the system exceeded by the trial frequency,  $J_o$  represents the total number of clamped-clamped (C-C) natural frequencies of all elements exceeded by the trial frequency (i.e.,  $|K_{DSM}(\omega)| = \infty$ ) and is calculated as

$$J_o = \sum_{k=1}^{NE} J_m \quad (0.7)$$

The term  $\text{sgn}\{K_{DSM}\}$  is the sign of  $K_{DSM}$ , and is determined by counting the number of negative elements along the leading diagonal of the upper triangularized matrix. This is accomplished after the  $K_{DSM}$  is fully assembled. The upper triangular matrix is sensitive to pivotal operations, such that, during the gauss elimination procedure, the rows can be pivoted but not the columns. Then, from equation (0.6) the final number of natural frequencies exceeded by the trial frequency for the entire beam is calculated. Using a numerical method any natural frequency can be converged upon. This research uses the bisection technique as the convergence method. The bisection method is a no fault method in determining the solution.

There also exist combined methods to speed up the convergence of the solution. When the bisection method brings the upper and lower limits on the eigenvalues sufficiently close, a quicker numerical procedure can be implemented such as linear interpolation presented by Hoorpah, Henchi and Dhatt (1994), Newton's method discussed by Hopper and Williams (1977), parabolic interpolation discussed by Simpson (1984), or inverse iteration method (refer to Williams and Kennedy, 1988; Hashemi, 1998).

## **2.6 Extracting the modes**

By implementing the Wittrick-William algorithm the resonant frequencies are established for the free vibration of a system. Difficulty arises from solving the equation for the modes of deformation due to the zero force vector residing on the right hand side:

$$[K(\omega_n)]\{w_n\} = \{0\} \quad (0.8)$$

where,  $F$  is the zero force vector corresponding to the free vibration of the structure. At the resonant frequency, the dynamic stiffness matrix cannot be inverted due to the zero determinant. To obtain a non-trivial solution the frequency variable is manipulated so that the frequency dependent stiffness matrix is altered slightly. This perturbation must be small as to not deviate from the solution significantly.

$$\tilde{\omega}_n = \omega_n (1 + 1.0 \times 10^{-i}) \quad (0.9)$$

where  $\tilde{\omega}_n$  is the altered frequency and  $i$  is any real number sufficiently large enough such that a small perturbation is created. This new frequency is then substituted into equation (0.8) leading to:

$$[K(\tilde{\omega}_n)]\{w_n\} = \{F\} \quad (0.10)$$

The force vector on the right side of equation (0.10) is also altered slightly.

$$\tilde{F} = F + 1.0 \times 10^{-10} \quad (0.11)$$

where  $\tilde{F}$  is the altered force vector. Then the modes can be evaluated by manipulating equation (0.10) to:

$$\{w_n\} = [K(\tilde{\omega}_n)]^{-1} \{\tilde{F}\} \quad (0.12)$$

The order of perturbation of the frequency variable  $\tilde{\omega}_n$  and the force vector  $\tilde{F}$  depends on the numerical precision. Using double precision the 10<sup>th</sup> order perturbation is acceptable to accurately describe the modes of deformation (Hashemi, 1998).

## **2.7 Conclusion**

The Wittrick-William technique plays an important part in determining the natural frequencies and modes of free vibration. This method is used for both, but not limited to the Dynamic Finite Element method and Dynamic Stiffness Matrix method where the use of a frequency dependent stiffness matrix leads to a non-linear eigenvalue problem. The technique can equally be used as a solver for the FEM (Roach and Hashemi, 2003). This

method is particularly advantageous with the capability of solving any range of frequencies.

## **Chapter 3 Composite Rigidities**

### **3.1 Introduction**

The application of fibre-reinforced composite materials in the aerospace industry extends from commercial to military aircraft, such as the Boeing F18, B2 Stealth Bomber, AV-8B Harrier (Jones, 1998). The attractiveness of composites lies in their mechanical properties; such as weight, strength, stiffness, corrosion resistance, fatigue life. Composites are widely used for control surfaces such as ailerons, flaps, stabilizers, rudders, as well as rotary and fixed wings. That is why the analysis of composite structures is imperative for aerospace industry. The main advantage of composites is their flexibility in design. Mechanical properties of the laminate can be altered simply by changing the stacking sequence, fibre lay-up and thickness of each ply which leads to optimization in a design process.

### **3.2 Assumptions**

The composite beam is modeled based on the chord-wise bending moment (about the z-axis) small compared to the span-wise moment (about the y axis, see Figure 3-2). The chord-wise moment is then neglected. The composite material pertaining to this research is a unidirectional fibre reinforced composite material. The given information of any unidirectional composite material is the elastic modulus in both the longitudinal and transverse axis (see Figures 3-1 and 3-2), Poison's ratio and the shear modulus in the principle directions.

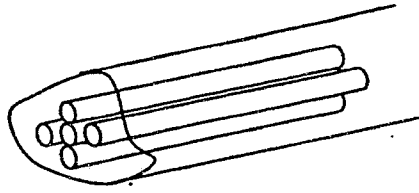


Figure 3-1: Unidirectional fibres surrounded by a matrix

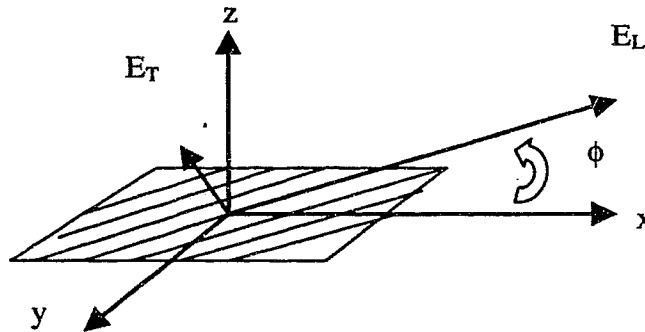


Figure 3-2: Coordinate transformation from principal directions to global  $(x,y,z)$  direction. Where  $E_L$  and  $E_T$  and the longitudinal and transverse elastic modulae.

### 3.3 Effective rigidities for a solid cross-section

The reduced stiffness constants in the material principle directions are:

$$Q_{12} = \frac{\nu_{LT} E_T}{1 - \nu_{LT} \nu_{TL}} = \nu_{LT} Q_{22} \quad (0.13)$$

$$Q_{22} = \frac{E_T}{1 - \nu_{LT} \nu_{TL}} = \frac{E_T}{1 - \frac{E_T}{E_L} \nu_{LT}^2} = \frac{E_T}{E_L} Q_{11} \quad (0.14)$$

$$Q_{66} = G_{LT} \quad (0.15)$$

where,  $E_L$ , is the elastic modulus in the longitudinal direction.  $E_T$ , is the elastic modulus in the transverse direction. Poisson's ratio is denoted by  $\nu_{LT}$  and the principal shear

modulus is denoted by  $G_{LT}$ . For a plane stress state these reduced stiffness constants are sufficient to describe the stress-strain relationship as follows:

$$\begin{bmatrix} \sigma_1 \\ \sigma_2 \\ \tau_{12} \end{bmatrix} = \begin{bmatrix} Q_{11} & Q_{12} & Q_{16} \\ Q_{12} & Q_{22} & Q_{26} \\ Q_{16} & Q_{26} & Q_{66} \end{bmatrix} \begin{bmatrix} \varepsilon_1 \\ \varepsilon_2 \\ \varepsilon_{12} \end{bmatrix} \quad (0.16)$$

In order to find the stresses and strains in the  $(x, y, z)$  coordinate system a simple rotational transformation is needed, as:

$$[\overline{Q}_{ij}] = [T]^{-1} [Q_{ij}] [T] \quad (0.17)$$

where  $T$  is the transformation matrix which is used to transform the reduced stiffness constants from the principal material fibre directions to a global  $(x, y, z)$  beam coordinates.

Then, the resulting transformed reduced stiffness constants for a unidirectional or orthotropic composite from its principal directions is (Berthelot, 1999):

$$\begin{aligned} \overline{Q}_{11} &= Q_{11} \cos^4 \phi + Q_{22} \sin^4 \phi + 2(Q_{12} + 2Q_{66}) \sin^2 \phi \cos^2 \phi \\ \overline{Q}_{12} &= (Q_{11} + Q_{22} - 4Q_{66}) \sin^2 \phi \cos^2 \phi + Q_{12} (\cos^4 \phi + \sin^4 \phi) \\ \overline{Q}_{16} &= (Q_{11} - Q_{12} - 2Q_{66}) \sin \phi \cos^3 \phi + (Q_{12} - Q_{22} + 2Q_{66}) \sin^3 \phi \cos \phi \\ \overline{Q}_{22} &= (Q_{11} \sin^4 \phi + 2(Q_{12} + Q_{66}) \sin^2 \phi \cos^2 \phi + Q_{22} \cos^4 \phi) \\ \overline{Q}_{26} &= (Q_{11} - Q_{12} - 2Q_{66}) \sin^3 \phi \cos \phi + (Q_{12} - Q_{22} + 2Q_{66}) \sin \phi \cos^3 \phi \\ \overline{Q}_{66} &= (Q_{11} + Q_{22} - 2(Q_{12} + Q_{66})) \sin^2 \phi \cos^2 \phi + Q_{66} (\sin^4 \phi + \cos^4 \phi) \end{aligned} \quad (0.18)$$

From Berthelot (1999) and Banerjee (1998), the in-plane resultant matrix  $N(x, y)$  is:

$$\begin{Bmatrix} N_x \\ N_y \\ N_{xy} \end{Bmatrix} = \int_{-1/2}^{1/2} \begin{Bmatrix} \sigma_1 \\ \sigma_2 \\ \tau_{12} \end{Bmatrix} dz \quad (0.19)$$

and the resultant moment is:

$$\begin{Bmatrix} M_x \\ M_y \\ M_{xy} \end{Bmatrix} = \int_{-t/2}^{t/2} z \begin{Bmatrix} \sigma_1 \\ \sigma_2 \\ \tau_{12} \end{Bmatrix} dz \quad (0.20)$$

Both equations (above) can be merged into a single equation commonly known as the “Constitutive Equation”. The constitutive equation describes the stiffness matrix of a laminate plate. The resultant forces and moments are functions of the in-plane strains and curvatures (Berthelot, 1999).

$$\begin{bmatrix} N_x \\ N_y \\ N_{xy} \\ M_x \\ M_y \\ M_{xy} \end{bmatrix} = \begin{bmatrix} A_{11} & A_{12} & A_{16} & B_{11} & B_{12} & B_{16} \\ A_{12} & A_{22} & A_{26} & B_{12} & B_{22} & B_{26} \\ A_{16} & A_{26} & A_{66} & B_{16} & B_{26} & B_{66} \\ B_{11} & B_{12} & B_{16} & D_{11} & D_{12} & D_{16} \\ B_{12} & B_{22} & B_{26} & D_{12} & D_{22} & D_{26} \\ B_{16} & B_{26} & B_{66} & D_{16} & D_{26} & D_{66} \end{bmatrix} \begin{bmatrix} \epsilon_{xx} \\ \epsilon_{yy} \\ \epsilon_{xy} \\ \kappa_x \\ \kappa_y \\ \kappa_{xy} \end{bmatrix} \quad (0.21)$$

The sub-matrix  $A$  is called the extensional stiffness matrix, sub-matrix  $B$  is called the coupling stiffness matrix and sub-matrix  $D$  is called the bending stiffness matrix (Berthelot, 1999). When the laminate is symmetric, by ply orientation and thickness, with respect to the mid-plane layer, the coupling matrix  $B$  is eliminated ( $B_{ij} = 0$ ). The coefficients corresponding to a bending-twist coupling are  $D_{12}$  and  $D_{26}$ .

The stiffness coefficients are defined by the following expressions from Berthelot (1999).

$$\begin{aligned} A_{ij} &= \sum_{k=1}^{NL} (\overline{Q_{ij}})_k (h_k - h_{k-1}) \\ B_{ij} &= \frac{1}{2} \sum_{k=1}^{NL} (\overline{Q_{ij}})_k (h_k^2 - h_{k-1}^2) \\ D_{ij} &= \frac{1}{3} \sum_{k=1}^{NL} (\overline{Q_{ij}})_k (h_k^3 - h_{k-1}^3) \end{aligned} \quad (0.22)$$

where  $h_k$  is the distance from the mid-plane of the laminate (Figure 3-3).

$$\begin{bmatrix} M_x \\ M_y \\ M_{xy} \end{bmatrix} = \begin{bmatrix} D_{11} & D_{12} & D_{16} \\ D_{12} & D_{22} & D_{26} \\ D_{16} & D_{26} & D_{66} \end{bmatrix} \begin{bmatrix} \kappa_x \\ \kappa_y \\ \kappa_{xy} \end{bmatrix} \quad (0.23)$$

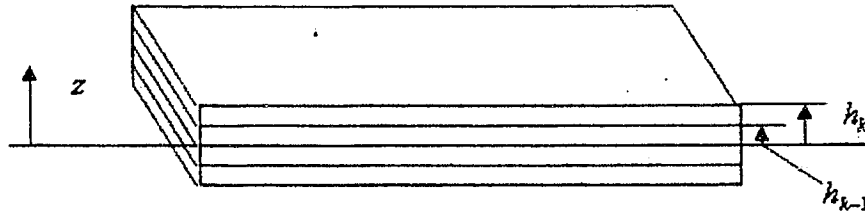


**Figure 3-3: Composite Laminate beam consisting of multiple plies, where  $h_k$  is the distance from the mid-plane of the composite.**

For a bending-torsion coupling behaviour the chord wise moment  $M_x$  is assumed to be zero so that the  $\kappa_x$  curvature can be eliminated from (above) and then the matrix (0.23) reduces to the following form:

$$\begin{bmatrix} M_y \\ M_{xy} \end{bmatrix} = \begin{bmatrix} D_{22} & D_{26} \\ D_{26} & D_{66} \end{bmatrix} - \begin{bmatrix} D_{12} \\ D_{16} \end{bmatrix} [D_{11}]^{-1} [D_{12} \quad D_{16}] \begin{bmatrix} \kappa_y \\ \kappa_{xy} \end{bmatrix} \quad (0.24)$$

The resulting matrix is then:

$$\begin{bmatrix} M_y \\ M_{xy} \end{bmatrix} = \begin{bmatrix} D_{22} - \frac{D_{12}^2}{D_{11}} & D_{26} - \frac{D_{12}D_{16}}{D_{11}} \\ D_{26} - \frac{D_{12}D_{16}}{D_{11}} & D_{66} - \frac{D_{16}^2}{D_{11}} \end{bmatrix} \begin{bmatrix} \kappa_y \\ \kappa_{xy} \end{bmatrix} \quad (0.25)$$

The bending and torque intensities are related to the resultant moment and torque by (Banerjee, 1998):

$$\begin{aligned} M &= -bM_y \\ T &= 2bM_{xy} \end{aligned} \quad (0.26)$$

where  $b$  is the base (chord) of the laminate. For small deflections, the curvatures can be related to the bending slope  $\theta$  and torsion twist  $\psi$  as follows:

$$\begin{aligned} \kappa_y &= -\theta \\ \kappa_{xy} &= 2\psi' \end{aligned} \quad (0.27)$$

so that the general form of the moment and torque is:

$$\begin{bmatrix} M \\ T \end{bmatrix} = \begin{bmatrix} EI & K \\ K & GJ \end{bmatrix} \begin{bmatrix} \theta' \\ \psi' \end{bmatrix} \quad (0.28)$$

where,

$$\begin{aligned} EI &= b \left( D_{22} - \frac{D_{12}^2}{D_{11}} \right) \\ GJ &= 4b \left( D_{66} - \frac{D_{16}^2}{D_{11}} \right) \\ K &= 2b \left( D_{26} - \frac{D_{12}D_{16}}{D_{11}} \right) \end{aligned} \quad (0.29)$$

The  $EI$ ,  $GJ$  and  $K$  represent the effective rigidities of the beam in the global ( $x, y, z$ ) coordinate system.  $EI$ ,  $GJ$ , and  $K$  represent, respectively, the bending rigidity, torsion rigidity and bending-torsion coupled rigidity. The effective rigidities are functions of ply angle, thickness, and stacking sequence.

### 3.4 Effective rigidities for a thin-walled box-beam section

The calculation of composite rigidities for a box-beam is presented by Armanios and Badir (1995) and Berdichevsky *et al* (1992). The Circumferentially Asymmetric Stiffness (CAS) configuration would produce a bend-twist coupling. The reduced axial stiffness  $A(s)$ , coupling stiffness  $B(s)$  and shear stiffness  $C(s)$  can then be developed from the constitutive equation (0.21) as:

$$\begin{aligned} A(s) &= A_{11} - \frac{(A_{12})^2}{A_{22}} \\ B(s) &= 2 \left( A_{16} - \frac{A_{12}A_{26}}{A_{22}} \right) \\ C(s) &= 4 \left( A_{66} - \frac{(A_{26})^2}{A_{22}} \right) \end{aligned} \quad (0.30)$$

The current rigidities are based on the following thin-walled assumptions:

$$d \ll L, \quad h \ll d, \quad h \ll R$$

where  $d$  is the depth,  $h$  is the height,  $L$  is the length of the beam and  $R$  is the radius of curvature (refer to

Figure 3-4 ) (Berdichevsky *et al* , 1992)..

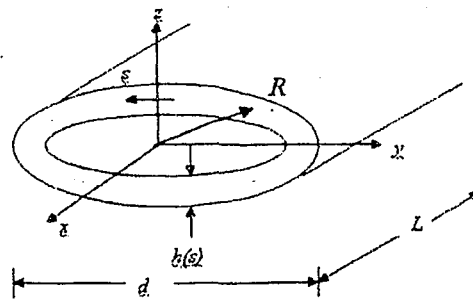


Figure 3-4: General cartesian coordinate system

The resulting effective rigidities are then obtained as:

$$EI = A \int z^2 ds - \frac{B_t}{2C_t} \left\{ a - \frac{A_e}{\left[ d + a \frac{C_t}{C_v} \right]} \right\} A_e \quad (0.31)$$

$$GJ = \frac{C_t}{2 \left[ d + a \frac{C_t}{C_v} \right]} A_e^2 \quad (0.32)$$

$$K = \frac{B_t}{2 \left[ d + a \frac{C_t}{C_v} \right]} A_e^2 \quad (0.33)$$

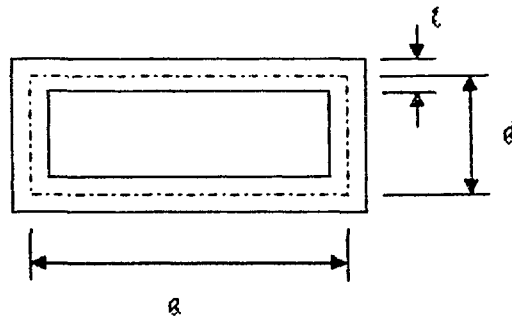


**Figure 3-5: Box beam with rectangular cross-section (Box-section)**

To differentiate the top and bottom panels from the side wall panels the subscripts  $t$  and  $v$  are used to represent top and sides, respectively. The inner area is denoted by  $A_e$ , variables  $d$  and  $a$  are, respectively, the depth and width of the box-section. These effective rigidities can then be used as the coefficients to the differential equations of motion governing the materially coupled bending-torsion vibration of composite wings analyzed in Chapters 4 and 5. The same equations will also be then extended to asymmetric airfoil cross-sections. A pre-processing program was developed in Matlab<sup>®</sup>

to calculate rigidity terms for various ply angles, laminates and cross-sectional configurations.

## **Chapter 4 Uniform Laminated Composite Wing Model**

### **4.1 Introduction**

In this chapter, the materially coupled bending-torsion vibration of laminated composite beam, based on an assembly of uniform beam elements, and using the Finite Element Method (FEM), Dynamic Stiffness Matrix (DSM) and Dynamic Finite Element (DFE) is presented. The DSM method is based on the exact solution to the governing differential equations of motion, as presented by Banerjee and Williams (1995). Therefore, for a uniform beam, the DSM needs only one element to achieve the exact natural frequencies. The DSM formulations can also be easily extended to approximate tapered geometry by using a piece-wise uniform stepped model. The FEM model is obtained using a Galerkin weighted residual method to formulate the element mass and stiffness matrices of the current uniform beam. In what follows, a Dynamic Finite Element method for the coupled vibration analysis of uniform and stepped composite beams is developed. The comparison is then made between the DFE results and those obtained from the FEM and DSM formulations in order to validate the proposed methodology.

### **4.2 Wing Model**

A cantilever composite beam with length  $L$  and a solid cross-section is the basis of the model (see Figure 4-1). All rigidities are assumed constant along  $y$  axis. The rigidities are: bending,  $EI$ , torsion,  $GJ$ , and coupled bending-torsion,  $K$ . The rigidities can be determined either experimentally or based on the theory presented in Chapter 3. The solid cross section is assumed to be symmetric with different fibre layer orientations (see Figure 4-1), where  $w$  is the translational displacement associated with bending and  $\psi$  is the rotational twist associated with torsion.

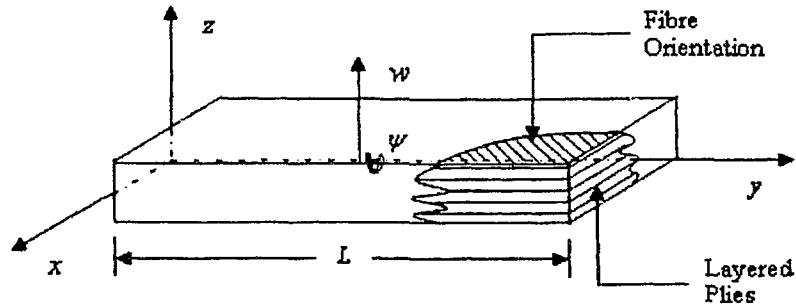


Figure 4-1: Composite Beam on a Right Handed Coordinate System.

### 4.3 Assumptions

The simplest model of a composite wing is represented by a uniform Euler-Bernoulli beam, where the bending slope is the derivative of the bending displacement with respect to the span-wise direction (Lilico *et al*, 1997). Shear deformation and rotary inertia are neglected by assuming a long slender beam. Further simplifications have been made by applying the St. Venant assumptions, which is a pure torsion state, and neglecting all warping effects. The beam is assumed to be composed of composite material with unidirectional fibre lay-up. With any composite, material couplings between extensional-twist and bending-twist arise from ply orientation and stacking sequence. This research will focus on the bending-twist couplings as the other coupling behaviours are being investigated by other researchers (see, for example, Roach and Hashemi, 2003).

### 4.4 DFE Formulation

The governing differential equations of motion for the materially coupled vibration of a uniform composite beam are (Banerjee, 1998):

$$EIw'''' + K\psi'''' + m\frac{\partial^2 w}{\partial t^2} = 0 \quad (0.34)$$

$$GJ\psi'''' + Kw'''' - I_\alpha\frac{\partial^2 \psi}{\partial t^2} = 0 \quad (0.35)$$

where  $w(y,t)$  denote the beam flexural displacement and  $\psi(y,t)$  is the torsion angle.  $EI$  and  $GJ$  denote flexural and torsion rigidities respectively,  $m$  is the mass per unit length and  $I_\alpha$  represents the polar mass moment of inertia per unit length of the wing. The material bend-twist coupling rigidity is represented by  $K$  and primes denote differentiation with respect to span wise position  $y$ . Based on the simple harmonic motion assumption, the following separation of variables is applied on the flexural and torsional displacements (sinusoidal variation with frequency  $\omega$ ).

$$\begin{aligned} w(y,t) &= w(y) \sin \omega t \\ \psi(y,t) &= \Psi(y) \sin \omega t \end{aligned} \quad (0.36)$$

Then with substitutions of (0.36) into (0.34) and (0.35), the differential equations can be re-written in the following form:

$$EIw'''' + K\Psi'''' - m\omega^2 w = 0 \quad (0.37)$$

$$GJ\Psi'''' + Kw'''' + I_\alpha\omega^2 \Psi = 0 \quad (0.38)$$

By implementing the Galerkin weighted residual method and integration by parts, the continuity requirements on the field variable are relaxed so that the integral weak form associated with equations (0.37) and (0.38) can then be obtained as:

$$\begin{aligned} W_f = \int_0^L [ &EI\delta w'' w'' + K\delta w'' \Psi'' - m\omega^2 \delta w w ] dy \\ &+ EI [\delta w w'' - \delta w' w']_0^L \\ &+ K [\delta w \Psi'' - \delta w \Psi']_0^L \end{aligned} \quad (0.39)$$

$$\begin{aligned}
W_i = \int_0^L [GJ \delta\Psi' \Psi' + K \delta\Psi' w'' + I_a \omega^2 \delta\Psi \Psi] dy \\
+ GJ [\delta\Psi \Psi']_0^L \\
+ K [\delta\Psi w'']_0^L
\end{aligned} \tag{0.40}$$

The above boundary terms can be associated with the Shear  $S(y)$ , Moment  $M(y)$ , and torque  $T(y)$  as:

$$S(y) = EI(y) \frac{\partial^3 w}{\partial x^3} + K(y) \frac{\partial^2 \Psi}{\partial x^2} \tag{0.41}$$

$$M(y) = -EI(y) \frac{\partial^2 w}{\partial y^2} - K(y) \frac{\partial^2 \Psi}{\partial y^2} \tag{0.42}$$

$$T(y) = GJ(y) \frac{\partial \Psi}{\partial y} + K(y) \frac{\partial^2 w}{\partial y^2} \tag{0.43}$$

Boundary conditions associated with clamped-free (cantilever) beam are  $w = w' = \Psi = 0$ , and all force boundary terms are zero at the tip ( $y=L$ ). The system is then discretized by 2-node 6-DOF beam elements (Figure 4-2).



Figure 4-2: A 2-node 6-DOF beam element

Principle of Virtual Work (PVW) is also satisfied such that:

$$W_T = W_1 + W_2 = W_{INT} - W_{EXT} = \sum_{k=1}^{NE} W^k - W_{EXT} = 0 \tag{0.44}$$

where,  $W^k$  represents element internal virtual work and  $W_{EXT} = 0$  for free vibrations. After two integrations by parts on the differential equation governing the flexural motion, the element internal virtual work can be written in the following form:

$$W^k = W_f^k(\xi) + W_t^k(\xi) \quad (0.45)$$

where,

$$\begin{aligned} W_f^k(\xi) = & \int_0^1 w \left[ \underbrace{\frac{EI}{l_k^3} \delta w^{(4)} - l_k m \omega^2 \delta w}_{(*)} \right] d\xi \\ & + \frac{EI}{l_k^3} [\delta w'' w' - \delta w''' w]_0^1 \\ & + \frac{K}{l_k^2} \int_0^1 \Psi' \delta w'' d\xi \end{aligned} \quad (0.46)$$

and,

$$\begin{aligned} W_t^k(\xi) = & \int_0^1 \Psi \left[ \underbrace{\frac{GJ}{l_k} \delta \Psi'' - l_k I_\alpha \omega^2 \delta \Psi}_{(**)} \right] d\xi \\ & + \frac{GJ}{l_k} [-\delta \Psi' \Psi]_0^1 \\ & - \frac{K}{l_k^2} \int_0^1 \delta \Psi' w'' d\xi \end{aligned} \quad (0.47)$$

The two above equations simply represent the bending and torsion contributions to the discretized internal virtual work for each element of length  $l_k$ .

The basis functions are then chosen based on the solutions to the differential equations of (\*) and (\*\*). For the first differential equation (0.46) pertaining to bending, the following process is applied to formulate the trigonometric shape functions according to Hashemi and Richard (1999). The torsion interpolation functions are also evaluated in a similar way.

#### 4.4.1 Frequency dependent trigonometric shape functions.

The non-nodal approximation for the flexural weighting function,  $\delta w(\xi)$ , and the field variable,  $w(\xi)$ , can be written as:

$$w(\xi) = \{P_f(\xi)\}^T \{a\} \quad (0.48)$$

Similarly for torsion:

$$\Psi(\xi) = \{P_t(\xi)\}^T \{b\} \quad (0.49)$$

where  $\delta w$ ,  $w$ ,  $\delta\Psi$ ,  $\Psi$  are discretized over a single element ( $0 \leq \xi \leq 1$ ). The basis functions of the approximation space are chosen as:

$$\{P_f(\xi)\}^T = \left[ \cos \alpha\xi \quad \frac{\sin \alpha\xi}{\alpha} \quad \frac{\cosh \alpha\xi - \cos \alpha\xi}{\alpha^2} \quad \frac{\sinh \alpha\xi - \sin \alpha\xi}{\alpha^3} \right] \quad (0.50)$$

and, for torsion as:

$$\{P_t(\xi)\}^T = \left[ \cos \gamma\xi \quad \frac{\sin \gamma\xi}{\gamma} \right] \quad (0.51)$$

where,

$$\alpha = \sqrt[4]{\frac{m\omega^2 L^4}{EI}} \quad (0.52)$$

$$\gamma = \sqrt{\frac{I_a \omega^2 l_k^2}{GJ}} \quad (0.53)$$

The basis functions are chosen as trigonometric terms based on the solution to the differential equations and were manipulated to reduce to Hermitian basis functions as

$\alpha \rightarrow 0$  and  $\gamma \rightarrow 0$ . It is important to note that Hermitian basis functions have been used in beam finite elements for many years, since they satisfy the “Completeness” and “Compatibility” requirements. “Completeness” is satisfied by including the lowest order admissible term. The compatibility condition is also satisfied. With these conditions satisfied, the DFE with its Hermitian based Dynamic Trigonometric Shape Functions (DTSF’s) is guaranteed to converge to the exact solution. Classical basis functions of the standard “Hermite” beam element are  $[1, \xi, \xi^2, \xi^3]$ . The bending and torsion trigonometric basis functions lead to standard cubic and linear ones by taking the limit as  $\alpha \rightarrow 0$  and  $\gamma \rightarrow 0$ , respectively. These variables are frequency dependent as seen above in equations (0.52) and (0.53). When the frequency approaches zero the DTSF’s reduce to polynomial basis functions which lead to satisfying the required conditions of compatibility and completeness.

For the first bending basis function:

$$\lim_{\alpha \rightarrow 0} \cos \alpha \xi = 1 \quad (0.54)$$

The second basis function leads to:

$$\lim_{\alpha \rightarrow 0} \frac{\sin \alpha \xi}{\alpha} = \xi \quad (0.55)$$

The third basis function leads to:

$$\lim_{\alpha \rightarrow 0} \frac{\cosh \alpha \xi - \cos \alpha \xi}{\alpha^2} = \xi^2 \quad (0.56)$$

The fourth basis function leads to:

$$\lim_{\alpha \rightarrow 0} \frac{\sinh \alpha \xi - \sin \alpha \xi}{\alpha^3} = \frac{\xi^3}{3} \quad (0.57)$$

The coefficients  $\langle \delta a \rangle$ ,  $\langle a \rangle$ ,  $\langle \delta b \rangle$ , and  $\langle b \rangle$  have no physical meaning and can be replaced by nodal variables for bending  $\langle \delta w_1, \delta w_1', \delta w_2, \delta w_2' \rangle$  and  $\langle w_1, w_1', w_2, w_2' \rangle$  and for torsion  $\langle \delta \Psi_1, \delta \Psi_2 \rangle$  and  $\langle \Psi_1, \Psi_2 \rangle$ . The derivation of bending shape functions are only considered in the following procedure, since, the torsion shape functions will follow the same development. Following the same systematic method as in FEM, one can write:

$$\{\delta w_n\} = [P_n]\{\delta a\} \quad (0.58)$$

$$\{w_n\} = [P_n]\{a\} \quad (0.59)$$

Then,

$$[P_{n_f}] = \begin{bmatrix} 1 & 0 & 0 & 0 \\ 0 & 1 & 0 & 0 \\ \cos(\alpha) & \frac{\sin(\alpha)}{\alpha} & \frac{\cosh(\alpha) - \cos(\alpha)}{\alpha^2} & \frac{\sinh(\alpha) - \sin(\alpha)}{\alpha^3} \\ -\alpha \sin(\alpha) & \cos(\alpha) & \frac{\alpha \sinh(\alpha) + \alpha \sin(\alpha)}{\alpha^2} & \frac{\alpha \cosh(\alpha) - \cos(\alpha)}{\alpha^3} \end{bmatrix} \quad (0.60)$$

The nodal approximations for element variables  $w(\xi)$  and  $\Psi(\xi)$  can then be rewritten as:

$$\delta w(\xi) = \{P_f(\xi)\}^T [P_{n_f}]^{-1} \{\delta w_n\} = \{N(\xi, \omega)\}^T \{\delta w_n\} \quad (0.61)$$

$$w(\xi) = \{P_f(\xi)\}^T [P_{n_f}]^{-1} \{w_n\} = \{N(\xi, \omega)\}^T \{w_n\} \quad (0.62)$$

Then,

$$\begin{aligned}
w(\xi) &= \{P_f(\xi)\}^T [P_n]_f^{-1} \{W_n\} = \{N(\xi)_f\}^T \{w\} \\
\Psi(\xi) &= \{P_f(\xi)\}^T [P_n]_f^{-1} \{\Psi_n\} = \{N(\xi)_f\}^T \{\Psi\}
\end{aligned}
\tag{0.63}$$

Expressions (0.63) can then be rearranged as:  $[w(\xi) \Psi(\xi)]^T = [N]\{u_n\}$ , where  $\{u_n\} = \langle w_1 \ w'_1 \ \Psi_1 \ w_2 \ w'_2 \ \Psi_2 \rangle^T$  is the element displacements (i.e., degrees of freedom) and  $[N]$  represents the dynamic shape functions in matrix form

$$[N] = \begin{Bmatrix} N(\xi, \omega)_f \\ N(\xi, \omega)_f \end{Bmatrix} = \begin{bmatrix} N_1(\xi, \omega)_f & N_2(\xi, \omega)_f & 0 & N_3(\xi, \omega)_f & N_4(\xi, \omega)_f & 0 \\ 0 & 0 & N_1(\xi, \omega)_f & 0 & 0 & N_2(\xi, \omega)_f \end{bmatrix}
\tag{0.64}$$

The four trigonometric shape functions pertaining to bending are (Hashemi and Richard 1999; Hashemi, 1998):

$$N_1 = \{ \cosh(\alpha) \cos(\alpha\xi - \alpha) - \cos(\alpha\xi) + \cos(\alpha) \cosh(\alpha\xi - \alpha) - \cosh(\alpha\xi) - \sin(\alpha) \sinh(\alpha\xi - \alpha) + \sinh(\alpha) \sin(\alpha\xi - \alpha) \} / \text{DEN}
\tag{0.65}$$

$$N_2 = \frac{1}{\alpha} \{ \cosh(\alpha) \sin(\alpha\xi - \alpha) - \sin(\alpha\xi) + \sin(\alpha) \cosh(\alpha\xi - \alpha) + \cos(\alpha) \sinh(\alpha\xi - \alpha) + \sinh(\alpha) \cos(\alpha\xi - \alpha) - \sinh(\alpha\xi) \} / \text{DEN}
\tag{0.66}$$

$$N_3 = \{ -\cosh(\alpha\xi - \alpha) + \cosh(\alpha\xi) \cos(\alpha) + \cos(\alpha\xi) \cosh(\alpha) - \cos(\alpha\xi - \alpha) + \sinh(\alpha\xi) \sin(\alpha) - \sin(\alpha\xi) \sinh(\alpha) \} / \text{DEN}
\tag{0.67}$$

$$N_4 = \frac{1}{\alpha} \{ -\sinh(\alpha\xi - \alpha) - \cosh(\alpha\xi) \sin(\alpha) - \cos(\alpha\xi) \sinh(\alpha) - \sin(\alpha\xi - \alpha) + \sinh(\alpha\xi) \cos(\alpha) + \sin(\alpha\xi) \cosh(\alpha) \} / \text{DEN}
\tag{0.68}$$

$$\text{DEN} = (2 \cosh(\alpha) \cos(\alpha) - 2)
\tag{0.69}$$

For torsion:

$$N_{r,1} = \frac{\sin \gamma(1-\xi)}{\sin \gamma} \quad (0.70)$$

$$N_{r,2} = \frac{\sin \gamma \xi}{\sin \gamma} \quad (0.71)$$

The six shape functions are plotted individually for first four natural frequencies of free coupled vibration of a uniform composite wing (see Figures 4-3 through 4-8). These shape functions are the approximations to the solution of the governing differential equations of motion.

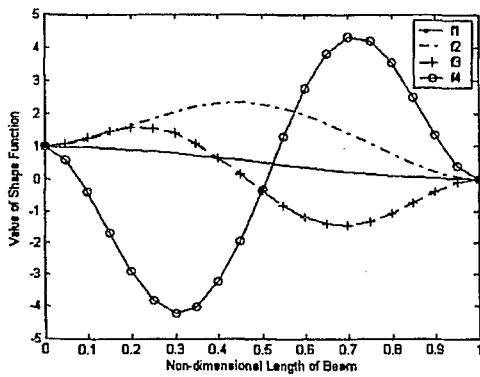


Figure 4-3: First flexural shape function plotted for the first 4 natural frequencies of a uniform beam

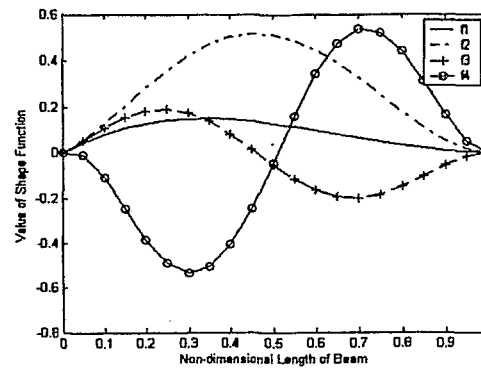


Figure 4-4: Second flexural shape function plotted for the first 4 natural frequencies of a uniform beam.

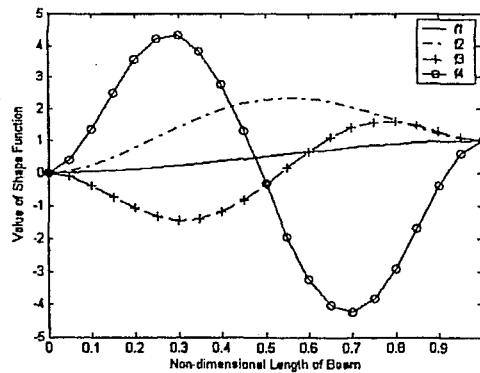


Figure 4-5: Third flexural shape function plotted for the first 4 natural frequencies of a uniform beam.

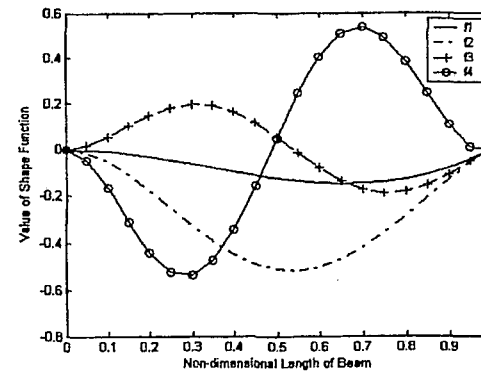
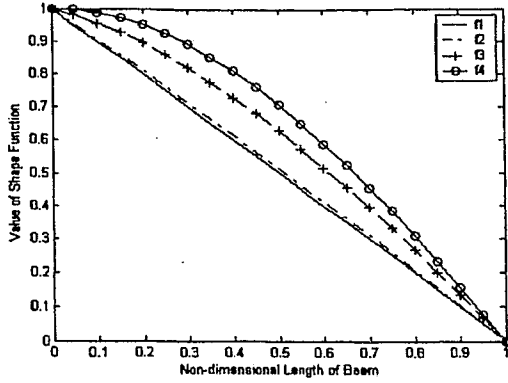
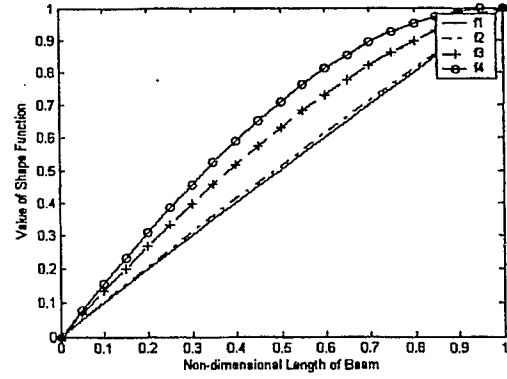


Figure 4-6: Fourth flexural shape function plotted for the first 4 natural frequencies of a uniform beam



**Figure 4-7: First torsional shape function plotted for the first 4 natural frequencies of a uniform beam.**



**Figure 4-8: Second torsional shape function plotted for the first 4 natural frequencies of a uniform beam.**

The above shape function plots display the inter-element continuity required to satisfy the compatibility condition. With the frequency dependent trigonometric shape functions determined, the dynamic finite element matrix can be constructed from equations (0.46) and (0.47). The DFE matrix can be expressed in two matrices as:

$$K_{DFE} = K_{UNCOUPLED} + K_{COUPLED} \quad (0.72)$$

The uncoupled matrix is obtained from the boundary term expressions extracted from the integration by parts. The coupled matrix is formulated from the integral expressions representing the coupling terms in both equations (0.46) and (0.47). The symmetry of coupled matrix can be seen in the equivalence in both integral expressions.

$$K_{UNCOUPLED} = \begin{bmatrix} \frac{EI}{l_k^3} \{N_1'''\}_0 & \frac{EI}{l_k^3} \{-N_1''\}_0 & 0 & \frac{EI}{l_k^3} \{-N_1'''\}_1 & \frac{EI}{l_k^3} \{N_1''\}_1 & 0 \\ \frac{EI}{l_k^3} \{N_2'''\}_0 & \frac{EI}{l_k^3} \{-N_2''\}_0 & 0 & \frac{EI}{l_k^3} \{-N_2'''\}_1 & \frac{EI}{l_k^3} \{N_2''\}_1 & 0 \\ 0 & 0 & \frac{GJ}{l_k} \{-N_{t1}'\}_0 & 0 & 0 & \frac{GJ}{l_k} \{N_{t1}'\}_1 \\ \frac{EI}{l_k^3} \{N_3'''\}_0 & \frac{EI}{l_k^3} \{-N_3''\}_0 & 0 & \frac{EI}{l_k^3} \{-N_3'''\}_1 & \frac{EI}{l_k^3} \{N_3''\}_1 & 0 \\ \frac{EI}{l_k^3} \{N_4'''\}_0 & \frac{EI}{l_k^3} \{-N_4''\}_0 & 0 & \frac{EI}{l_k^3} \{-N_4'''\}_1 & \frac{EI}{l_k^3} \{N_4''\}_1 & 0 \\ 0 & 0 & \frac{GJ}{l_k} \{-N_{t2}'\}_0 & 0 & 0 & \frac{GJ}{l_k} \{N_{t2}'\}_1 \end{bmatrix} \quad (0.73)$$

$$K_{COUPLED} = \int_0^l \frac{K}{l_k^2} \begin{bmatrix} 0 & 0 & \{N_1''N_{i1}\} & 0 & 0 & \{N_1''N_{i2}\} \\ 0 & 0 & \{N_2''N_{i1}\} & 0 & 0 & \{N_2''N_{i2}\} \\ \{N_1''N_{i1}\} & \{N_2''N_{i1}\} & 0 & \{N_3''N_{i1}\} & \{N_4''N_{i1}\} & 0 \\ 0 & 0 & \{N_3''N_{i1}\} & 0 & 0 & \{N_3''N_{i2}\} \\ 0 & 0 & \{N_4''N_{i1}\} & 0 & 0 & \{N_4''N_{i2}\} \\ \{N_1''N_{i2}\} & \{N_2''N_{i2}\} & 0 & \{N_3''N_{i2}\} & \{N_4''N_{i2}\} & 0 \end{bmatrix} d\xi \quad (0.74)$$

$K_{DFE}$  represents the dynamic finite element matrix which is now ready for assembly in the usual finite element way. The coupled matrix is integrated symbolically to ensure the final dynamic finite element matrix is purely algebraic. With all expressions in the DFE matrix symbolically computed, there is no need for a numerical integration which decreases the required computational time. The symbolic integrations for the coupled matrix in equation (0.74) are carried using MAPLE©.

## 4.5 Numerical Results

Here the coupled vibrations of the composite wing configurations are considered. First, a uniform glass/epoxy wing beam model is analyzed. The second example represents a stepped piece-wise uniform cantilever composite beam. The natural frequencies and modes of vibration are studied. The DFE results are compared with those obtained from DSM and FEM approaches.

### 4.5.1 Free vibration of a uniform beam

The beam is composed of glass/epoxy composite material and made up of unidirectional plies with fibre angles in each ply set to  $+15^\circ$ . The beam can be considered equivalent to a single thick ply (Banerjee and Williams, 1995) with a thickness of 3.18 mm and width of 12.7 mm. The material and geometric properties determined by Banerjee (1998), Banerjee and Williams (1996) and Banerjee and Williams (1995). The principle rigidities are experimentally found by Teh and Huang (1980) displayed in Table 4-1 and the effective rigidities are:

Effective bending rigidity,  $EI = 0.2865 \text{ Nm}^2$ ;  
Torsion rigidity,  $GJ = 0.1891 \text{ Nm}^2$ ;  
Bending-torsion coupling rigidity,  $K = 0.1143 \text{ Nm}^2$ ;  
Mass per unit length,  $m = 0.0544 \text{ kg/m}$ ;  
Mass moment of inertia per unit length,  $I_{\omega} = 7.77 \times 10^{-7} \text{ kg.m}$   
Length of the beam,  $L = 0.1905 \text{ m}$ .

**Table 4-1: Material Properties of a glass/epoxy Laminate**

$E_L$	9.71 GPa
$E_T$	3.25 GPa
$G_{LT}$	0.9025 GPa
$\nu_{LT}$	0.29
Thickness	3.18 mm

The variations of bending rigidity,  $EI$ , torsion rigidity,  $GJ$ , and bending-torsion coupled stiffness,  $K$ , as functions of different ply angles displayed in Figure 4-9. This plot is particularly important for optimization since a wing composed of fibre-reinforced composite material can be designed for any desired stiffness and corresponding frequency response. A greater flexibility is available with composites which is not necessarily restricted to the plot shown in Figure 4-9: Plot of Rigidities vs Ply angle for a glass/epoxy composite. Different stacking sequences and ply thickness lead to a much greater domain of possible stiffness properties. Different stacking configurations will be considered in Chapter 5.

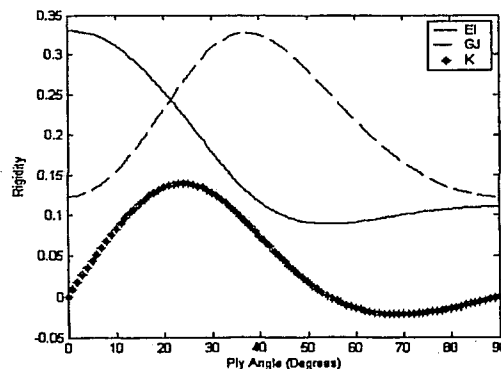


**Figure 4-9: Plot of Rigidities vs Ply angle for a glass/epoxy composite.**

The convergence results for the 1<sup>st</sup> four natural frequencies of a uniform glass/epoxy composite beam are presented in Figure 4-10 and the corresponding modes are found in the following Figure 4-10. It is observed that the DFE and the FEM converge nearly at the same rate for the first three natural frequencies. The DFE converges faster than the FEM for the fourth natural frequency (refer to Figure 4-10). This higher convergence rate can be attributed to the mode behaviour at this natural frequency. The fourth natural frequency is predominately torsion (refer to Figure 4-11 (d)). It has been observed that torsion plays a more important role at higher frequencies and the DFE converges significantly faster than the FEM as the frequency number is increased (Borneman and Hashemi, 2003).

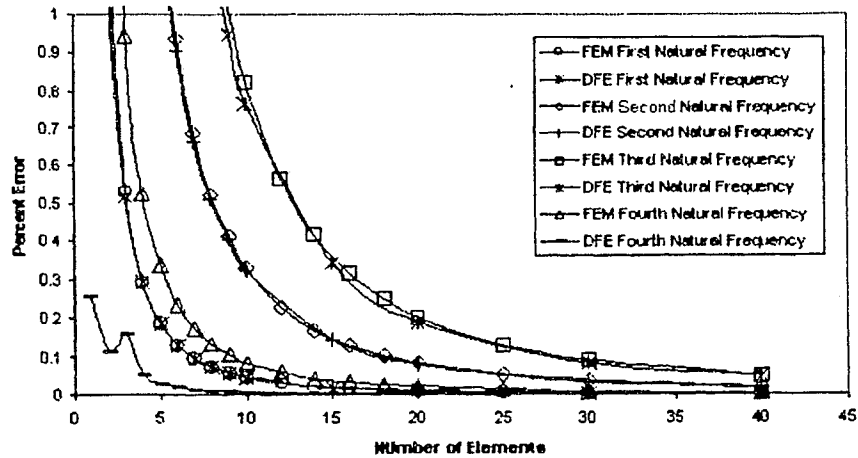
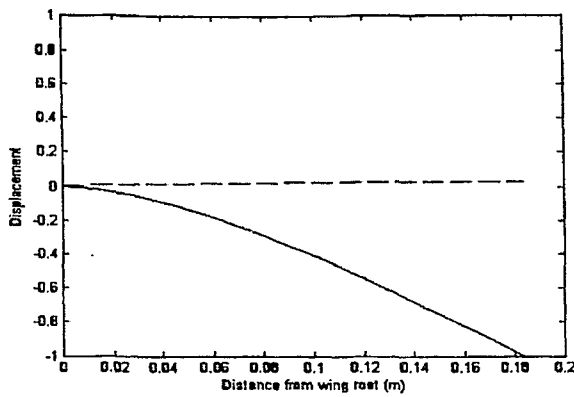
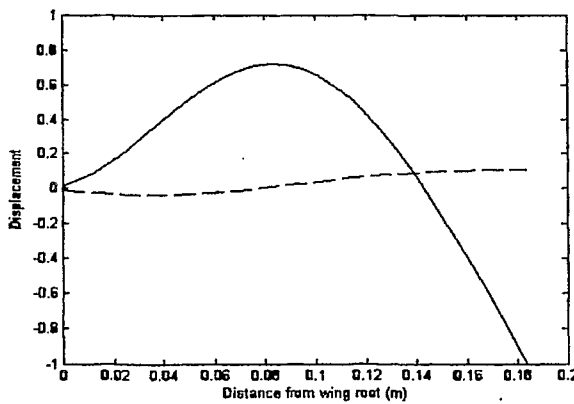
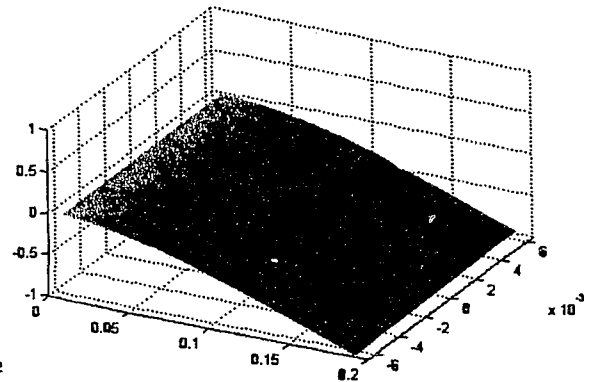


**Figure 4-10: Convergence of DFE and FEM for the first four natural frequencies of a uniform composite wing. Percent Error is relative to the exact values obtained from the DSM (Banerjee and Williams, 1995).**

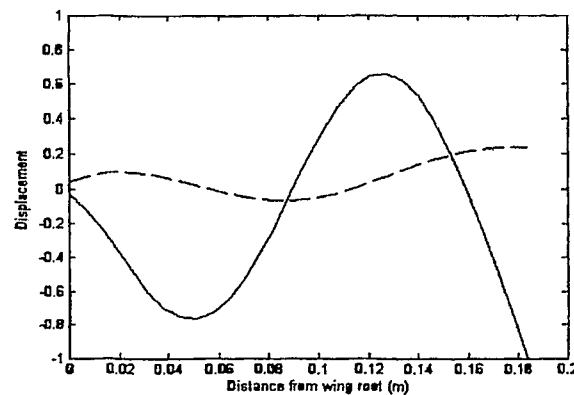
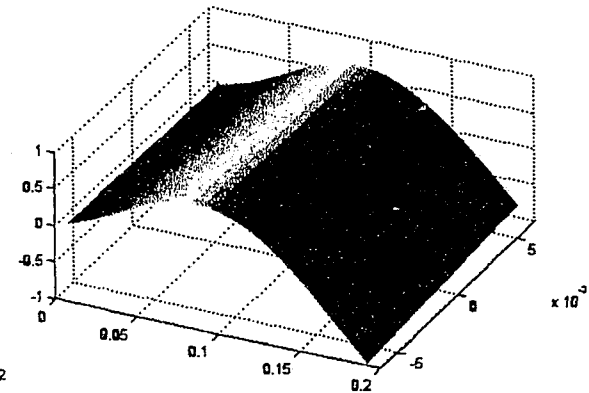
The two and three dimensional modes of deformation are also plotted in 4-11 (a)-(d) to give a visual representation of the behaviour of the wing when vibrating at the first four natural frequencies. All modes both 2D and 3-D have been normalized to properly distinguish the modes as bending, torsion or bending-torsion. Numerical values of the first five natural frequencies using various methods are presented in Table 4-2.



(a)



(b)



(c)

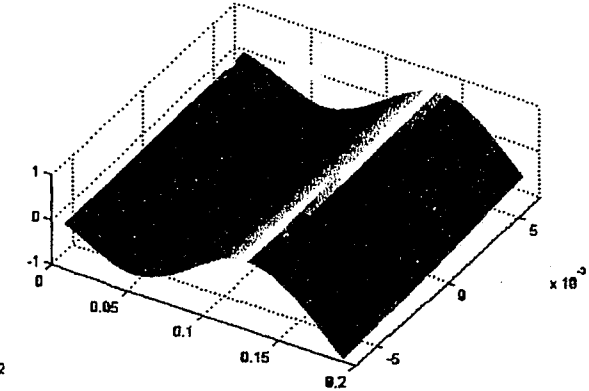


**Figure 4-11: Natural modes of free vibration for a coupled bending-torsion uniform composite beam. (a) First Natural mode; (b) 2<sup>nd</sup> Natural mode; (c) 3<sup>rd</sup> Natural mode; Each 2D mode displacement due to torsion is represented by a dashed (--) line and bending is represented by a solid (-) line.**

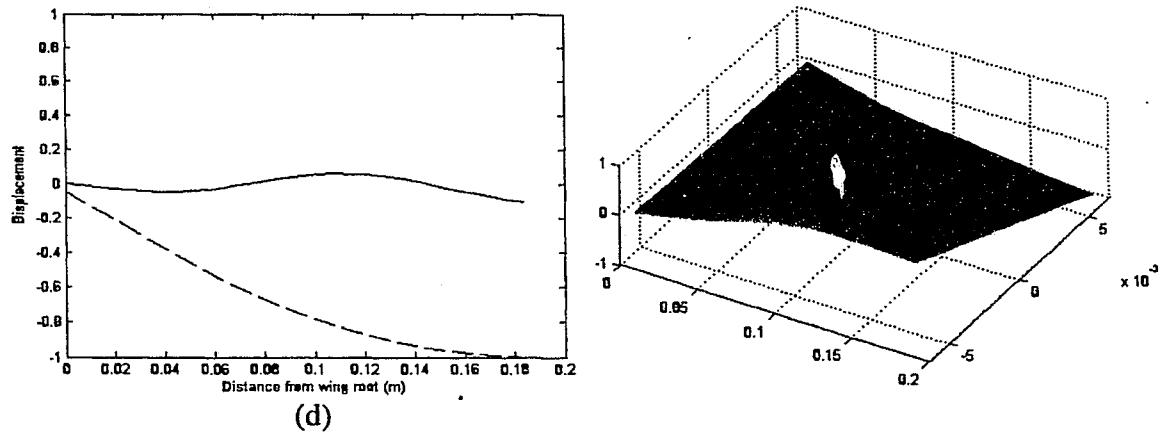


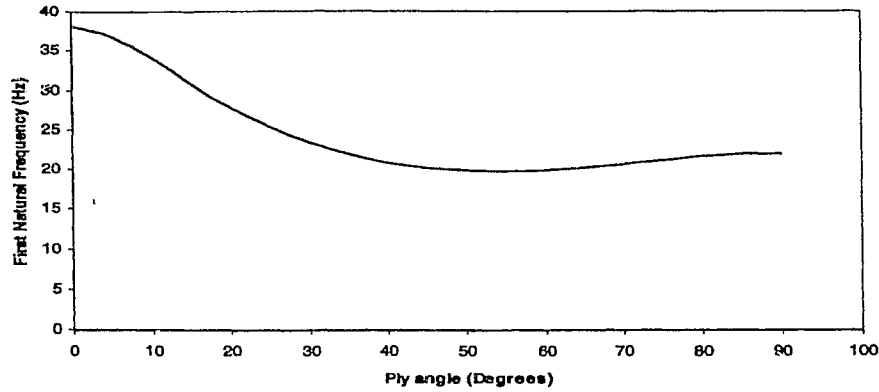
Figure 4-12: Natural modes of free vibration for a coupled bending-torsion uniform composite beam. (d) 4<sup>th</sup> Natural mode. Each 2D mode displacement due to torsion is represented by a dashed (--) line and bending is represented by a solid (-) line.

Table 4-2: Numerical values of the first five natural frequencies (Hz) using various methods are presented. 'B' denotes a predominant bending mode and 'T' denotes a predominant torsion mode.

Natural Frequencies of a Uniform Composite Beam 15° lay-up (Hz)			
Natural Frequency	FEM 20 Using Elements	DFE Using 20 Elements	DSM 1 Element (Exact)
1 <sup>st</sup>	30.82	30.82 B	30.82
2 <sup>nd</sup>	192.87	192.87 B	192.72
3 <sup>rd</sup>	538.47	538.42 B	537.38
4 <sup>th</sup>	648.87	648.74 T	648.73
5 <sup>th</sup>	1053.87	1053.46 B	1049.73

The exact results for the DSM are confirmed by the earlier works published by Banerjee (1998), Banerjee and Williams (1996), Banerjee and Williams (1995) for the first four natural frequencies.

Figures 4-12 to 4-16 display the variations of natural frequencies for a uniform beam over a range of ply angles. These figures are particularly useful for a quick reference of the ply angle for a desired frequency response. The uniform beam is composed of glass/epoxy composite material with the same dimensions as the first uniform model described in section 4.5.



**Figure 4-13: Variations in the first natural frequency for different ply orientations**

From Figure 4-13 it is observed that the first natural frequency starts at its highest point at zero degrees. The natural frequency then decreases and levels out to a constant value at approximately 50 degrees. Similar trends in the second natural frequency are observed where the natural frequency levels at approximately 45 degrees ply orientation in Figure 4-14.

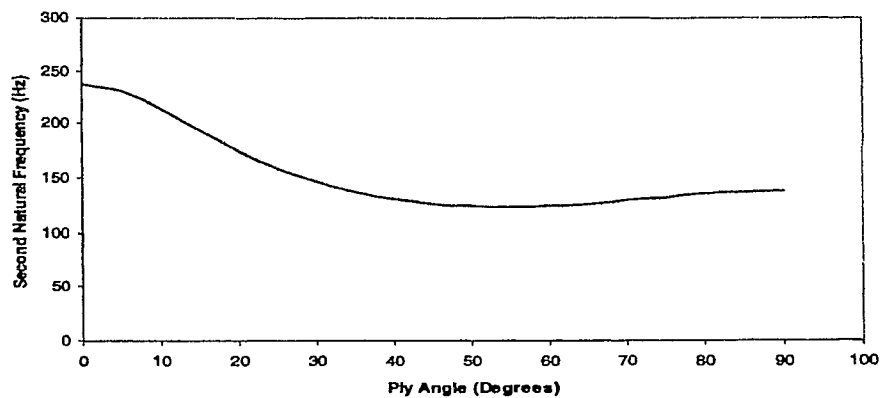


**Figure 4-14: Variations in the second natural frequency for different ply orientations**

The third natural frequency (Figure 4-15) again levels at nearly 50 degrees much like the first mode but an additional increase exists at the initial range from 0-12 degrees. The differences associated with variations in frequency can be attributed to the stronger influence of torsion on the higher modes of materially coupled vibration. This is observed especially in the fourth mode of vibration (Figure 4-16). The fourth mode displays

predominance in torsion (refer to the mode shape from Figure 4-11 (d)). Figure 4-16 deviates from the original trends found in the first two modes with greater fluctuations in frequency with different ply lay-ups

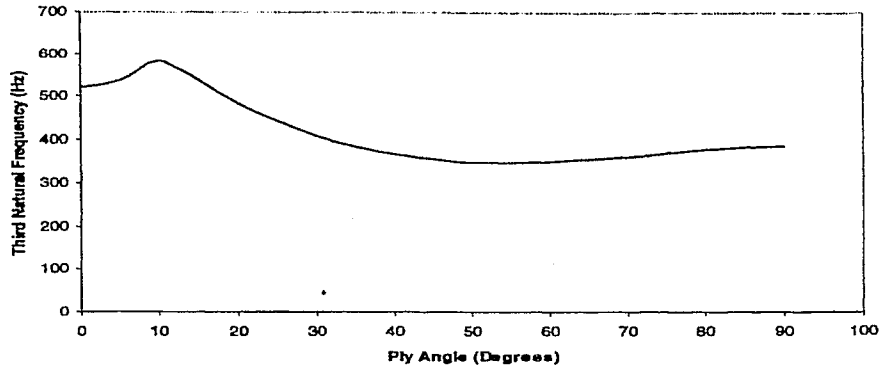


**Figure 4-15: Variations in the third natural frequency for different ply orientations**

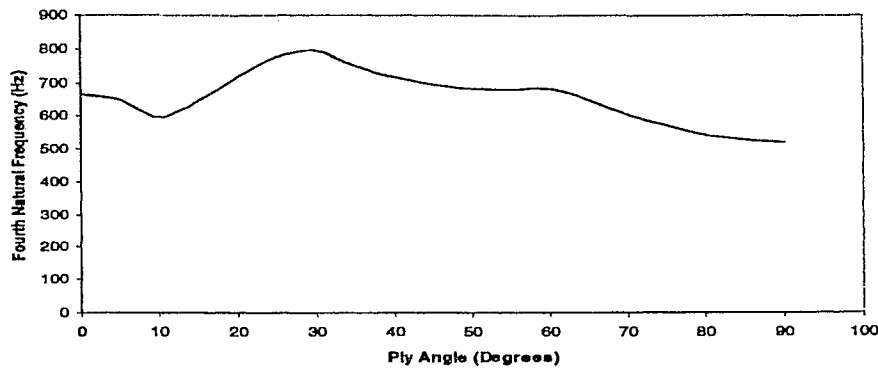


**Figure 4-16: Variations in the fourth natural frequency for different ply orientations**

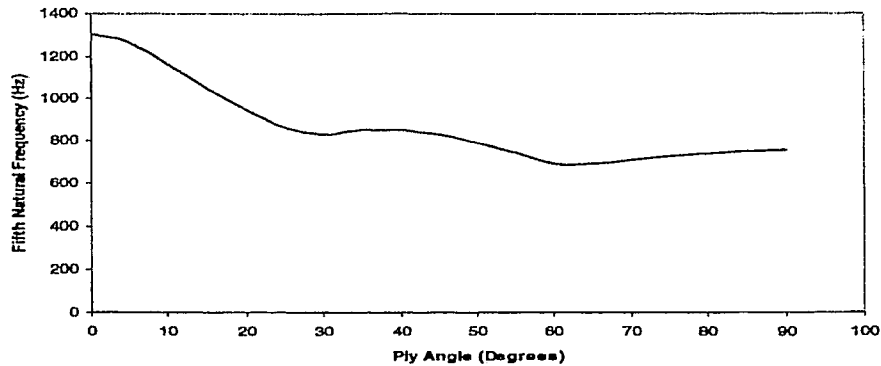


**Figure 4-17: Variations in the fifth natural frequency for different ply orientations**

The fifth natural frequency in Figure 4-17 returns to the original trend found in the first two predominantly bending modes of vibration (refer to Table 4-2). By extending the results to the fifth mode a correlation is observed between the influence of torsion and the fluctuations in frequency with ply orientation.

### 4.5.2 Numerical example for a step beam

More complex geometries such as tapered wings are usually constructed using piecewise uniform steps. The convergence results for a step beam constructed with three steps can be found in Figure 4-17 and Figure 4-18. The beam rigidities at its root ( $EI, GJ, K$ ) are identical to those of the previous uniform composite beam example and each step has the length of  $L/3$ . The second and third steps have the rigidity parameters equal to two-thirds and one-third of those for the root, respectively.

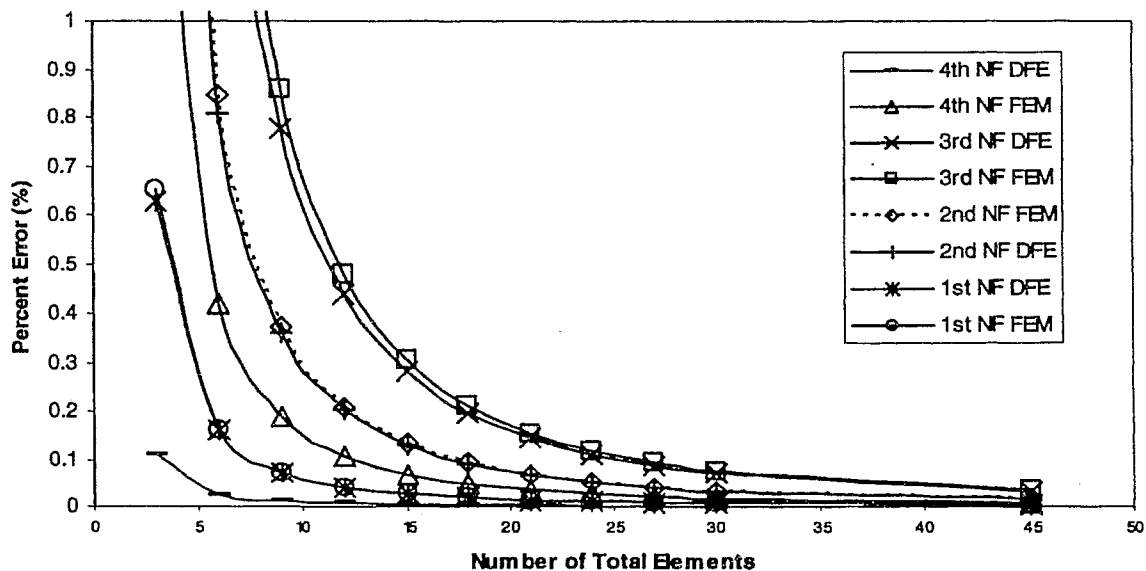


Figure 4-18: Convergence for a step beam formed from three steps using the FEM and DFE for the first 4 natural frequencies. 'NF' represents Natural Frequency.

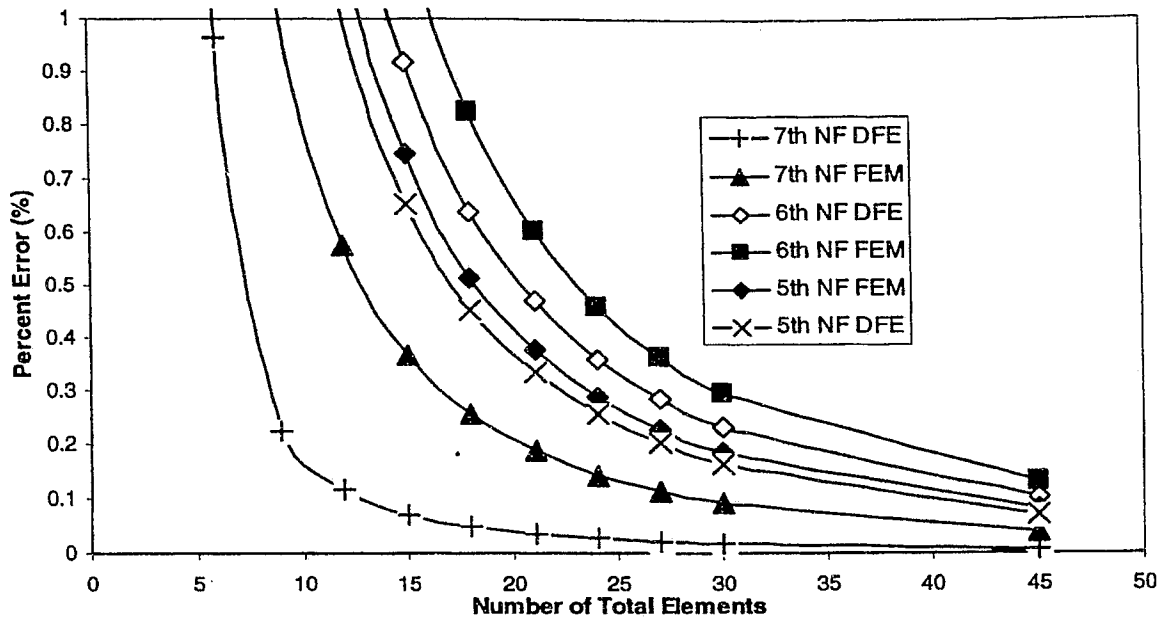


Figure 4-19: Convergence for a step beam formed from three steps using the FEM and DFE for the 5<sup>th</sup>, 6<sup>th</sup>, 7<sup>th</sup> natural frequencies.

The percent error in Figures 4-17 and 4-18 is calculated based on the exact values obtained using the DSM method. The first three natural frequencies converged at nearly the same rate as the FEM (see also Borneman and Hashemi, 2003). It is observed from Figures 4-17 and 4-18 that the DFE converges quicker than the FEM for higher frequencies. If a tapered formulation was used it would include the addition of deviator terms to compensate for the constant parameters assumed over each element. That would increase the convergence rates, and is the factor which distinguishes DFE from DSM method.

#### 4.6 Conclusions

The DFE displays significantly better convergence than the FEM for higher modes in the cases of the uniform and stepped composite beam. The modes of materially coupled vibration have been classified based on predominance of either bending or torsion and correlations have been drawn based on the higher influence of twist on particular

frequencies. Given the fact that the DFE approach is based on a general FEM type formulation the method can be easily extended to more complex element geometries such as tapered elements which will be covered in Chapter 5.

## Chapter 5 Tapered Wing Model

### 5.1 Introduction

A Dynamic Finite Element (DFE) formulation for the free vibration analysis of materially coupled uniform composite beam elements was developed in the previous chapter. In the present chapter, the DFE matrix for a generally tapered beam element is presented using frequency dependent trigonometric shape functions found in chapter 4. A homogeneous analysis of aircraft wings, rudders, helicopter blades, rotors, has been prepared using tapered beam elements for an accurate formulation of the frequency response. Tapered beams have been studied by various authors using the DSM (Banerjee and Williams, 1985) and the DFE (Hashemi and Richard, 1999 and Hashemi, 1998). The DSM and FEM approximate a taper using uniform steps as seen in the section 4.5.2. The proposed DFE uses steps also; however, the addition of refining terms known as deviator terms alters the formulation to better represent a taper geometry. The deviators will be discussed in more depth in the DFE formulation (see also Borneman and Hashemi (2003) and Hashemi and Borneman (2004)).

### 5.2 Wing Model

A simplified beam representation for a tapered composite wing of length  $L$  and solid rectangular cross section is illustrated in Figure 5-1. Bending-torsion material coupling behaviour usually present in composite material is due to the unbalanced lay up. The beam model is characterized by bending rigidity  $EI$ , torsion rigidity  $GJ$ , and coupled bending-torsion rigidity,  $K$ . Here, a symmetric laminate configuration is considered that consists of fibre orientations and thickness which are symmetric across the mid-plane of the laminate. Symmetric laminates result in bending-torsion couplings. The rigidities can be determined using classical laminate theory presented by Jones (1998), Berthelot

(1999) and Banerjee (1998). The beam element considered consists of 3 DOF per node; bending displacement, bending slope and torsion angle, which results in a final 6 x 6 element matrix (refer to Figure 4-2). The bending displacement is denoted by  $w(x,t)$  and torsion twist denoted by  $\psi(x,t)$ , where  $x$  is the distance spanning the beam and  $l_k$  is the element length.

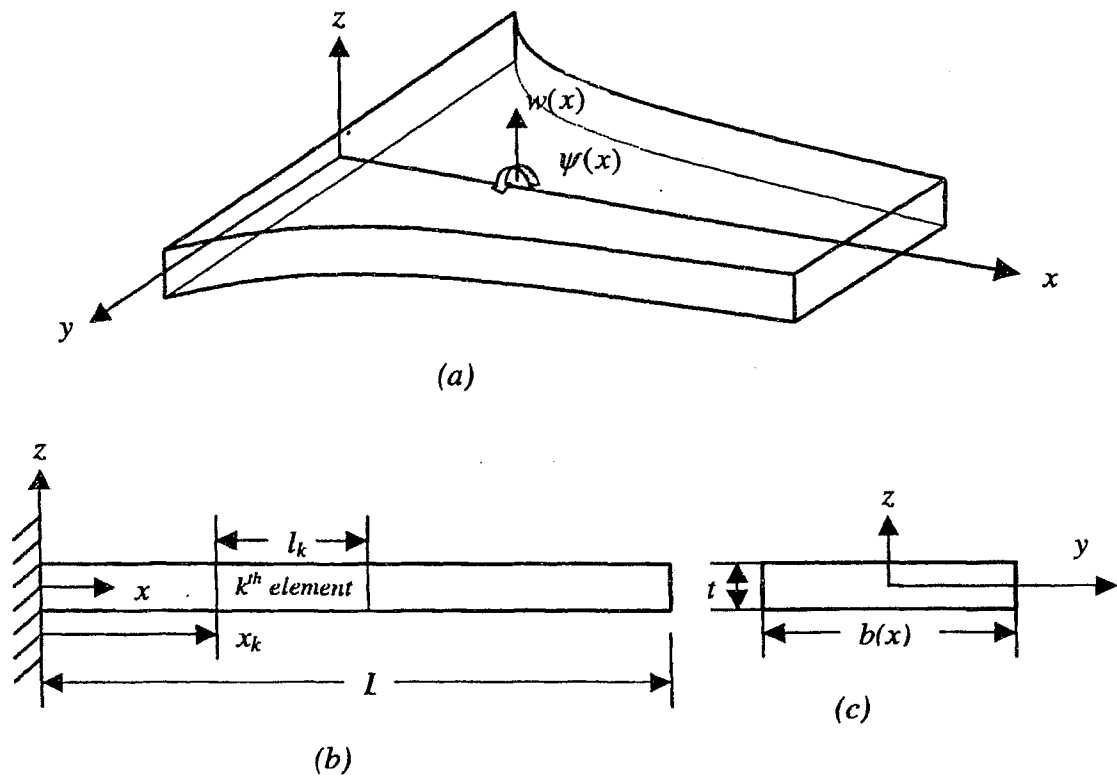


Figure 5-1: (a) Tapered beam in Global  $(x, y, z)$  coordinate system. (b) Side view in  $(x, z)$  plane. (c) Beam cross-section.

### 5.3 Assumptions

A constant thickness general taper is first considered (i.e., the beam does not taper by thickness of the multilayer composite). The mechanical and geometric properties can change with a contracting base. Next, the thickness will be changed along the span-wise

direction by stepping the thickness. Due to feasibility reasons in design, the thickness must be stepped by multiples of layer reduction. The constitutive relationship between stresses and strains is applied using classical laminate theory presented in Chapter 2. The Euler-Bernoulli bending and St. Venant torsion beam theories are employed. Shear deformation, rotary inertia and warping effects are neglected.

The variations in beam's mechanical and geometric properties can be considered as (Banerjee and Williams, 1985):

$$b(x) = b_r \left(1 + c \frac{x}{L}\right)^n \quad (5.1a) \quad GJ(x) = GJ_r \left(1 + c \frac{x}{L}\right)^{n+2} \quad (5.1c)$$

$$A(x) = A_r \left(1 + c \frac{x}{L}\right)^n \quad (5.1b) \quad EI(x) = EI_r \left(1 + c \frac{x}{L}\right)^{n+2} \quad (5.1d)$$

$$I_\alpha(x) = \rho A(x) \frac{1}{12} (h^2 + b(x)^2) \quad (5.1e) \quad K(x) = K_r \left(1 + c \frac{x}{L}\right)^{n+2} \quad (5.1f)$$

where  $b_r, A_r, I_\alpha, GJ_r, EI_r$  and  $K_r$  are, respectively, reference beam model's width, cross-sectional area, mass moment of inertia, torsion rigidity, bending rigidity and coupled bending torsion rigidity and are usually taken at the wing root. The constant 'c' must be greater -1 to ensure the beam does not taper to zero before the end of the beam.  $n$  is usually 1 or 2 depending on the degree of taper.

## 5.4 DFE Formulation

The differential equations governing the free vibrations of a materially coupled laminated composite beam, incorporating variable properties are (Weisshaar, 1980):

$$\frac{\partial^2}{\partial x^2} \left( EI(x) \frac{\partial^2 w}{\partial x^2} \right) + \frac{\partial^2}{\partial x^2} \left( K(x) \frac{\partial \psi}{\partial x} \right) + m(x) \frac{\partial^2 w}{\partial t^2} = 0 \quad (5.2)$$

$$\frac{\partial}{\partial x} \left( GJ(x) \frac{\partial \psi}{\partial x} \right) + \frac{\partial}{\partial x} \left( K(x) \frac{\partial^2 w}{\partial x^2} \right) - I_\alpha \frac{\partial^2 \psi}{\partial t^2} = 0 \quad (5.3)$$

The displacements can be assumed to have a sinusoidal variation with frequency  $\omega$  as:

$$\begin{aligned} w(x, t) &= w(x) \sin \omega t \\ \psi(x, t) &= \Psi(x) \sin \omega t \end{aligned} \quad (5.4)$$

The sinusoidal variations from (5.4) can be substituted into equation (5.2) and (5.3) so that the governing equations of motion can be re-written as solely x dependent

$$\frac{\partial^2}{\partial x^2} \left( EI(x) \frac{\partial^2 w}{\partial x^2} \right) + \frac{\partial^2}{\partial x^2} \left( K(x) \frac{\partial \Psi}{\partial x} \right) - m(x) w \omega^2 = 0 \quad (5.5)$$

$$\frac{\partial}{\partial x} \left( GJ(x) \frac{\partial \Psi}{\partial x} \right) + \frac{\partial}{\partial x} \left( K(x) \frac{\partial^2 w}{\partial x^2} \right) + I_\alpha(x) \Psi \omega^2 = 0 \quad (5.6)$$

The weighted residual method is employed and the integral form is altered to the weak form after two integrations by parts for the flexural portion and one integration by parts for the twisting portion. By re-writing the virtual work expression the inter-element continuity requirements are relaxed so that the approximation space for  $w$  is  $C^1$ .

$$\begin{aligned} W_f &= \int_0^L \left( EI(x) \delta w'' w'' + K(x) \delta w'' \Psi' - m(x) \omega^2 \delta w w \right) dx \\ &+ \left[ (EI(x) w'' + K(x) \Psi')' \delta w \right]_0^L - \left[ (EI(x) w'' + K(x) \Psi') \delta w' \right]_0^L \end{aligned} \quad (5.7)$$

$$\begin{aligned} W_t &= \int_0^L \left[ -GJ(x) \delta \Psi' \Psi' - K(x) \delta \Psi' w'' + I_\alpha(x) \omega^2 \delta \Psi \Psi \right] dx \\ &+ GJ(x) [\delta \Psi \Psi']_0^L + K(x) [\delta \Psi w'']_0^L \end{aligned} \quad (5.8)$$

The resultant shear force,  $S(x)$ , bending moment,  $M(x)$ , and torsional moment,  $T(x)$ , are based on the sign convention in Figure 5-2:

$$S(x) = \frac{\partial}{\partial x} \left( EI(x) \frac{\partial^2 w}{\partial x^2} + K(x) \frac{\partial \Psi}{\partial x} \right) \quad (5.9a)$$

$$M(x) = -EI(x) \frac{\partial^2 w}{\partial x^2} - K(x) \frac{\partial \Psi}{\partial x} \quad (5.9b)$$

$$T(x) = GJ(x) \frac{\partial \Psi}{\partial x} + K(x) \frac{\partial^2 w}{\partial x^2} \quad (5.9c)$$

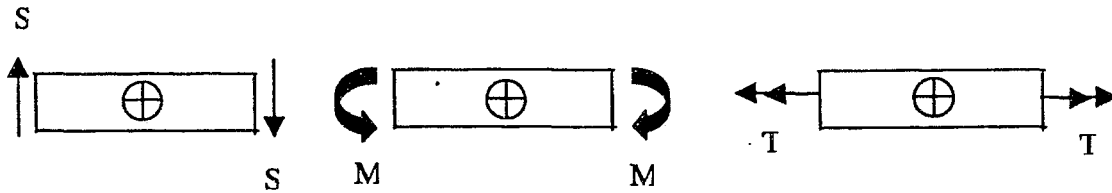


Figure 5-2 Sign Convention, where  $S$  denotes the transverse force,  $M$  denotes the bending moment and  $T$  denotes the torque

Boundary conditions associated to clamped-free (cantilever) structure are such that all virtual displacements are zero at the wing root (i.e., Fixed end,  $x=0$ ) and all boundary force terms are equal to zero at the wing tip ( $x=L$ ):

$$\delta w = \delta \theta = \delta \Psi = 0 \quad \text{at } x = 0 \quad (5.10)$$

$$S = M = T = 0 \quad \text{at } x = L \quad (5.11)$$

The system is now discretized over the length of the beam where the principle of virtual work is satisfied:

$$W_T = W_1 + W_2 = W_{INT} - W_{EXT} = \sum_{k=1}^{NE} W^k - W_{EXT} = 0 \quad (5.12)$$

where  $\xi = x/l_k$ , The bending and torsion contributions to the elemental virtual work,  $W_f^k$ , and  $W_t^k$ , respectively, are:

$$\begin{aligned}
W_f^k(\xi) = & \int_0^l \underbrace{\left[ \frac{1}{l_k^3} (EI(\xi) \delta w''')'' - m(\xi) l_k \omega^2 \delta w \right]}_{(*)} w d\xi \\
& + \left[ \frac{EI(\xi)}{l_k^3} \delta w'' w' \right]_0^l - \left[ \frac{1}{l_k^3} (EI(\xi) \delta w''')' w \right]_0^l + \frac{K(\xi)}{l_k^2} \int_0^l \Psi' \delta w'' d\xi
\end{aligned} \tag{5.13}$$

$$\begin{aligned}
W_t^k(\xi) = & \int_0^l \underbrace{\left[ -\frac{1}{l_k} (GJ(\xi) \delta \Psi')' - I_\alpha(\xi) l_k \omega^2 \delta \Psi \right]}_{(**)} \Psi d\xi \\
& + \frac{GJ(\xi)}{l_k} [\delta \Psi' \Psi]_0^l + \frac{K(\xi)}{l_k^2} \int_0^l w'' \delta \Psi' d\xi
\end{aligned} \tag{5.14}$$

The coupling terms in (5.13) and (5.14) are equivalent and when written in matrix form they are only different by their dimensions. The coupling terms in the weak form ensure symmetry of the final element DFE matrix. Similar to the DSM the average parameters over each element for  $EI(\xi)$ ,  $m(\xi)$ ,  $GJ(\xi)$ ,  $I_\alpha(\xi)$ ,  $K(\xi)$ , are used in the DFE such that the two expressions for flexural and twist are written as follows:

$$\begin{aligned}
W_f^k(\xi) = & \int_0^l \underbrace{\left[ \frac{1}{l_k^3} EI_{ave} \delta w'''' - m_{ave} l_k \omega^2 \delta w \right]}_{(*)} w d\xi \\
& + \left[ \frac{EI_{ave}}{l_k^3} \delta w'' w' \right]_0^l - \left[ \frac{1}{l_k^3} EI_{ave} \delta w'''' w \right]_0^l + \frac{K_{ave}}{l_k^2} \int_0^l \Psi' \delta w'' d\xi
\end{aligned} \tag{5.15}$$

$$\begin{aligned}
W_t^k(\xi) = & \int_0^l \underbrace{\left[ -\frac{1}{l_k} GJ_{ave} \delta \Psi'' - I_{\alpha,ave} l_k \omega^2 \delta \Psi \right]}_{(**)} \Psi d\xi \\
& + \frac{GJ_{ave}}{l_k} [\delta \Psi' \Psi]_0^l + \frac{K_{ave}}{l_k^2} \int_0^l w'' \delta \Psi' d\xi
\end{aligned} \tag{5.16}$$

The Dynamic Trigonometric Shape Functions (DTSF's) are chosen such that the integral expressions (\*) and (\*\*) are zero. The DFE element matrix is constructed by the addition of the uncoupled matrix and the coupled matrix as:

$$K_{DFE} = K_{UNCOUPLED} + K_{COUPLED} \quad (5.17)$$

where,

$$K_{UNCOUPLED} = \begin{bmatrix} \frac{EI}{l_k^3} \{N_1'''\}_0 & \frac{EI}{l_k^3} \{-N_1''\}_0 & 0 & \frac{EI}{l_k^3} \{-N_1'''\}_1 & \frac{EI}{l_k^3} \{N_1''\}_1 & 0 \\ \frac{EI}{l_k^3} \{N_2'''\}_0 & \frac{EI}{l_k^3} \{-N_2''\}_0 & 0 & \frac{EI}{l_k^3} \{-N_2'''\}_1 & \frac{EI}{l_k^3} \{N_2''\}_1 & 0 \\ 0 & 0 & \frac{GJ}{l_k} \{-N_{t1}'\}_0 & 0 & 0 & \frac{GJ}{l_k} \{N_{t1}'\}_1 \\ \frac{EI}{l_k^3} \{N_3'''\}_0 & \frac{EI}{l_k^3} \{-N_3''\}_0 & 0 & \frac{EI}{l_k^3} \{-N_3'''\}_1 & \frac{EI}{l_k^3} \{N_3''\}_1 & 0 \\ \frac{EI}{l_k^3} \{N_4'''\}_0 & \frac{EI}{l_k^3} \{-N_4''\}_0 & 0 & \frac{EI}{l_k^3} \{-N_4'''\}_1 & \frac{EI}{l_k^3} \{N_4''\}_1 & 0 \\ 0 & 0 & \frac{GJ}{l_k} \{-N_{t2}'\}_0 & 0 & 0 & \frac{GJ}{l_k} \{N_{t2}'\}_1 \end{bmatrix}$$

$$K_{COUPLED} = \frac{K}{l_k^2} \int_0^1 \begin{bmatrix} 0 & 0 & N_1'' N_{t1}' & 0 & 0 & N_1'' N_{t2}' \\ 0 & 0 & N_2'' N_{t1}' & 0 & 0 & N_2'' N_{t2}' \\ N_1'' N_{t1}' & N_2'' N_{t1}' & 0 & N_3'' N_{t1}' & N_4'' N_{t1}' & 0 \\ 0 & 0 & N_3'' N_{t1}' & 0 & 0 & N_3'' N_{t2}' \\ 0 & 0 & N_4'' N_{t1}' & 0 & 0 & N_4'' N_{t2}' \\ N_1'' N_{t2}' & N_2'' N_{t2}' & 0 & N_3'' N_{t2}' & N_4'' N_{t2}' & 0 \end{bmatrix} d\xi$$

The uncoupled matrix is formulated from the boundary terms extracted from the integration by parts. The coupled matrix is formulated from the integral expressions in both equations (5.15) and (5.16).

#### 5.4.1 Application of deviators.

As it was mentioned earlier, the DFE takes the average over each element much like the DSM for  $EI(\xi)$ ,  $m(\xi)$ ,  $GJ(\xi)$ ,  $I_\alpha(\xi)$  and  $K(\xi)$ . These average parameters can then be

adjusted to an exact representation of the element by including deviator terms. Deviator terms subtract the average parameters and add the exact variation parameters. The two expressions for flexural and twist from equations (5.7 and 5.8) can therefore be re-written as:

$$\begin{aligned}
W_f = & \int_{x_j}^{x_{j+1}} \left[ EI_{ave}(x) \delta w'' w'' - m_{ave}(x) \omega^2 \delta w w + K_{ave}(x) \delta w'' \Psi' \right] dx \\
& + \int_{x_j}^{x_{j+1}} \left[ \underbrace{-(EI_{ave} - EI(x))}_{EI_{DEV}} \delta w'' w'' - \underbrace{(K_{ave} - K(x))}_{K_{B,DEV}} \delta w'' \Psi' + \underbrace{(m_{ave} - m(x))}_{m_{DEV}} \omega^2 \delta w w \right] dx
\end{aligned} \tag{5.18}$$

$$\begin{aligned}
W_t = & \int_{x_j}^{x_{j+1}} \left[ GJ_{ave} \delta \Psi' \Psi' + K_{ave} \delta \Psi' w'' - I_{\alpha,ave} \omega^2 \delta \Psi \Psi \right] dx \\
& + \int_{x_j}^{x_{j+1}} \left[ \underbrace{-(GJ_{ave} - GJ(x))}_{GJ_{DEV}} \delta \Psi' \Psi' - \underbrace{(K_{ave} - K(x))}_{K_{I,DEV}} \delta \Psi' w'' + \underbrace{(I_{\alpha,ave} - I_{\alpha}(x))}_{I_{\alpha,DEV}} \omega^2 \delta \Psi \Psi \right] dx
\end{aligned} \tag{5.19}$$

The element integral expressions in equations (5.18, 5.19) can then be simplified similar to equations (5.13, 5.14) to yield the element equations for a tapered beam as:

$$\begin{aligned}
W^K = & \underbrace{\frac{EI_{ave}}{l_k^3} [\delta w'' w'' - \delta w''' w]_0^1 + \frac{GJ_{ave}}{l_k} [\delta \Psi' \Psi]_0^1}_{Uncoupled\ Terms} \\
& + \frac{K_{ave}}{l_k^2} \int_0^1 \Psi' \delta w'' d\xi + \frac{K_{ave}}{l_k^2} \int_0^1 w'' \delta \Psi' d\xi + DEV
\end{aligned} \tag{5.20}$$

where,

$$\begin{aligned}
DEV = & \frac{1}{l_k^3} \int_0^1 (-EI_{ave} + EI(\xi)) \langle N'' \rangle \{N''\} d\xi + \frac{1}{l_k} \int_0^1 (GJ_{ave} - GJ(\xi)) \langle N_t' \rangle \{N_t'\} d\xi \\
& + l_k \omega^2 \int_0^1 (m_{ave} - m(\xi)) \langle N \rangle \{N\} d\xi + l_k \omega^2 \int_0^1 (I_{\alpha,ave} - I_{\alpha}(\xi)) \langle N_t \rangle \{N_t\} d\xi \\
& + \frac{1}{l_k^2} \int_0^1 (-K_{ave} + K(\xi)) \langle N'' \rangle \{N_t'\} d\xi + \frac{1}{l_k^2} \int_0^1 (-K_{ave} + K(\xi)) \langle N_t' \rangle \{N''\} d\xi
\end{aligned} \tag{5.21}$$

The integral DEV expressions (5.21) were to be originally evaluated numerically for each trial frequency,  $\omega$ . The closed form analytical solution to the above deviator terms was later evaluated using MAPLE<sup>®</sup> symbolic math, and has increased computational efficiency greatly. The result, in this case, is a frequency dependent DFE stiffness matrix expressed in purely algebraic form. Element matrices are then assembled in the usual FEM way and the boundary conditions are introduced as a clamped-free cantilevered beam (e.g., using the penalty method (Cook, 2001 and Bathe, 1982)). Finally natural frequencies are found using a dedicated numerical bisection method in conjunction with the Wittrick-Williams root counting algorithm presented as by Wittrick and Williams (1971), Wittrick and Williams (1982) and Wittrick and Williams (1983) (see Chapter 2 for more details).

## ***5.5 Application of the Theory and Examples of Linearly Tapered Wings***

To validate the DFE method a linearly tapered wing is first studied. The wing is modeled with beam elements for various taper ratios and the resulting natural frequencies are compared to other existing methods. For this example the wing only tapers by a contracting chord in the span-wise direction. The next example represents a dual tapered wing by chord and thickness, with different ply orientations and stacking sequences. It is important to note that the tapered thickness is created by changing the ply numbers along the wing length, similar to the stepped case. Consequently, there would be no need to apply deviators for the thickness variations.

### ***5.5.1 Numerical tests for a linearly tapered beam.***

The wing model is composed of glass/epoxy composite material with 15 degree fibre lay-up. All mechanical and geometric properties at the wing root are the same as the uniform beam case studied earlier in Chapter 4. The coefficient  $c$  from equation (5.1(a-f)) is set at its minimum -1 for the maximum possible taper. The reasoning for such a large taper is to

show how faster the DFE will converge to the exact natural frequencies compared to the FEM and DSM. To approximate a tapered configuration, all three methods DFE, DSM, and FEM originally use piecewise uniform steps. The DFE then has the advantage of applying this refining technique by including deviator terms.

The 15 degree lay-up was initially used in order to reproduce and to confirm the calculations of effective rigidities with Banerjee (1998), Banerjee and Williams (1996), and Banerjee and Williams (1995). As a result, the same natural frequencies of a uniform beam presented in Chapter 4, were again obtained from the present DFE. The principal rigidities and Poisson's ratio are experimentally obtained (Teoh and Huang, 1976) (refer to Table 5-1).

**Table 5-1 Material Properties of a glass/ epoxy composite Laminate.**

$E_L$	9.71 GPa
$E_T$	3.25 GPa
$G_{LT}$	0.9025 GPa
$\nu_{LT}$	.29
<b>Thickness</b>	3.18 mm

Referring to Figure 4-9 in Chapter 4, shows the variations of the effective rigidities vs ply angle for a glass/epoxy composite laminate. The 15 degree fibre angle falls into the range of maximum bending-torsion coupled rigidity. The natural modes of free vibration as result display this coupled vibration behaviour in the following section. The values of the natural frequencies for the linearly tapered composite wing, using the same root properties as used in the chapter 4 for a uniform beam, are presented in Table 5-2. The wing studied in this example is assumed to have a taper coefficient  $c=-1$ .

**Table 5-2: The first five natural frequencies (Hz) of a linearly tapered wing composed of glass/epoxy composite material, with a taper coefficient of  $c=-1$**

Mode no.	FEM 200 Elements	DSM 20 Elements	Percent Error	DFE 20 Elements	Percent Error
1 <sup>st</sup>	62.73	62.55	0.0028	62.74	0.0001
2 <sup>nd</sup>	271.96	270.39	0.0058	272.19	0.0008
3 <sup>rd</sup>	660.68	654.78	0.0089	662.01	0.0020
4 <sup>th</sup>	1219.89	1205.21	0.0120	1224.40	0.0037
5 <sup>th</sup>	1845.77	1837.64	0.0044	1843.57	0.0012

Then, the resulting convergence results for various deviator terms are displayed in Figures 5-3 (a), (b), (c), (d), (e). The maximum taper ratio was used since it reflects the effectiveness of various deviator terms in the DFE versus the other methods. Since there are no published results for this tapered composite configuration the reference values have been determined using 200 finite elements.

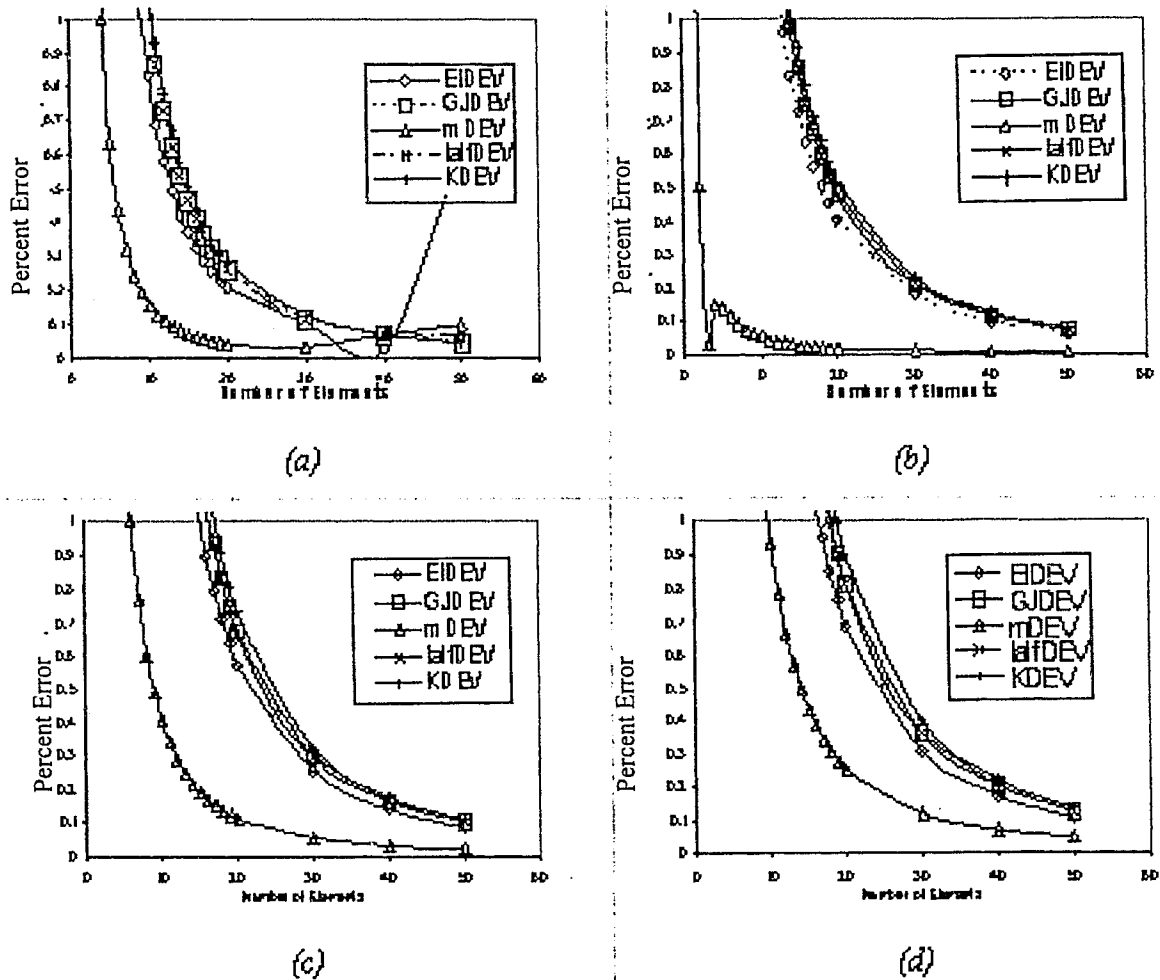
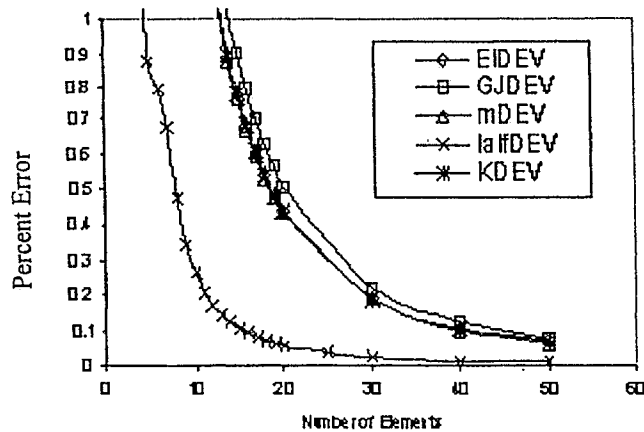


Figure 5-3: Comparative study between DFE convergence rates for the first five natural frequencies of a linearly tapered composite wing ( $c=1$ ) incorporating different deviator terms: (a) The first; (b) The second; (c) The third; (d) The fourth. 'EIDEV', represents the bending rigidity deviator; 'GJDEV', represents the torsion rigidity deviator; 'KDEV' represents the coupled bending-torsion rigidity deviator, 'MDEV' represents the mass deviator; 'IalfDEV', represents the mass moment of inertia deviator.



(e)

**Figure 5-4: Comparative study between DFE convergence rates for the first five natural frequencies of a linearly tapered composite wing ( $c=1$ ) incorporating different deviator terms: (e) The fifth natural frequencies. 'EIDEV', represents the bending rigidity deviator; 'GJDEV', represents the torsion rigidity deviator; 'KDEV' represents the coupled bending-torsion rigidity deviator, 'MDEV' represents the mass deviator; 'IalfDEV', represents the mass moment of inertia deviator.**

The effect of deviator terms were compared individually based on convergence for various natural frequencies (Figures 5-3 (a), (b), (c), (d) and (e)). The mass deviator is the most significant term with the highest convergence rate for the first four natural frequencies. The fifth natural frequency showed the fastest convergence with the mass moment of inertia deviator (see Figure 5-3 (e)). The importance of the mass deviator matrix is consistent with mass matrix used in the FEM. That means, if a lumped mass matrix was used in the FEM the quality of the results would have been less desired compared to the consistent mass matrix. From the modes in Figures 5-5 to 5-9 the 5<sup>th</sup> natural frequency is a predominantly torsion mode which explains why the mass moment of inertia deviator shows greater significance. Further, the normalized modes presented in Figures 5-5 to 5.9, show the increased influence of torsion on the higher modes of free vibration. The first mode is predominantly bending with little torsion displacement whereas the fifth mode is predominantly torsion displacement. These modes characterize the coupled bending torsion behaviour accurately with 30 elements used for each mode. Using 30 elements for each mode was sufficient to obtain a smooth curve for the modal displacements.

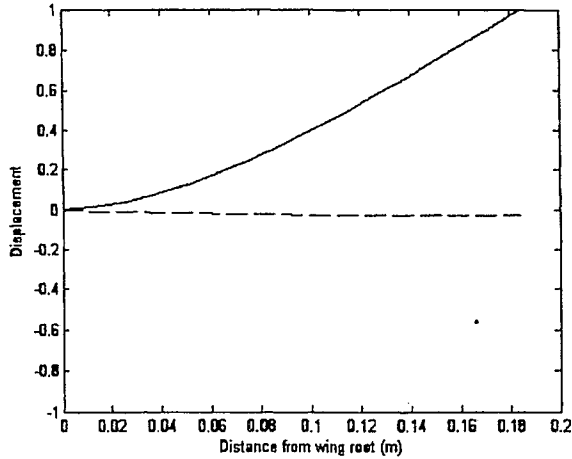


Figure 5-5: 1<sup>st</sup> normalized natural mode of a tapered composite wing. A solid line (-) represents bending displacement and dashed line (--) represents torsion displacement.

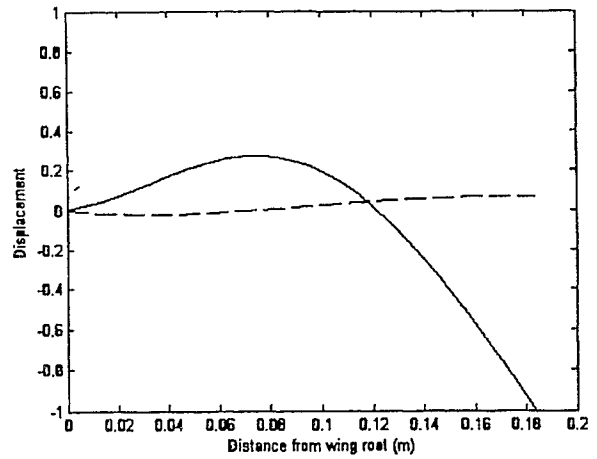


Figure 5-6: 2<sup>nd</sup> normalized natural mode of a tapered composite wing. A solid line (-) represents bending displacement and dashed line (--) represents torsion displacement.

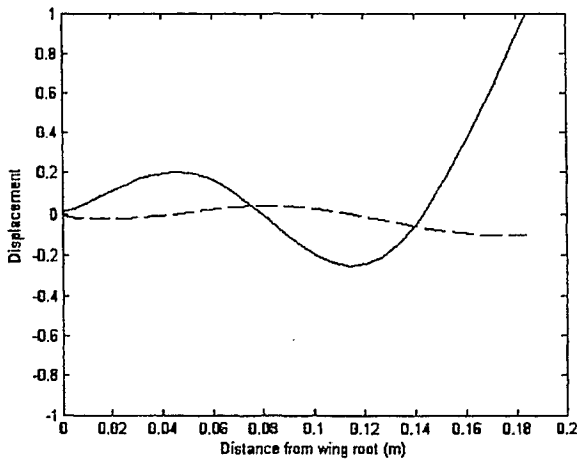


Figure 5-7: 3<sup>rd</sup> normalized natural mode of a tapered composite wing. A solid line (-) represents bending displacement and dashed line (--) represents torsion displacement.

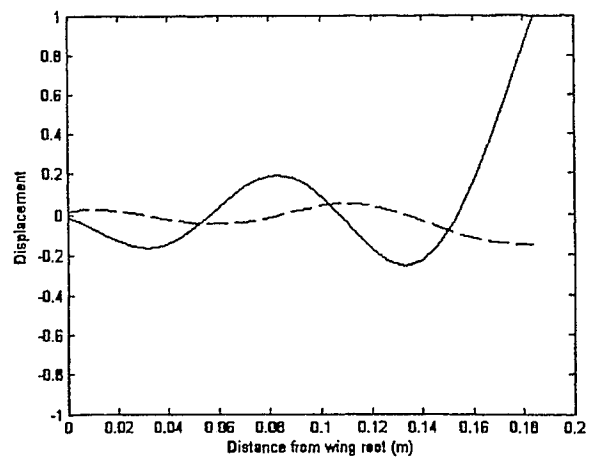
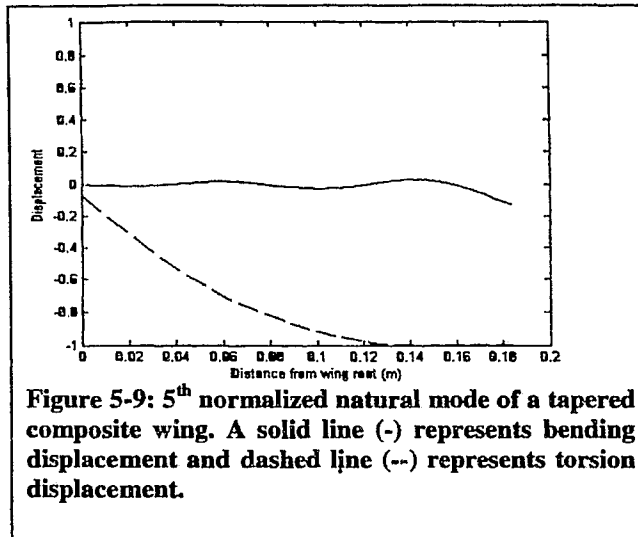


Figure 5-8: 4<sup>th</sup> normalized natural mode of a tapered composite wing. A solid line (-) represents bending displacement and dashed line (--) represents torsion displacement.



Fewer DFE elements are often required to converge accurately to the natural frequencies. Figure 5-10 shows that the principal natural frequency converges approximately to its exact value with only 20 elements. Convergence tests were carried out and revealed that the Refined Dynamic Finite Element (RDFE) including deviator terms has the fastest convergence (see Figures 5-10 to 5-12).

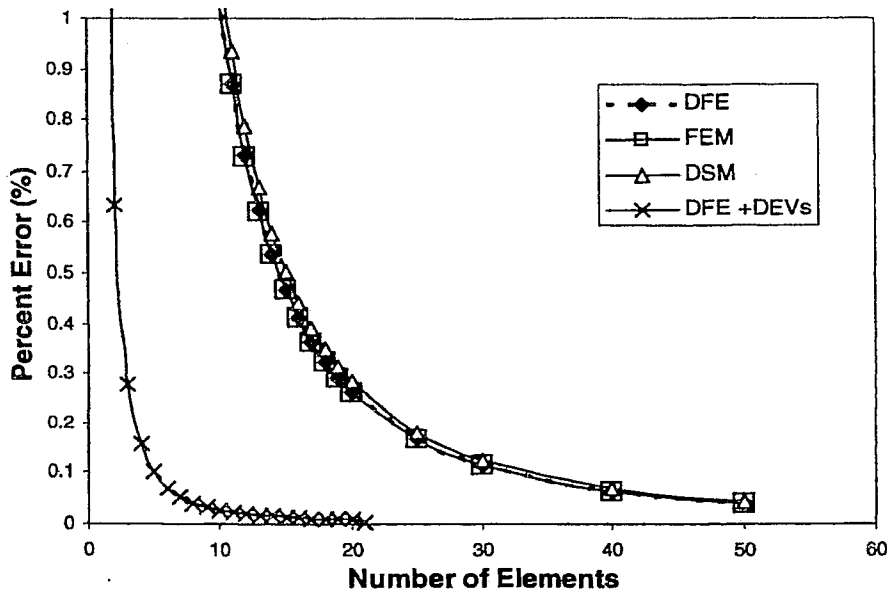


Figure 5-10: Convergence of DFE, FEM, DSM and DFE +DEVs for the first natural frequency.

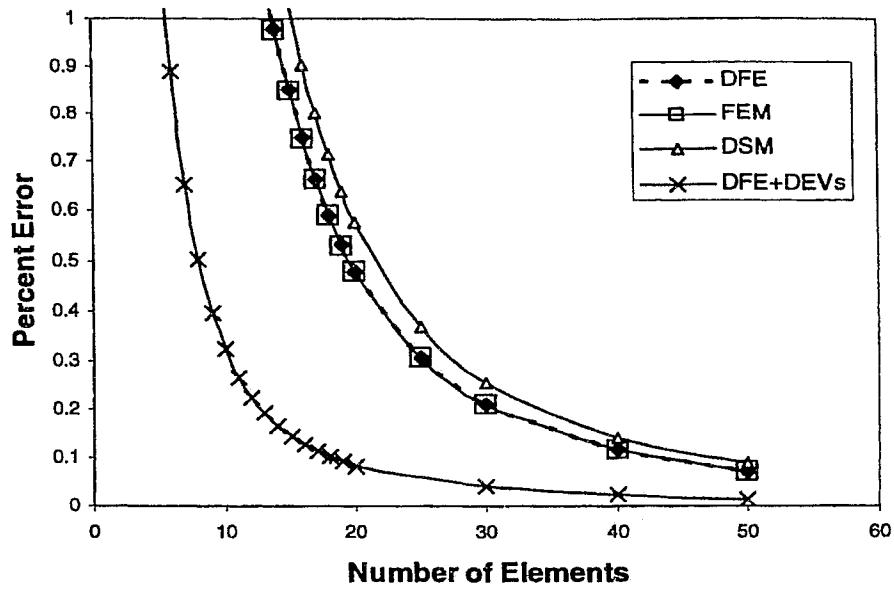


Figure 5-11: Convergence of DFE, FEM, DSM and DFE +DEVs for the second natural frequency

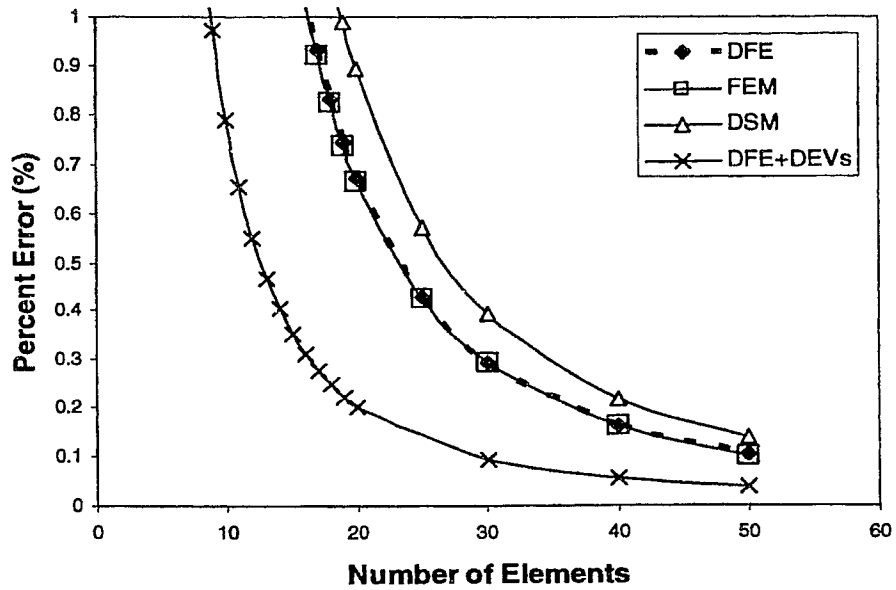


Figure 5-12: Convergence of DFE, FEM, DSM and DFE +DEVs for the third natural frequency

It has been observed that the DFE without its deviator matrix yields results almost identical to the FEM. The FEM is based on fixed polynomial basis functions and a consistent mass matrix is used. The DFE, DSM and FEM use the same centre element averaging for a tapered beam element parameters. For the linearly tapered wing the nodal values for rigidities, mass and cross-sectional area have been defined in equation (5.1). The DSM has the slowest convergence for the first three natural frequencies (Figures 5-10 to 5-12). The convergence for the DFE increased considerably when the deviator matrix was included. The RDFE with deviators converged to the exact solution for the first natural frequency with only 20 elements (see Figure 5-10). The reference values are based on a mesh of 200 classical finite elements, where the cubic "Hermite" and linear interpolation functions are used to approximate the bending and torsion displacements, respectively.

The DFE was then tested on beams with lower taper angles. The current glass/epoxy tapered beam configuration was then tapered with a less excessive taper coefficient of -0.5 yielding a taper angle of approximately 1 degree from the horizontal. The convergence tests revealed that in this case the DFE did not consistently converge faster than the other methods to the exact solution for all frequencies. In fact, according to Figures 5-13 to 5-15, the DFE only converged faster for the 1<sup>st</sup> fundamental natural frequency. The FEM resulted in the highest convergence rate for the second natural frequency (Figure 5-14), whereas, for the 3<sup>rd</sup> natural frequency (Figure 5-15), the best convergence was obtained from the DSM. In Table 5-3, presented is the first three natural frequencies for a 1 degree tapered wing and the corresponding percent error relative to 150 classical finite elements

**Table 5-3: Comparison study based on small taper angles. The natural frequencies are for a 1 degree tapered composite glass/epoxy wing.**

Mode no.	DFE 20 elements	Percent error	DSM 20 elements	Percent error	FEM 20 elements	Percent error
1 <sup>st</sup>	37.83	0.0001	37.80	0.0006	37.81	0.0004
2 <sup>nd</sup>	206.13	0.0008	205.84	0.0006	206.01	0.0002
3 <sup>rd</sup>	553.56	0.0019	552.16	0.0007	553.27	0.0013

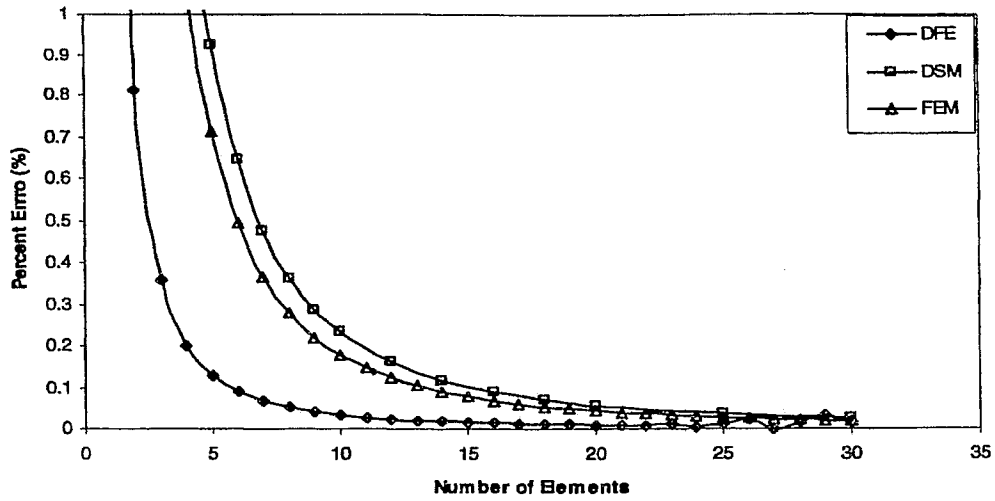


**Figure 5-13: Convergence for the first natural frequency for a glass/epoxy 1 degree tapered beam**

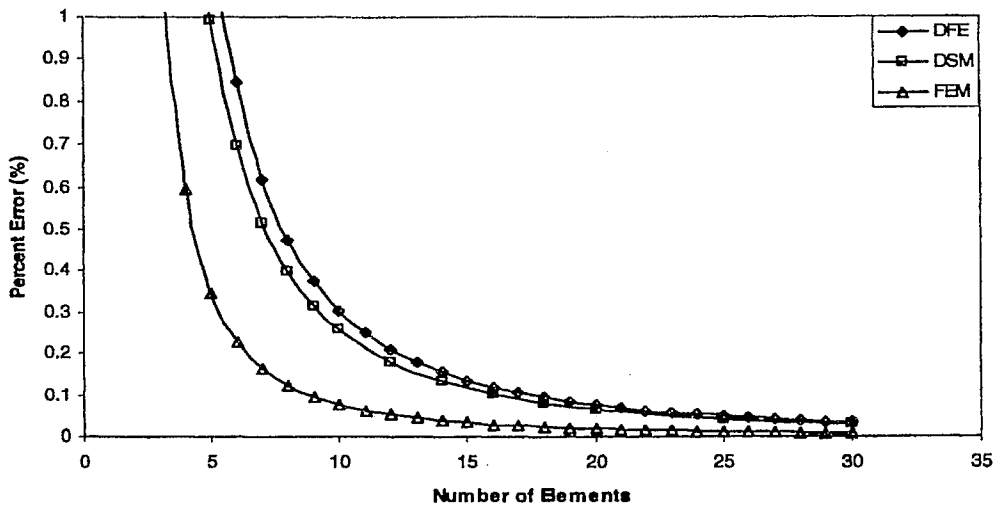


**Figure 5-14: Convergence for the second natural frequency for a glass/epoxy 1 degree tapered beam.**

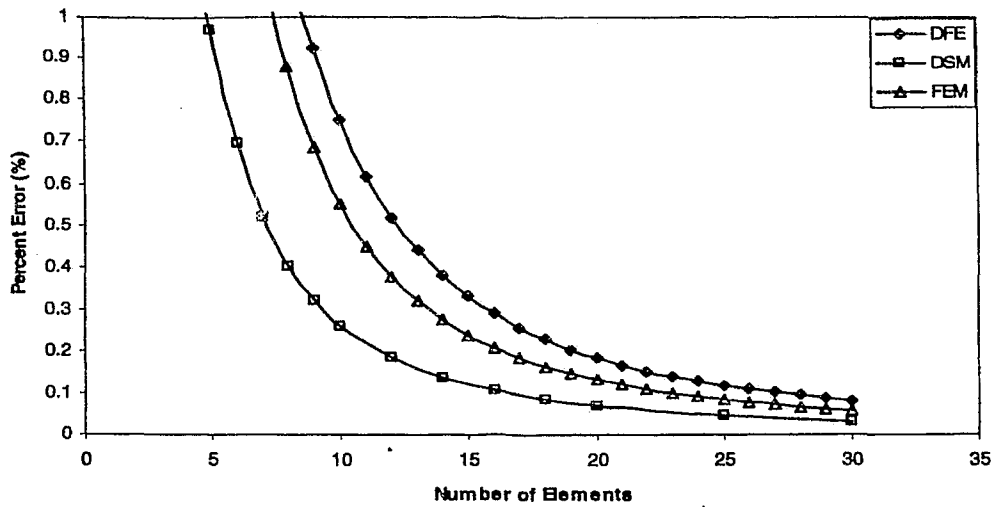


**Figure 5-15: Convergence for the third natural frequency for a glass/epoxy 1 degree tapered beam.**

In order to determine the reason why the DFE does not consistently yield good convergence for all frequencies, the convergence results were plotted for RDFE with and without its deviator matrices in Figure 5-16. As it can be observed from Figures 5-14 and 5-15 the DFE has slower convergence for the second and third natural frequencies when deviators are used.

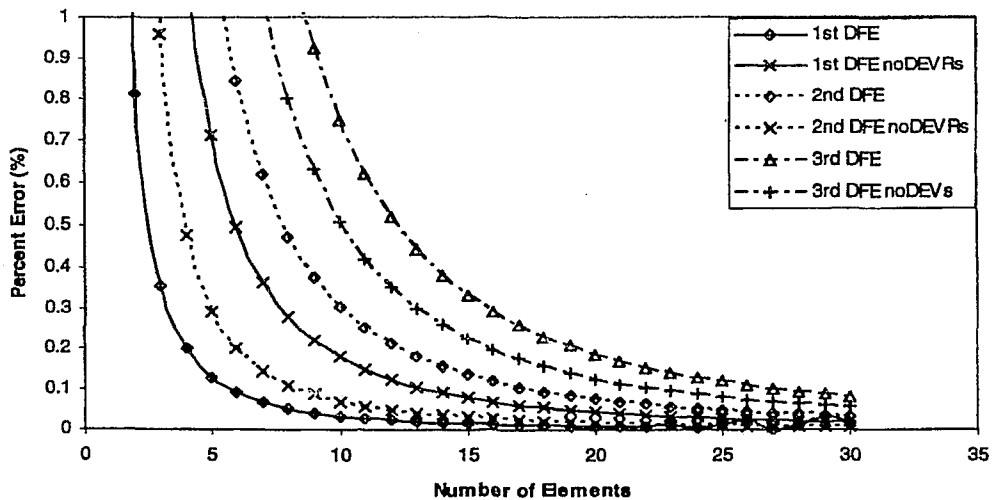


**Figure 5-16: Convergence of the DFE with and without deviators for the first three natural frequencies**

This behaviour can be attributed to the fact that for very small taper angles the effectiveness of the DFE refining terms known as deviators terms are less pronounced. This is due to the numerical errors and it is expanded in the following section.

### **5.5.2 Limitations on dynamic finite element deviators.**

Deviator expressions stem from the weak form of the differential equations of motion. These deviators are generally the difference between the average and exact representation of the element. Considering the example of a tapered wing, the DFE originally uses uniform beam elements to approximate the geometry. Then the application of deviators, essentially adjust the uniform (i.e., constant parameters) elements to better represent a tapered geometry (i.e., variable coefficients) leading to a more accurate wing-beam RDFE model. The power of these terms has been confirmed by Hashemi (1998) and Hashemi and Richard (1999) for the analysis of homogenous metallic beams and blades, and discussed by Hashemi and Borneman (2003) and Hashemi and Borneman (2004) for composite beams. Deviators do in fact increase the convergence of the DFE which is seen through out this research (see Figures 5-5 to 5-8).

The deviator matrix is constructed from multiple sub deviator matrices depending on the formulation and the model adopted for the structure. For the example of a tapered wing with variable coefficients in the governing differential equation such as mass,  $m(x)$ , mass moment of inertia,  $I_a(x)$ , bending,  $EI(x)$ , torsion,  $GJ(x)$ , and bending-torsion coupling,  $K(x)$ , which are each used to derive the deviator matrix (refer to equation 5.21). For a linearly tapered wing and using the properties in Table 5.1 the individual convergences for each deviator are observed in Figures 5-4 (a) through 5-4(e).

As discussed in section 5.5, these compensating matrices, particularly the mass and mass moment of inertia deviators generally increase the convergence rates of the natural frequencies (refer to Figs 5-4 (a)-(e)).

Although deviators generally increase the DFE convergence, there are instances where the application of these matrices produced undesirable results. With the introduction of numerical error, the addition of deviators can result in a decrease in convergence, particularly for very low taper ratio models that can be sufficiently approximated using

uniform beam elements. “An acceptable FE formulation converges to the exact solution of the mathematical model as the mesh is indefinitely refined (neglecting errors due to finite precision computer arithmetic)” (see Cook, Malkus, Plesha and Witt (2001) pp. 161). It is important to distinguish when deviators will increase or decrease convergence. Unfortunately the numerical error differs from one model to another based on the complexity of the formulation. This issue will also be discussed in chapter 6 for the geometrical and material bending-torsion coupled model.

A parameter study revealed that for the present model consisting of a solid rectangular cross-section the numerical error associated with the deviator terms is most pronounced for tapers less than 10 degrees (refer to Figure 5-17).

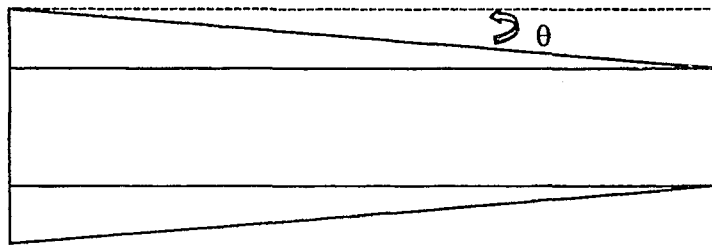


**Figure 5-17: Illustration of composite wing taper angle**

The deviators used for taper angles greater than 10 degrees result in more consistent convergence. This consistency in results suffers for taper angles between 5-10 degrees. The consistency is based on the convergence of each deviator matrix. It is observed that for  $5^\circ < \theta < 10^\circ$  some deviators increase the convergence rate while some decrease the convergence. Due to this inconsistency it is not recommended to use deviators for this range. For very small taper angles  $0^\circ < \theta < 5^\circ$  adding the deviators only decreased the DFE convergence (see Figures 5-14 and 5-15).

If the DFE can approximate a tapered geometry using uniform elements to a reasonable accuracy then there is no need to include the numerical error by implementing a deviator matrix. If the taper angle is large enough, in this example greater than 10 degrees, the deviator terms will positively affect the DFE convergence rate. The deviator matrices are a distinct advantage that the DFE has over the other methods (FEM, DSM)

although one has to be aware of the limitation on these deviators particularly for highly complex models.

### 5.5.3 A dually tapered wing model.

Here, a dually tapered wing model is considered. The wing geometry is presented in Figure 5-18. The composite material used for this example is Cytek 5245-T800 carbon fibre/epoxy. The mechanical properties of this laminate are displayed in Table 5-4 (see Taylor and Butler, 1997) and the wing dimensions are given in Table 5-5. The free vibration of wings with different lay-ups is presented for a dual varying geometry (i.e., linearly tapered by chord and stepped in thickness).

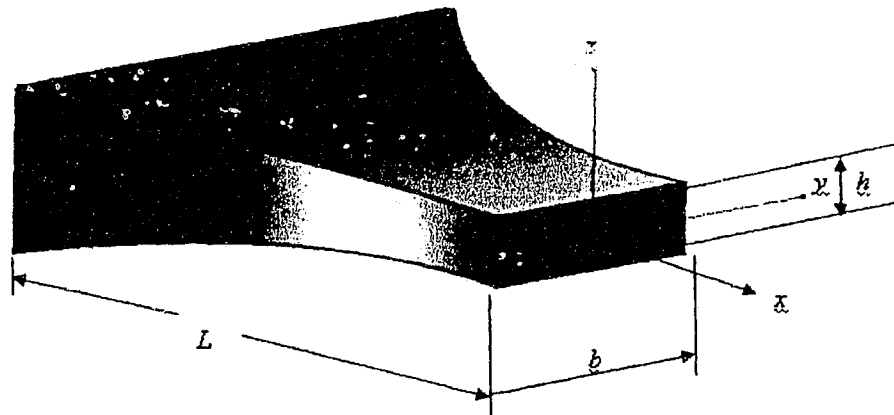


Figure 5-18: Dually tapered Cytek 5245-T800 carbon fibre/epoxy wing geometry

Table 5-4 Material Properties of Cytek 5445-T800 Carbon fibre/epoxy

$E_L$	165 GPa
$E_T$	8.8 GPa
$G_{LT}$	5.0 GPa
$\nu_L$	0.30
$\rho$	1550 Kg/m <sup>3</sup>

Table 5-5 Wing Dimensions and configuration.

Lay-up #1	$[(30)_4 / (-30)_4]_S$
Taper Coefficient	-0.5
Lay-up #2	$[(45)_4 / (-45)_4]_S$
Taper Coefficient	-0.75
Layer Thickness	0.125 mm
Length	0.1905 m
Root Chord	50.8 mm

The composite wing considered for lay-up #1 consisted of 16 uniform layers at the root and reduced along the span-wise direction by four layers per step. Four steps are used with thicknesses of 2 mm and 0.5 mm at the root and tip, respectively. The convergence test results for the first natural frequency are shown in Figure 5-19. It is observed that for this frequency the convergence reaches 100 % accuracy with only 16 elements and then fluctuates with greater than 24 elements. These fluctuations are not uncommon as the FEM exhibits the same behaviour with a greater number of elements. The fluctuations are a result of numerical error associated with large global assemblies.

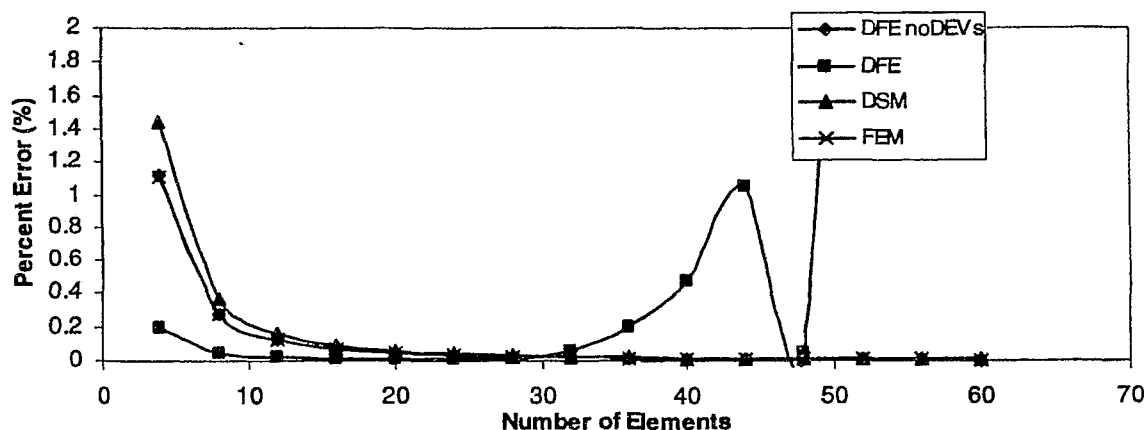


Figure 5-19: First natural frequency for Lay-up #1 with a  $c=-0.5$ .

The convergence results for the second natural frequency are displayed in Figure 5-20. For this mode the convergence of the DFE without deviators results in better convergence due to the limitations of the deviators discussed in section 5.5.1. Data trends in the Figures 5-19 to 5-21 for the first, second and third natural frequencies show similar convergence for the FEM and DFE (omitting the deviators expressions) with the DSM resulting in the slowest convergence. Similarities between the DFE and FEM are expected since both are Galerkin based formulations.

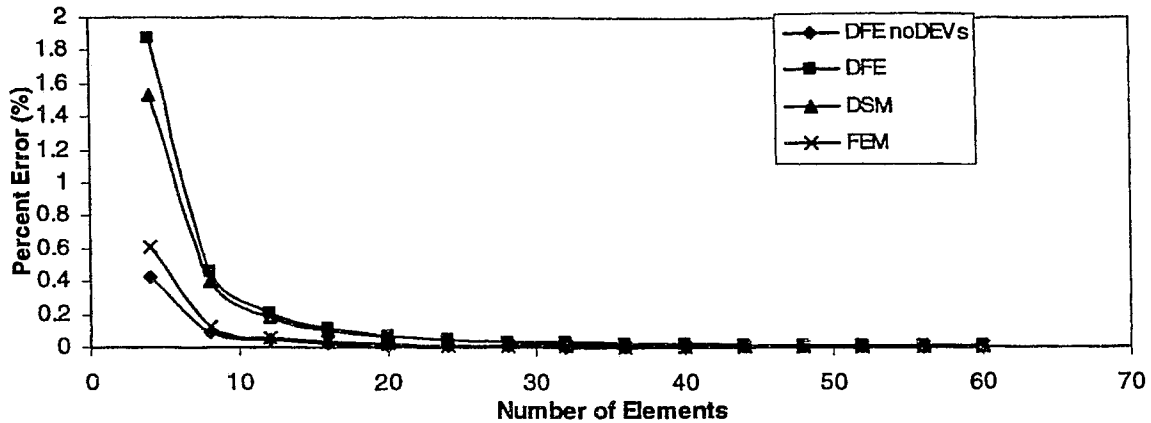


Figure 5-20: Second Natural Frequency for Lay-up #1 with a  $c=-0.5$

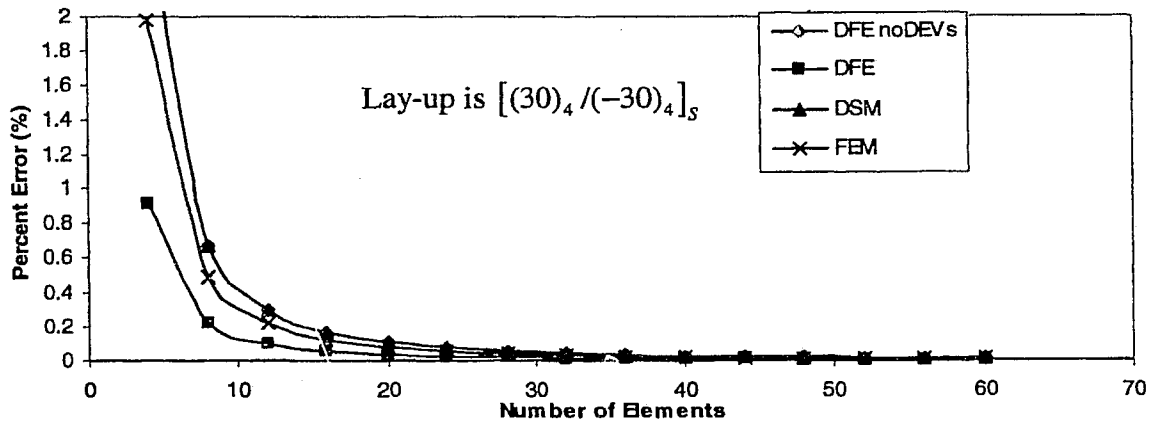


Figure 5-21: Third Natural Frequency for Lay-up #1 with a  $c=-0.5$ .

The main difference is in the shape functions. The DFE uses Dynamic Trigonometric Shape Functions (DTSF's), whereas FEM uses fixed polynomial shape functions. In previous applications of the DFE (see Hashemi and Richard (1999), Hashemi (1998)) the trigonometric shape functions have always satisfied the natural (free) boundary conditions. For composites beams where the addition of an extra coupling term is used, the present trigonometric shape functions become less effective since the natural boundary conditions are not satisfied, thus resulting in similar convergence between DFE and FEM. It is with the deviator terms that the DFE is distinguished from the FEM and DSM.

In contrast to the  $[(30)_4/(-30)_4]_S$  symmetric stacking sequence, a  $[(45)_4/(-45)_4]_S$  stacking sequence was also tested. The increased taper resulted in much more consistent convergences for the RDFE. For the first natural frequency (Figure 5-22) the DFE converges to the exact solution with only 8 elements and intermittently converges more rapidly than the other methods for the 2<sup>nd</sup>, 3<sup>rd</sup> and 4<sup>th</sup> frequencies (see Figures 5-23 to 5.25).

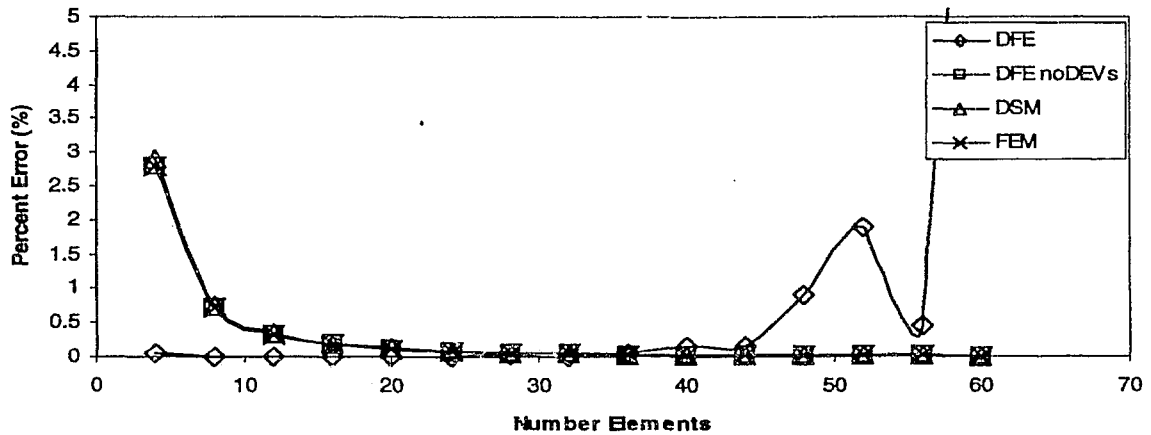


Figure 5-22: First natural frequency for Lay-up #2 where  $c=-0.75$

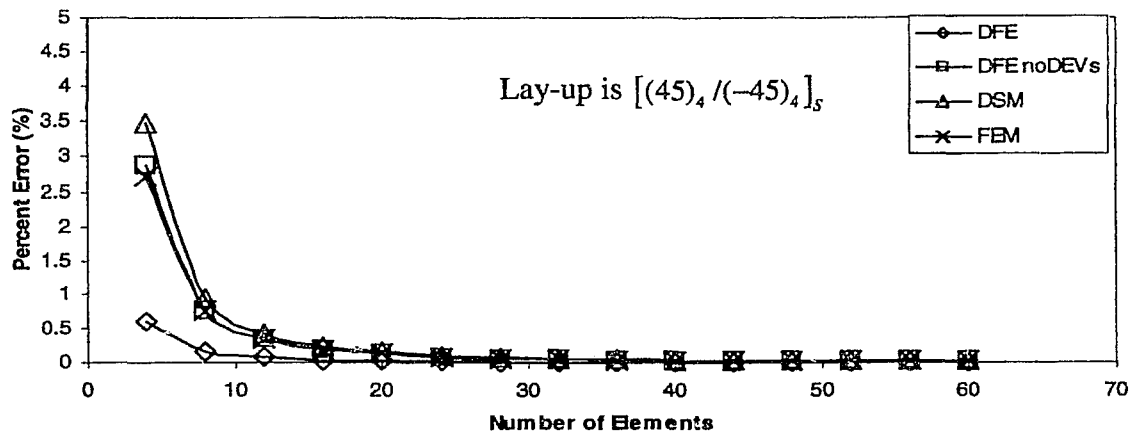


Figure 5-23: Second natural frequency for Lay-up #2 where  $c=-0.75$

For the 3<sup>rd</sup> natural frequency, the RDFE behaviour is slightly different for small number of elements, however, the DFE does still have the fastest convergence. To verify whether the RDFE would converge faster at higher modes, a convergence test for the fourth natural frequency was also carried. According to Figure 5-25 the fourth natural frequency still favours the RDFE. It is observed that by using a higher taper coefficient, the

effectiveness of the deviators is more pronounced resulting in consistently faster convergence. The more complex the system, the better the RDFE converges compared to the other existing methods.

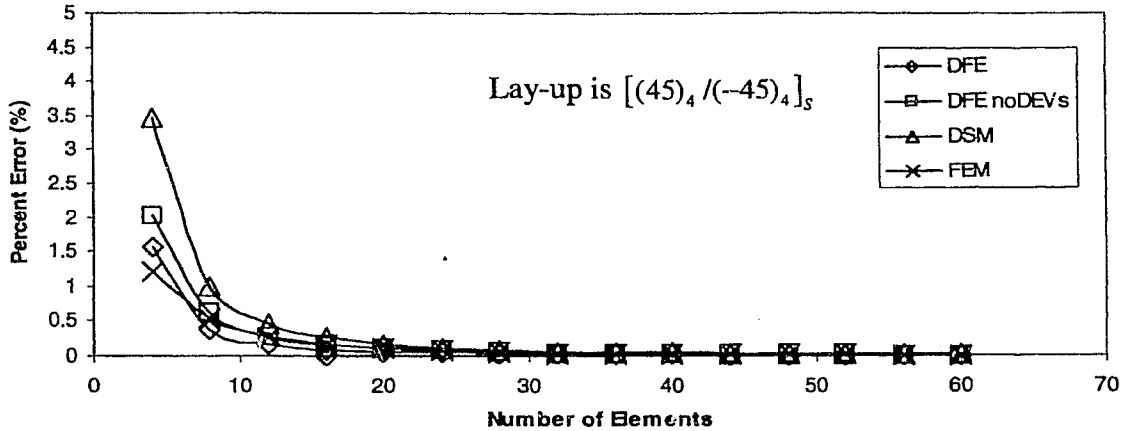


Figure 5-24: Third natural frequency for Lay-up #2 where  $c=-0.75$

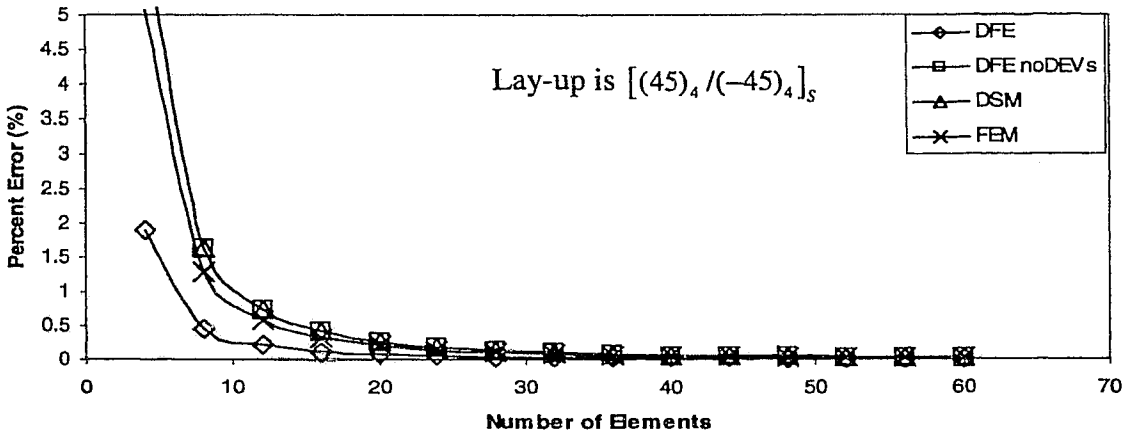


Figure 5-25: Fourth natural frequency for Lay-up #2 where  $c=-0.75$

Table 5-6: The fundamental natural frequencies (Hz) of a carbon fibre/epoxy wing with a -0.75 taper coefficient

Natural Frequency	FEM Using 300 Elements (Benchmark)	DFE Using 20 Elements	DSM Using 20 Elements	FEM 20 Elements
1 <sup>st</sup>	42.65	42.65	42.60	42.60
2nd	208.15	208.20	207.84	207.90
3rd	538.76	539.08	537.87	538.23
4th	957.52	956.83	955.01	955.53

## **5.6 Conclusion**

The DFE formulation for the free vibration analysis of a uniform and tapered composite Euler-Bernoulli beam is presented. Natural frequencies and modes of free vibration have been determined and classified for two types of materials and multiple stacking sequences. The classification of these modes falls into bending, torsion, or bending-torsion modes which are characteristics of composite material. The DFE matrix is completely closed form based on trigonometric shape functions. Preliminary work entailed extensive symbolic integrations that were undertaken using MAPLE<sup>®</sup> software version 8. Based on the results obtained, the DFE shows faster convergence than the FEM and DSM. This is particularly true in the case of highly tapered beams where deviator terms are used to adjust the DFE matrix to generate a more accurate representation of the element (i.e., RDFE). It is important to acknowledge the limitations on these deviators as for some cases they adversely affect the convergence rates, by adding numerical errors. The numerical error associated with more complex elements is less pronounced as the deviators increase the convergence significantly. From the observed results, the DSM accurately converges quickly to the solution for simple uniform elements. The FEM is fast and is best suited for multiple frequency outputs. The RDFE with its refining terms is validated in contrast to the other existing methods for its fast convergence to the solution particularly for higher modes of free vibration and for more complex elements. With the RDFE validated for tapered beam configurations, the formulation can then be advantageously extended to more realistic wing cross-sections such as box-beam section discussed in Chapter 6.

# Chapter 6 Geometric and Material Coupled Wing Model

## 6.1 Introduction

The materially coupled composite, uniform and piece-wise uniform stepped wing beams were analysed in Chapter 4. The tapered wing configurations were then presented and discussed in Chapter 5. In this chapter, the wing model is extended to more complex configurations exhibiting not only the material but also geometrical couplings. Using a wing-box model for the wing cross-section and a circumferentially asymmetric stiffness (CAS) configuration for the composite ply lay-up, a more realistic composite wing model is generated. In the previous chapters, only material coupling was considered which arises from an unbalanced ply lay-up or symmetric stacking sequence. An additional geometric coupling arises from the cross-sectional geometry of the wing.

The present wing model, (Figure 6-2(a)) is modeled as a symmetric configuration where the materially coupled behaviour is characterized by bending-torsion coupled stiffness  $K$ . The added geometric coupling is a consequence of an offset of the mass centre axis,  $G_s$ , from the geometrical elastic axis,  $E_s$ , denoted by  $x_\alpha$ . Any structural component located in front of the leading spar or behind the rear spar is considered not to contribute to the rigidity of the wing (Lillico, Butler, Guo and Banerjee, 1997). The omitted components do however contribute to the mass and inertia of the wing such that the mass centre, initially located at the geometric centre of the box, shifts slightly towards the rear of the wing-box (refer to Figure 6-2(b)).

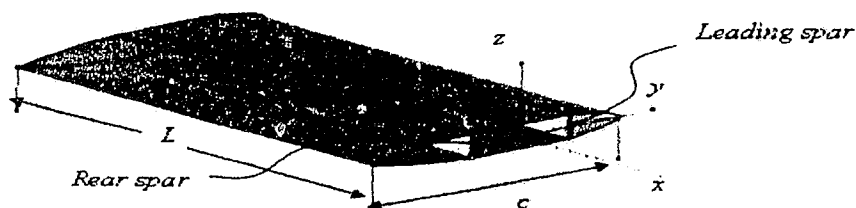
## 6.2 Model, Hypotheses and Simplifying Assumptions

The proposed wing model is constructed as a wing-box, where  $L$  is the span-wise length and  $c$  is the wing chord. The lateral bending and twist displacements are governed by

Euler-Bernoulli and St. Venant beam theories, respectively. Shear deformation, rotary inertia, commonly associated with Timoshenko beam theory, as well as warping effects are neglected.

Different stacking sequence and/or thickness of the thin-walled box-beam result in different coupling behaviours. For a circumferentially asymmetric stiffness (CAS) configuration the axial stiffness,  $A$ , must remain constant in all walls of the cross-section. The coupling stiffness,  $B$ , in opposite members is of the opposite sign as stated by Armanios and Badir (1995) and Berdichevsky *et al* (1992). As a result of axial stiffness,  $A$ , remaining constant, the corresponding thickness must also remain constant. Chandra *et al.* (1990) consider a symmetric configuration for a box-beam which consists of opposite walls having the same stacking sequence, although the stacking sequences between the horizontal and vertical members need not be the same. The CAS and symmetric configurations both lead to a bending-torsion coupled response for thin-walled beams.

The second configuration considered by Armanios and Badir (1995) and Berdichevsky *et al* (1992) was a circumferentially uniform stiffness configuration (CUS) where  $A$ ,  $B$ ,  $C$ , axial, coupling and shear stiffness, respectively, are constant throughout the circumference of the cross-section. Chandra *et al.* (1990) built-up similar configurations where the stacking sequence of opposite walls is of oppositely stacked, what they call anti-symmetric configuration. Anti-symmetric or CUS configurations are beyond the scope of this research and will not be discussed further. The CAS or symmetric configuration leads a bending-torsion coupled wing which will be used to model the wing-box composite plies.



(a)

Figure 6-1: (a) 3-D drawing of a composite wing cross-section airfoil, with length =  $L$ .

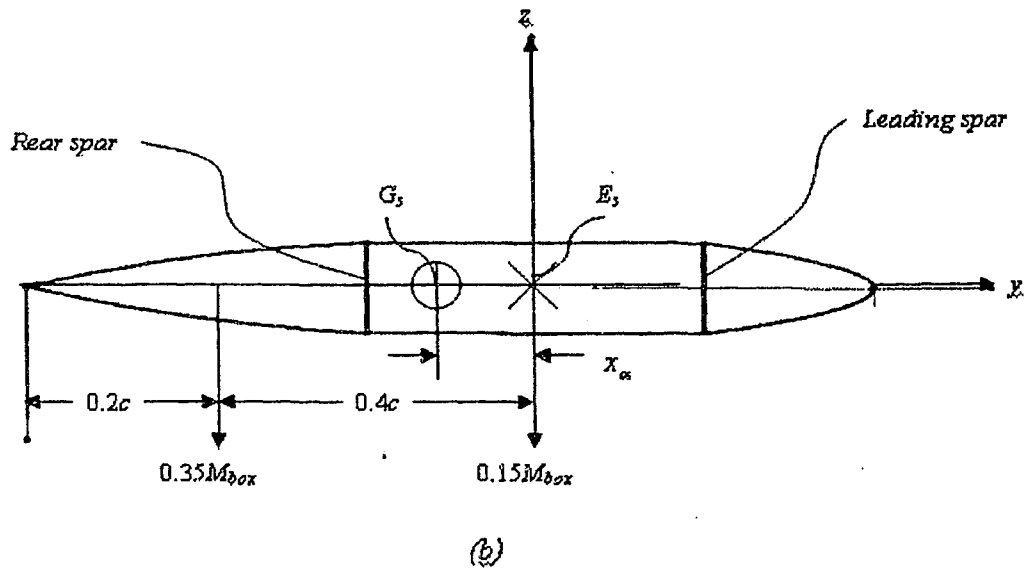


Figure 6-2: (b) Cross-section of a wing-box, where  $c$  is the chord length,  $M_{box}$  is the wing-box mass,  $E_s$  and  $G_s$  are, respectively, the geometric elastic centre and mass centre axis.

### 6.3 Theory

The differential equations governing the motion for the free vibration of laminated composite wings (presented in Figures 6-1(a, b)) with geometric couplings are given by Lillico *et al* (1997) as:

$$\frac{\partial^2}{\partial x^2} \left( EI(x) \frac{\partial^2 w}{\partial x^2} \right) + \frac{\partial^2}{\partial x^2} \left( K(x) \frac{\partial \psi}{\partial x} \right) + m(x) \frac{\partial^2 w}{\partial t^2} - m(x) x_\alpha \frac{\partial^2 \psi}{\partial t^2} = 0 \quad (0.75)$$

$$\frac{\partial}{\partial x} \left( GJ(x) \frac{\partial \psi}{\partial x} \right) + \frac{\partial}{\partial x} \left( K(x) \frac{\partial^2 w}{\partial x^2} \right) + m(x) x_\alpha \frac{\partial^2 w}{\partial t^2} - I_\alpha(x) \frac{\partial^2 \psi}{\partial t^2} = 0 \quad (0.76)$$

The displacements can be assumed to have a sinusoidal variation with frequency  $\omega$  as:

$$\begin{aligned} w(x, t) &= w(x) \sin \omega t \\ \psi(x, t) &= \Psi(x) \sin \omega t \end{aligned} \quad (0.77)$$

The Weighted Residual Method (WRM) is employed and the integral form is re-written in the following weak form

$$W_f = \int_0^L \left[ EI(x) \delta w'' w'' + K(x) \delta w'' \Psi' - m(x) \omega^2 \delta w w + m(x) \omega^2 x_\alpha \delta w \Psi \right] dx \quad (0.78)$$

$$+ \left[ (EI(x) w'' + K(x) \Psi')' \delta w \right]_0^L - \left[ (EI(x) w'' + K(x) \Psi') \delta w' \right]_0^L$$

$$W_t = \int_0^L \left[ -GJ(x) \delta \Psi' \Psi' - K(x) \delta \Psi' w'' + I_\alpha(x) \omega^2 \delta \Psi \Psi - m(x) \omega^2 x_\alpha \delta \Psi w \right] dx \quad (0.79)$$

$$+ GJ(x) \left[ \delta \Psi \Psi' \right]_0^L + K(x) \left[ \delta \Psi w'' \right]_0^L$$

where two integrations by parts for the flexural portion and one integration by parts for the twisting portion have been applied. Similar to Chapter 5, by re-writing the integral equation the inter-element continuity requirements are relaxed so that once again the approximation spaces for  $w$  and  $\phi$  satisfy the  $C^1$  and  $C^0$  continuity requirements, respectively. Then, the resulting shear force,  $S(x)$ , bending moment,  $M(x)$ , and torsional moment,  $T(x)$ , are:

$$S(x) = \frac{\partial}{\partial x} \left( EI(x) \frac{\partial^2 w}{\partial x^2} + K(x) \frac{\partial \Psi}{\partial x} \right) \quad (0.80)$$

$$M(x) = -EI(x) \frac{\partial^2 w}{\partial x^2} - K(x) \frac{\partial \Psi}{\partial x} \quad (0.81)$$

$$T(x) = GJ(x) \frac{\partial \Psi}{\partial x} + K(x) \frac{\partial^2 w}{\partial x^2} \quad (0.82)$$

The sign conventions are similar to those already used in Chapters 4 and 5. Boundary conditions associated to clamped-free (cantilever) structure are such that all virtual and real displacements are zero at wing root ( $x=0$ ) and all resulting forces are equal to zero at wing tip ( $x=L$ ). Hence,

$$\delta w = \delta \theta = \delta \Psi = 0 \quad \text{at } x = 0 \quad (0.83)$$

Consequently,

$$S = M = T = 0 \quad \text{at } x = L \quad (0.84)$$

Expressions (0.78) and (0.79) also satisfy the Principle of Virtual Work (PVW) similar to formulation in Chapter 5. The system is then discretized by 2-node 6-DOF uniform beam elements over the length of the beam. The wing can be discretized to a local domain  $\xi = [0,1]$  (i.e., reference element) where,  $\xi = x/L$ . The uniform element virtual work expressions for bending and torsion contributions can then be written as:

$$\begin{aligned} W_f^k(\xi) = & \int_0^1 \underbrace{\left[ \frac{1}{l_k^3} (EI(\xi) \delta w'')'' - m(\xi) l_k \omega^2 \delta w \right]}_{(*)} w d\xi \\ & + \frac{EI}{l_k^3} [\delta w'' w' - \delta w''' w]_0^1 + \frac{K}{l_k^2} \int_0^1 \Psi' \delta w'' d\xi + m x_\alpha l_k \omega^2 \int_0^1 \delta w \Psi d\xi \end{aligned} \quad (0.85)$$

and

$$\begin{aligned} W_t^k(\xi) = & \int_0^1 \underbrace{\left[ -\frac{1}{l_k} (GJ(\xi) \delta \Psi')' - I_\alpha(\xi) l_k \omega^2 \delta \Psi \right]}_{(**)} \Psi d\xi \\ & + \frac{GJ}{l_k} [\delta \Psi' \Psi]_0^1 + \frac{K}{l_k^2} \int_0^1 w'' \delta \Psi' d\xi + m x_\alpha l_k \omega^2 \int_0^1 w \delta \Psi d\xi \end{aligned} \quad (0.86)$$

The coupling terms in equations (0.85) and (0.86) are equivalent and when written in matrix form they are only different by their dimensions. The coupling terms in the weak form retain symmetry of the final element DFE matrix. The DFE takes the average over each element (similar to the DSM) for  $EI(\xi)$ ,  $m(\xi)$ ,  $GJ(\xi)$ ,  $I_\alpha(\xi)$  and  $K(\xi)$ . Therefore, after a certain number of additional integration by parts, the expressions for flexural and twist are found as:

$$\begin{aligned}
W_f^k(\xi) = & \int_0^1 \underbrace{\left[ \frac{1}{l_k^3} EI_{ave} \delta w''' - m_{ave} l_k \omega^2 \delta w \right]}_{(*)} w d\xi \\
& + \frac{EI_{ave}}{l_k^3} [\delta w'' w' - \delta w''' w]_0^1 + \frac{K_{ave}}{l_k^2} \int_0^1 \Psi' \delta w'' d\xi \\
& + (mx_\alpha)_{ave} l_k \omega^2 \int_0^1 \delta w \Psi d\xi
\end{aligned} \tag{0.87}$$

and,

$$\begin{aligned}
W_i^k(\xi) = & \int_0^1 \underbrace{\left[ -\frac{1}{l_k} GJ_{ave} \delta \Psi'' - I_{\alpha,ave} l_k \omega^2 \delta \Psi \right]}_{(**)} \Psi d\xi \\
& + \frac{GJ_{ave}}{l_k} [\delta \Psi' \Psi]_0^1 + \frac{K_{ave}}{l_k^2} \int_0^1 w'' \delta \Psi' d\xi \\
& + (mx_\alpha)_{ave} l_k \omega^2 \int_0^1 w \delta \Psi d\xi
\end{aligned} \tag{0.88}$$

such that,

$$W^k(\xi) = W_f^k(\xi) + W_i^k(\xi) \tag{0.89}$$

The Dynamic Trigonometric Shape Functions (DTSF's) are then defined such that the integral expressions (\*) and (\*\*) are zero. The variable mechanical properties are averaged differently compared to the previous models developed. The following integral averaging technique is employed to allow for flexibility in the model,

$$\Gamma_{ave} = \frac{1}{b-a} \int_a^b \Gamma(x) dx \tag{0.90}$$

so that the dually coupled wing-beam, exhibiting material and geometric couplings, can be easily extended to higher order taper configurations.  $\Gamma$  can be any mechanical property varying along the wing span (refer to Figure 6-2).

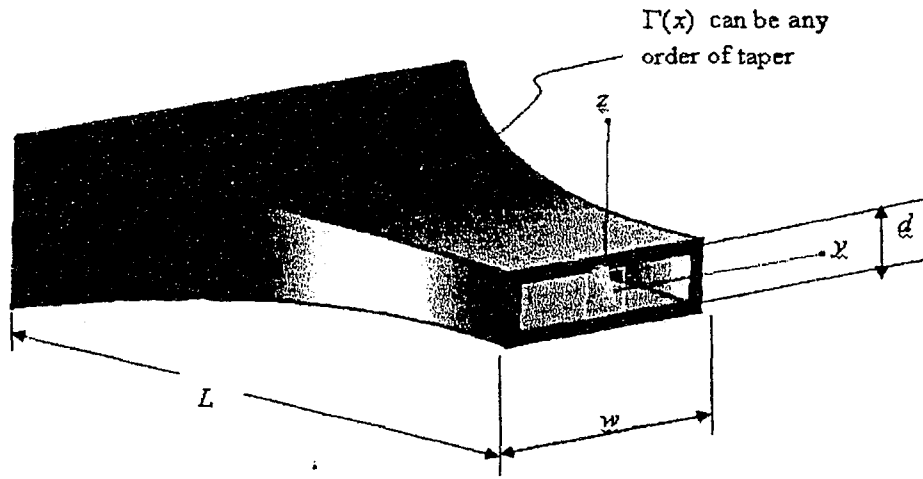


Figure 6-3: : Dually tapered composite wing-box

Finally, the approximations to the field and test variable  $w$ ,  $\Psi$ ,  $\delta w$  and  $\delta \Psi$  are substituted into the above equations and the corresponding DFE matrices are obtained as:

$$K_{UNCOUPLED} = \begin{bmatrix} \frac{EI}{l_k^3} \{N_1''''\}_0 & \frac{EI}{l_k^3} \{-N_1''\}_0 & 0 & \frac{EI}{l_k^3} \{-N_1''''\}_1 & \frac{EI}{l_k^3} \{N_1''\}_1 & 0 \\ \frac{EI}{l_k^3} \{N_2''''\}_0 & \frac{EI}{l_k^3} \{-N_2''\}_0 & 0 & \frac{EI}{l_k^3} \{-N_2''''\}_1 & \frac{EI}{l_k^3} \{N_2''\}_1 & 0 \\ 0 & L 0 & \frac{GJ}{l_k} \{-N_{r1}'\}_0 & 0 & w 0 & \frac{GJ}{l_k} \{N_{r1}'\}_1 \\ \frac{EI}{l_k^3} \{N_3''''\}_0 & \frac{EI}{l_k^3} \{-N_3''\}_0 & 0 & \frac{EI}{l_k^3} \{-N_3''''\}_1 & \frac{EI}{l_k^3} \{N_3''\}_1 & 0 \\ \frac{EI}{l_k^3} \{N_4''''\}_0 & \frac{EI}{l_k^3} \{-N_4''\}_0 & 0 & \frac{EI}{l_k^3} \{-N_4''''\}_1 & \frac{EI}{l_k^3} \{N_4''\}_1 & 0 \\ 0 & 0 & \frac{GJ}{l_k} \{-N_{r2}'\}_0 & 0 & 0 & \frac{GJ}{l_k} \{N_{r2}'\}_1 \end{bmatrix} \quad (0.91)$$

$$K_{Geometric} = l_k \omega^2 m x_\alpha \int_0^L \begin{bmatrix} 0 & 0 & N_1 N_{r1} & 0 & 0 & N_1 N_{r2} \\ 0 & 0 & N_2 N_{r1} & 0 & 0 & N_2 N_{r2} \\ N_1 N_{r1} & N_2 N_{r1} & 0 & N_3 N_{r1} & N_4 N_{r1} & 0 \\ 0 & 0 & N_3 N_{r1} & 0 & 0 & N_3 N_{r2} \\ 0 & 0 & N_4 N_{r1} & 0 & 0 & N_4 N_{r2} \\ N_1 N_{r2} & N_2 N_{r2} & 0 & N_3 N_{r2} & N_4 N_{r2} & 0 \end{bmatrix} d\xi \quad (0.92)$$

$$K_{Material} = \frac{K}{l_k^2} \int_0^l \begin{bmatrix} 0 & 0 & N_1'' N_{11}' & 0 & 0 & N_1'' N_{12}' \\ 0 & 0 & N_2'' N_{11}' & 0 & 0 & N_2'' N_{12}' \\ N_1'' N_{11}' & N_2'' N_{11}' & 0 & N_3'' N_{11}' & N_4'' N_{11}' & 0 \\ 0 & 0 & N_3'' N_{11}' & 0 & 0 & N_3'' N_{12}' \\ 0 & 0 & N_4'' N_{11}' & 0 & 0 & N_4'' N_{12}' \\ N_1'' N_{12}' & N_2'' N_{12}' & 0 & N_3'' N_{12}' & N_4'' N_{12}' & 0 \end{bmatrix} d\xi \quad (0.93)$$

Similar to equation (5.18) and (5.19) deviator expressions can also be added to refine the dynamic stiffness matrix RDFE to incorporate variable mechanical and/or geometric parameters:

$$\begin{aligned} W_f = & \int_{x_j}^{x_{j+1}} \left[ EI_{ave} \delta w'' w'' + K_{ave} \delta w'' \Psi' - m_{ave} \omega^2 \delta w w + (m x_\alpha)_{ave} \omega^2 \delta w \Psi \right] dx \\ & + \int_{x_j}^{x_{j+1}} \left[ \underbrace{(-EI_{ave} + EI(x))}_{EI_{DEV}} \delta w'' w'' + \underbrace{(-K_{ave} + K(x))}_{K_{B,DEV}} \delta w'' \Psi' \right] dx \\ & + \int_{x_j}^{x_{j+1}} \left[ \underbrace{-(-m_{ave} + m(x))}_{m_{DEV}} \omega^2 \delta w w + \underbrace{(-(m x_\alpha)_{ave} + m(x) x_\alpha(x))}_{m x_{\alpha,DEV}} \Psi \delta w \right] dx \end{aligned} \quad (0.94)$$

$$\begin{aligned} W_t = & \int_{x_j}^{x_{j+1}} \left[ GJ_{ave} \delta \Psi' \Psi' + K_{ave} \delta \Psi' w'' - I_{\alpha,ave} \omega^2 \delta \Psi \Psi + (m x_\alpha)_{ave} \omega^2 \delta \Psi w \right] dx \\ & + \int_{x_j}^{x_{j+1}} \left[ \underbrace{(-GJ_{ave} + GJ(x))}_{GJ_{DEV}} \delta \Psi' \Psi' + \underbrace{(-K_{ave} + K(x))}_{K_{t,DEV}} \delta \Psi' w'' \right] dx \\ & + \int_{x_j}^{x_{j+1}} \left[ \underbrace{-(-I_{\alpha,ave} + I_\alpha(x))}_{I_{\alpha,DEV}} \omega^2 \delta \Psi \Psi + \underbrace{(-(m x_\alpha)_{ave} + m(x) x_\alpha(x))}_{m x_{\alpha,DEV}} \delta \Psi w \right] dx \end{aligned} \quad (0.95)$$

The only major difference between equations (0.94) and (0.95) and equations (5.18) and (5.19) is an added bending-torsion coupling associated with  $x_\alpha$  term. The deviator matrices are then constructed in the same way leading to:

$$\begin{aligned}
W^k = & \underbrace{\frac{EI_{ave}}{l_k^3} [\delta w'' w' - \delta w^m w]_0^l + \frac{GJ_{ave}}{l_k} [\delta \Psi' \Psi]_0^l}_{\text{Uncoupled terms}} \\
& + \underbrace{\frac{K_{ave}}{l_k^2} \int_0^l \Psi' \delta w'' d\xi + \frac{K_{ave}}{l_k^2} \int_0^l w'' \delta \Psi' d\xi}_{\text{Material Coupling terms}} \\
& + \underbrace{m x_\alpha \int_0^l \Psi \delta w d\xi + m x_\alpha \int_0^l w \delta \Psi d\xi + DEV's}_{\text{Geometric Coupling terms}}
\end{aligned} \tag{0.96}$$

where,

$$\begin{aligned}
DEV = & \frac{1}{l_k^3} \int_0^l (-EI_{ave} + EI(\xi)) \langle N'' \rangle \{N''\} d\xi + \frac{1}{l_k} \int_0^l (GJ_{ave} - GJ(\xi)) \langle N_i' \rangle \{N_i'\} d\xi \\
& + l_k \omega^2 \int_0^l (m_{ave} - m(\xi)) \langle N \rangle \{N\} d\xi + l_k \omega^2 \int_0^l (I_{ave} - I_\alpha(\xi)) \langle N_i \rangle \{N_i\} d\xi \\
& + \frac{1}{l_k^2} \int_0^l (-K_{ave} + K(\xi)) \langle N'' \rangle \{N_i'\} d\xi + \frac{1}{l_k^2} \int_0^l (-K_{ave} + K(\xi)) \langle N_i' \rangle \{N''\} d\xi
\end{aligned} \tag{0.97}$$

Due to the unavailability a closed form symbolic integration for the deviator terms. The deviator terms rely on a numerical 16 point gauss quadrature integration.

## 6.4 Numerical Tests

### 6.4.1 Example of a quadratic tapered wing.

For the composite wing-box (Figure 6-1(b)) with tabulated properties displayed in Table 6.1 the natural frequencies were determined for a quadratic tapered wing. Mechanical Properties are also displayed in the paper published by Eslimy-Isfahany and Banerjee (1997). For a CAS configuration the fibre orientation on, the top is [+15]<sub>2</sub> degrees, bottom [-15]<sub>2</sub> degrees and the sides [15/-15] degrees.

Using a pre-processor developed specifically for thin-walled Composite box-beams based on the formulation presented by Armanios and Badir (1995) and Berdichevsky *et al* (1992) the effective rigidities for graphite/epoxy are obtained to be  $EI = 4.43$  MPa for

bending,  $GJ= 1.19$  MPa for torsion and  $K=1.75$  MPa for coupled bending-torsion rigidities at the wing root. The effective rigidities of graphite/epoxy are plotted for multiple ply angles (Figure 6-3). From this figure the maximum value for the bending-torsion coupling rigidity is observed to occur at 15 degrees. Along the wing length, the stiffness properties will vary according to the order of taper.

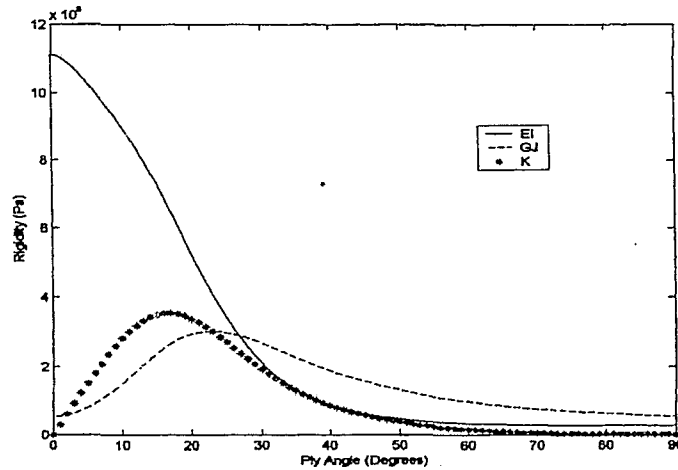


Figure 6-4: Plot of Rigidities vs Ply angle for a graphite/epoxy composite.

Table 6-1: Material Properties of a graphite/epoxy composite Laminate

$E_L$	206.92 GPa	Width	50.8 cm
$E_T$	5.17 GPa	Taper Coefficient	-0.5
$G_{LT}$	3.10 GPa	Depth	10.16 cm
$\nu_{TT}$	0.25	Taper Coefficient	-0.5
Thickness of Layer	1.016 mm	Length	2.03 m
Mass centre offset		-11.9 cm	

The convergence test results for the first three natural frequencies of the quadratic tapered wing are presented in Figures 6-4 to 6-6. The comparison is made between the numerical results obtained from the 'DFE with no deviators', 'RDFE incorporating the deviator terms' and the reference natural frequencies were obtained from 120 conventional beam Finite Elements. The FEM model is based on cubic Hermite and linear approximation for bending and torsion displacements, respectively, and a constant mass matrix.

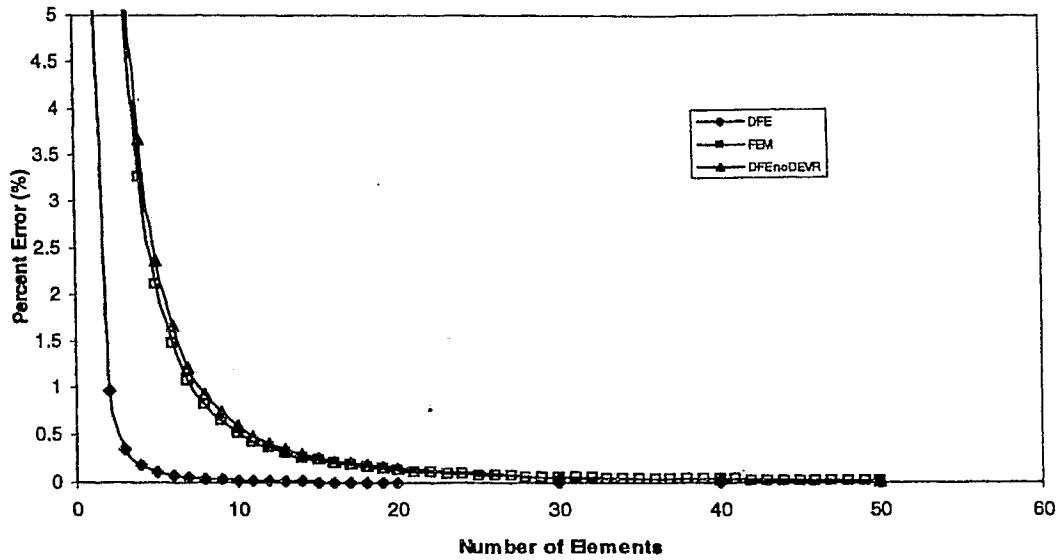


Figure 6-5: Convergence of dually quadratic tapered wing-box for the first natural frequency.

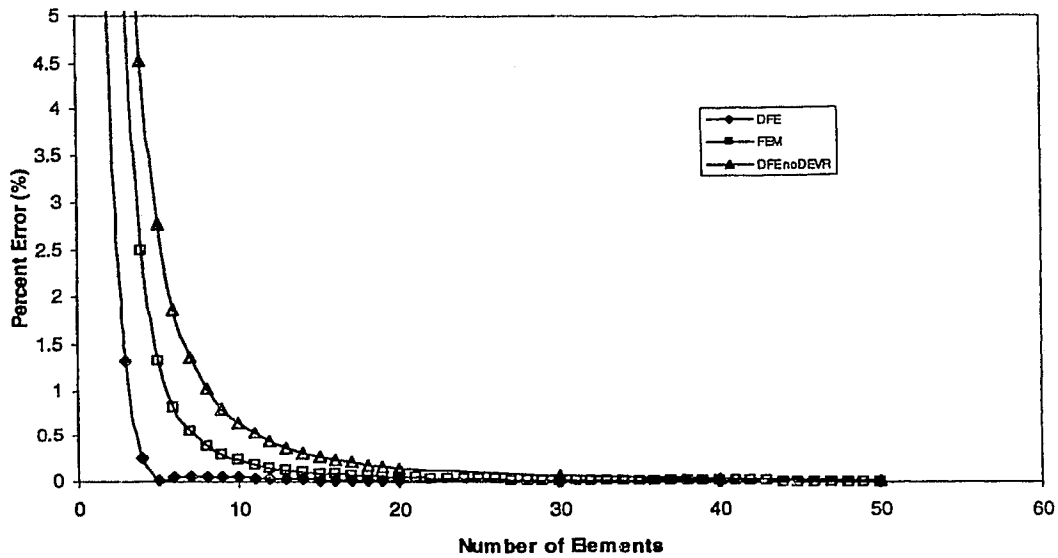


Figure 6-6: Convergence of dually quadratic tapered wing-box for the second natural frequency

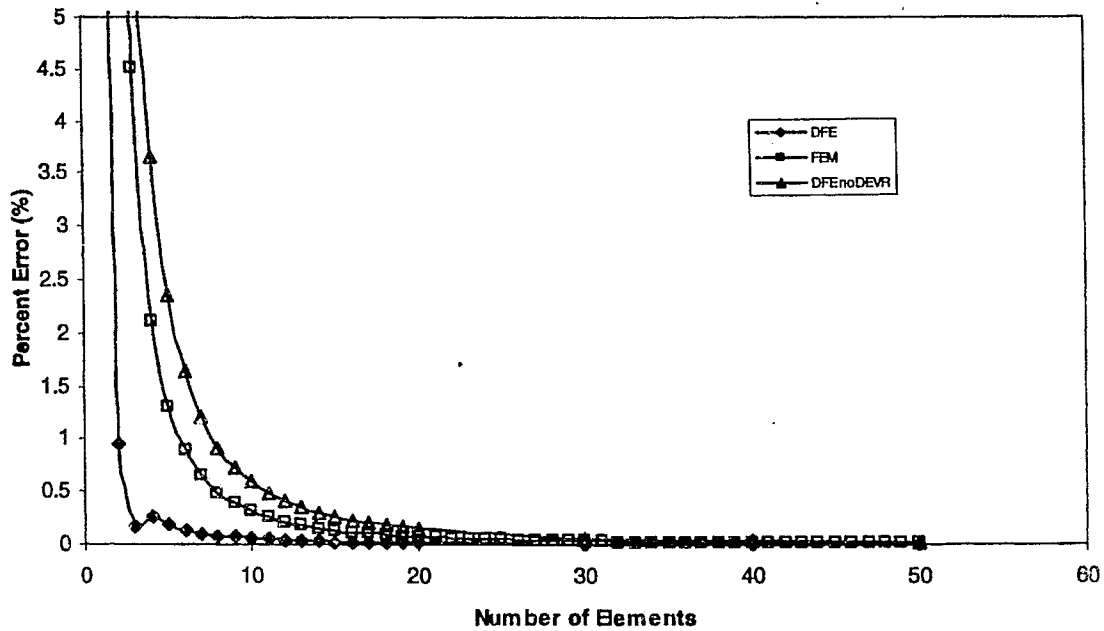


Figure 6-7: Convergence of dually quadratic tapered wing-box for the third natural frequency.

As it can be seen, in this case, the FEM converges faster than the DFE when deviators are not used. By including the deviator terms the convergence rates for all three frequencies increases significantly. This consistent convergence using the deviators shows that there are no apparent limitations on these terms. Referring to chapter 5, the deviators became more effective for higher taper angles. The quadratic tapered wing is now more complex such that the degrading effects resulting from numerical error is so small that they do not affect the positive refining results of the deviators.

A comparison is made between the fundamental natural frequencies of the graphite/epoxy composite wing obtained from FEM and DFE methods using different meshes. It is observed that the FEM errors for the first, second, and third natural frequencies, respectively, are approximately 20, 50 and 50 times higher than the corresponding DFE errors (see Table 6-2).

**Table 6-2: Fundamental frequencies in Hz for a graphite/epoxy quadratic tapered composite wing**

Mode number	120 elements FEM	10 elements DFE	ERROR	10 Elements FEM	ERROR
1 <sup>st</sup>	31.74	31.73	0.025 %	31.57	0.53 %
2 <sup>nd</sup>	74.36	74.40	0.050 %	74.19	0.24 %
3 <sup>rd</sup>	110.44	110.50	0.056 %	110.09	0.31 %

### 6.4.2 Cubic tapered wing.

Let us consider a dually cubic tapered wing-box with the same mechanical properties as in the previous example. The FEM and DFE convergence results for the wing's first 5 natural frequencies are presented in Figures 6-7 through 6-11. By implementing a cubic variation the deviators associated with the DFE method amplify the convergence in contrast to a linearly varying cross-section of low taper ratio seen previously in Chapter 5.

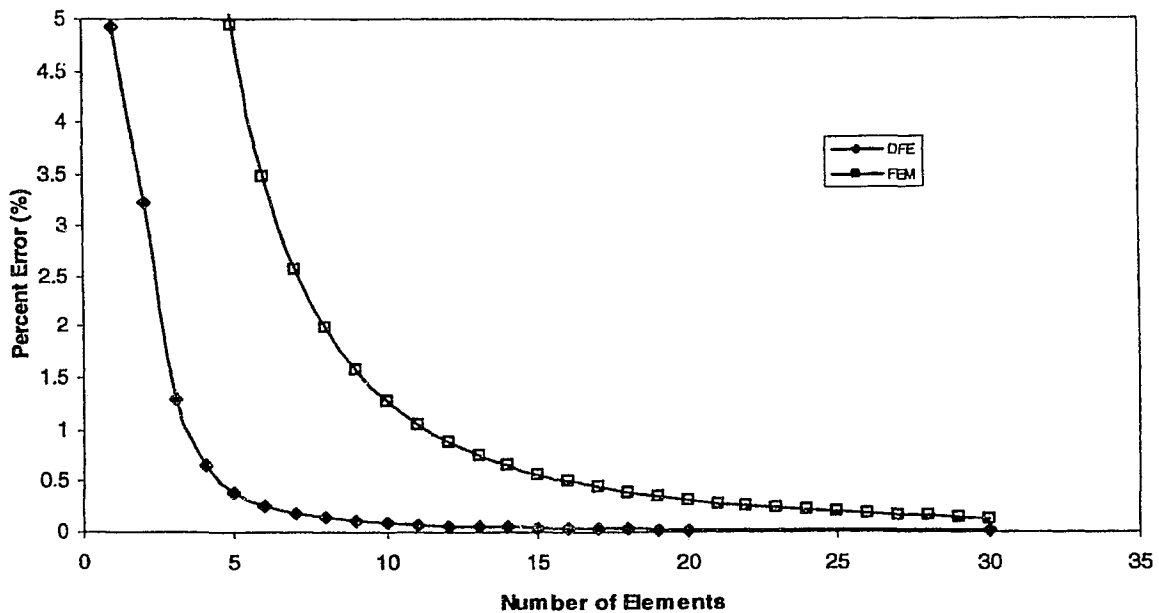


**Figure 6-8: Convergence of dually cubic tapered wing-box for the first natural frequency.**

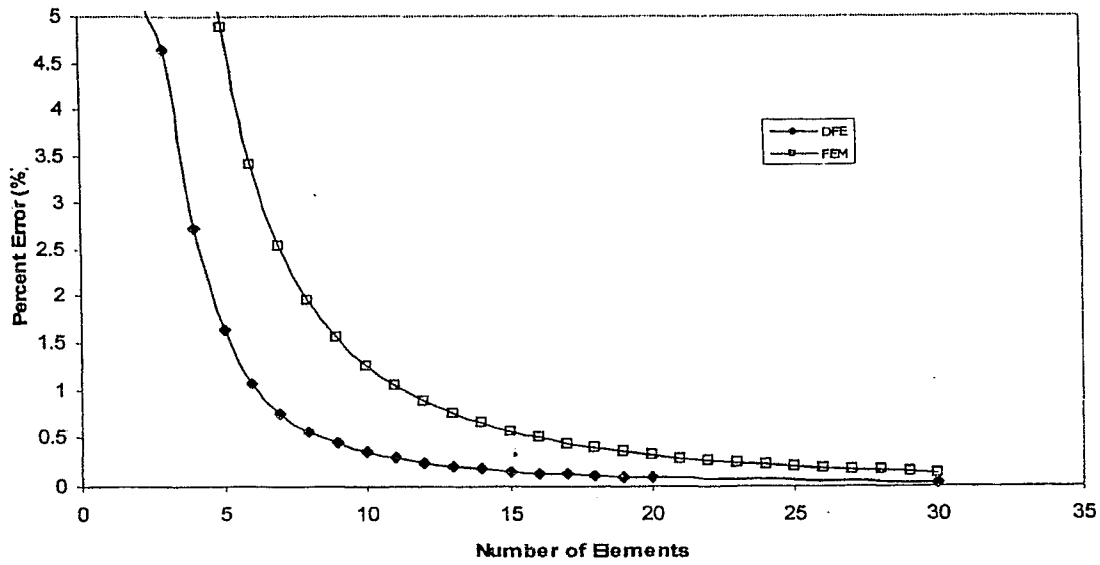


Figure 6-9: Convergence of dually cubic tapered wing-box for the second natural frequency.

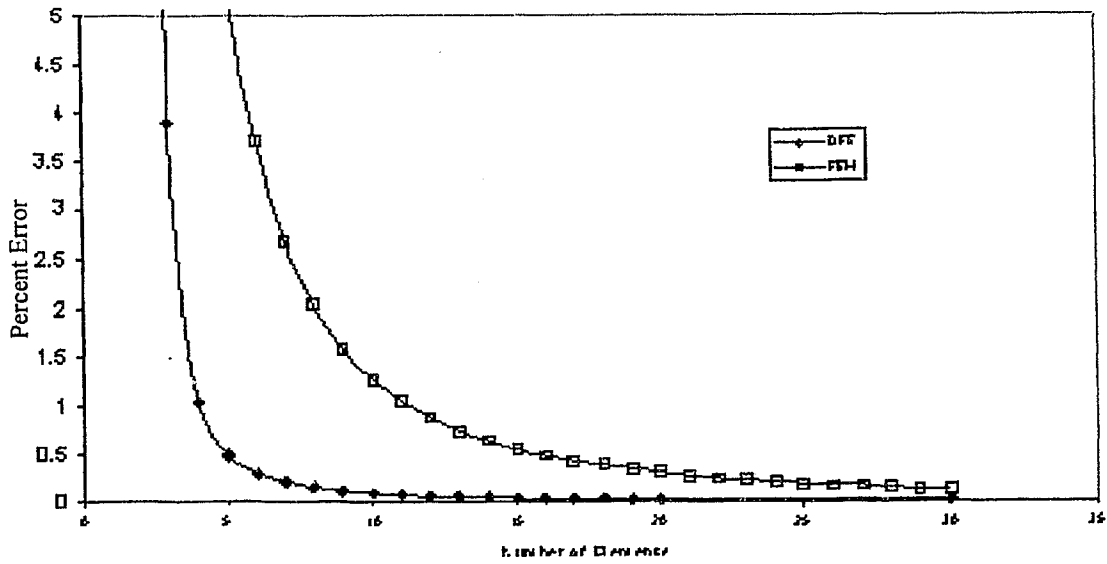


Figure 6-10: Convergence of dually cubic tapered wing-box for the third natural frequency.

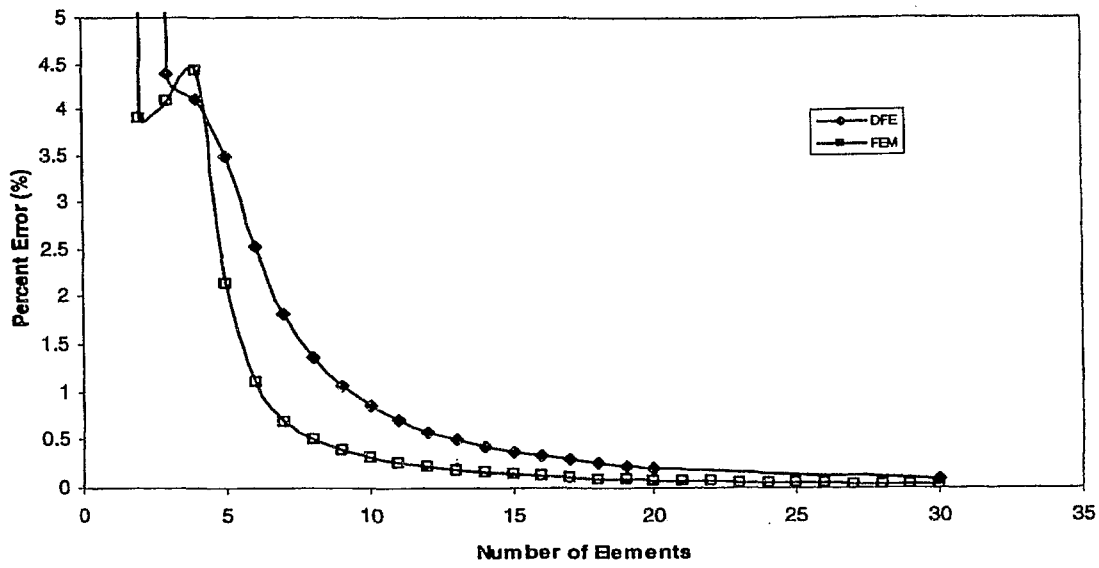


Figure 6-11: Convergence of dually cubic tapered wing-box for the fourth natural frequency.

Only for the fourth natural frequency (Figure 6-11) greater convergence rates are obtained from the FEM, which is irregular since all other convergence tests favoured the DFE. In order to further investigate these results, the numerical values for frequencies are presented in Table 6-3.

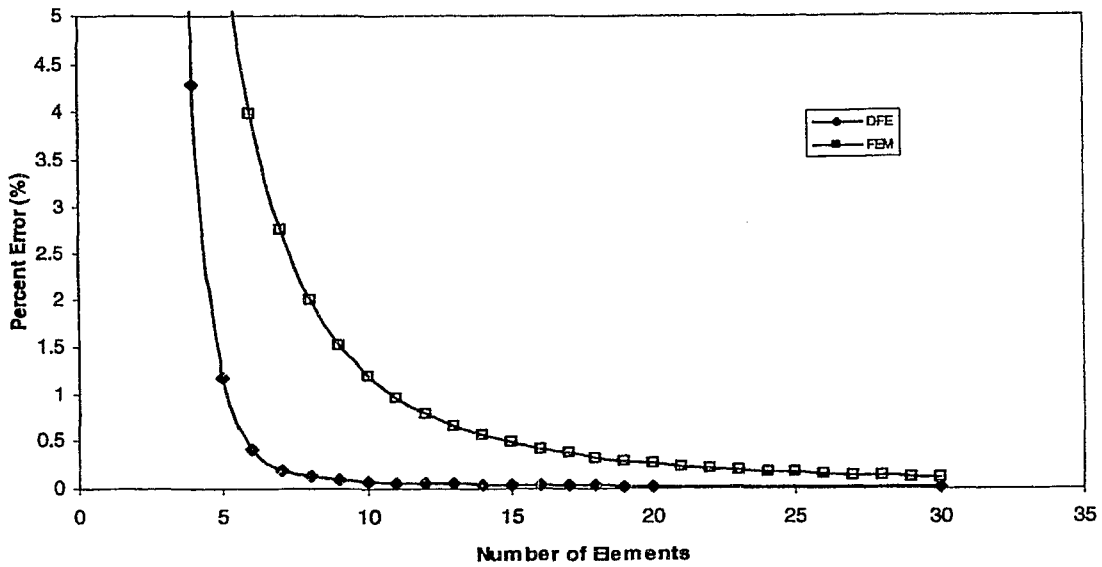
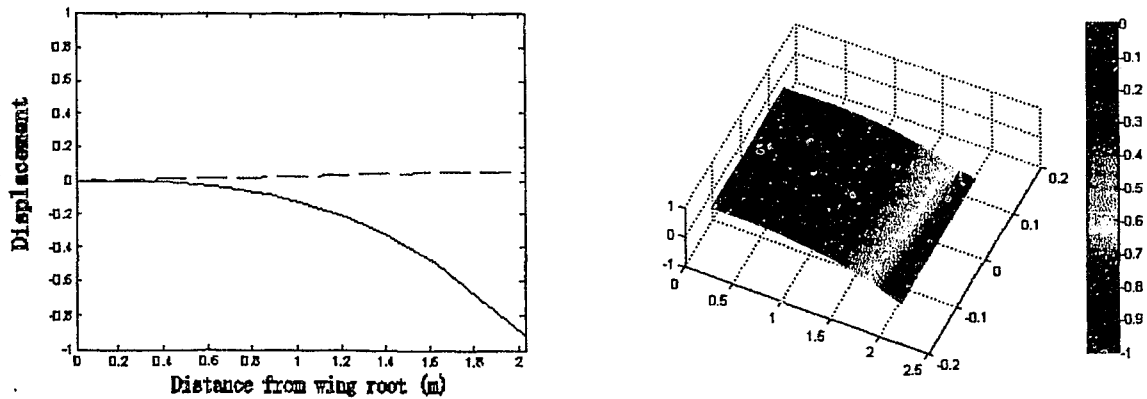


Figure 6-12: Convergence of dually cubic tapered wing-box for the fifth natural frequency.

**Table 6-3: Natural frequencies for a dually cubic tapered graphite/epoxy composite wing.**

Mode number	200 elements FEM (Hz)	10 elements DFE (Hz)	Percent error	10 Elements FEM (Hz)	Percent error
1 <sup>st</sup>	13.50	13.52 (B)	0.09	13.33	1.27
2 <sup>nd</sup>	40.58	40.72 (B)	0.35	40.07	1.26
3 <sup>rd</sup>	78.29	78.37 (T)	0.10	77.28	1.29
4 <sup>th</sup>	85.93	86.67 (BT)	0.86	85.65	0.32
5 <sup>th</sup>	131.36	131.46 (BT)	0.07	129.80	1.19

It is observed from the tabulated results that the DFE is significantly more accurate than the FEM by a factor of greater than 10. These results are expected as the DFE formulation is designed to be more accurate for complex elements such as the present dual cubic tapered model. The natural modes for the cubic tapered graphite/epoxy wing are displayed in Figure 6-13 to Figure 6-17. The modes of deformation have been plotted in both 2-D and 3-D spaces and have been normalized to better distinguish the modes as bending, torsion or coupled bending-torsion.



**Figure 6-13: First predominantly bending mode of vibration for a composite graphite/epoxy cubic tapered wing in both 2-D and 3-D plots. For the 2-D plot the bending displacement is represented by a solid line (-) and torsion is represented by a dashed line (--).**

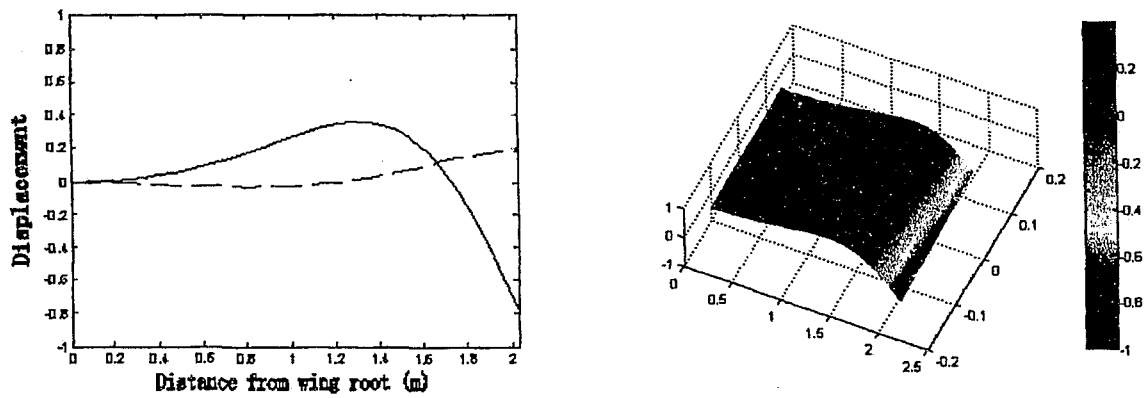


**Figure 6-14: Second predominantly bending mode of vibration for a composite graphite/epoxy cubic tapered wing in both 2-D and 3-D plots. For the 2-D plot the bending displacement is represented by a solid line (-) and torsion is represented by a dashed line (--).**

From the first two plots in Figure 6-13 and Figure 6-14 it can be seen that the modes are predominantly bending with slight influence of twist. For the higher modes a stronger influence of torsion is observed particularly for the third mode in Figure 6-15 where the mode is primarily torsion.

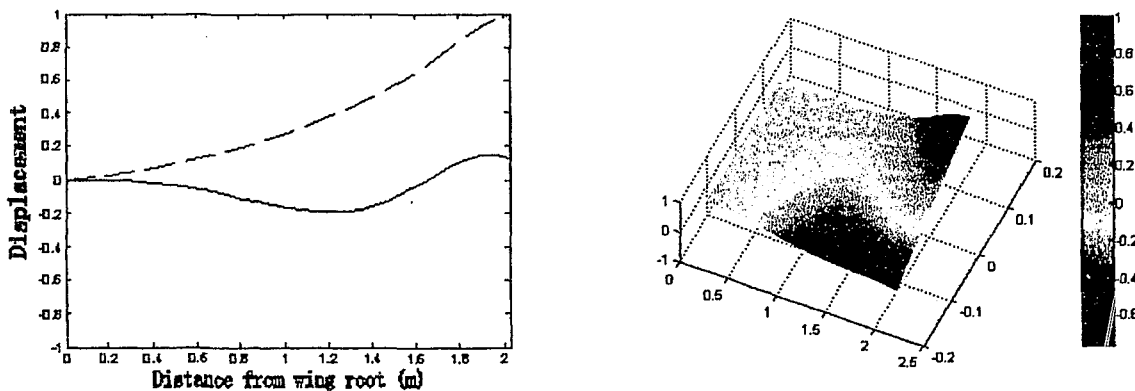


**Figure 6-15: Third predominantly torsion mode of vibration for a composite graphite/epoxy cubic tapered wing in both 2-D and 3-D plots. For the 2-D plot the bending displacement is represented by a solid line (-) and torsion is represented by a dashed line (--).**

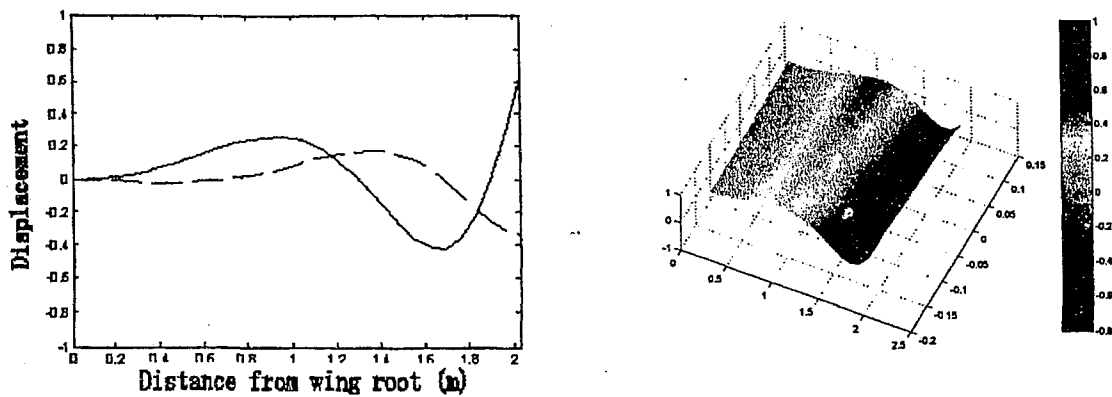


**Figure 6-16: Fourth bending-torsion mode of vibration for a composite graphite/epoxy cubic tapered wing in both 2D and 3-D plots. For the 2-D plot the bending displacement is represented by a solid line (-) and torsion is represented by a dashed line (--).**

The bending-torsion coupling is apparent in the last two modes extracted, in Figure 6-16 and Figure 6-17 for the fourth and fifth free vibration modes. Although the interpolated surface plot used in MATLAB<sup>®</sup> is exceptionally useful in visualizing these modes the cubic taper has been stretched into a rectangular surface such that the 3-D surface plots are not necessarily to scale, but can still be useful differentiating the modes as bending or torsion.

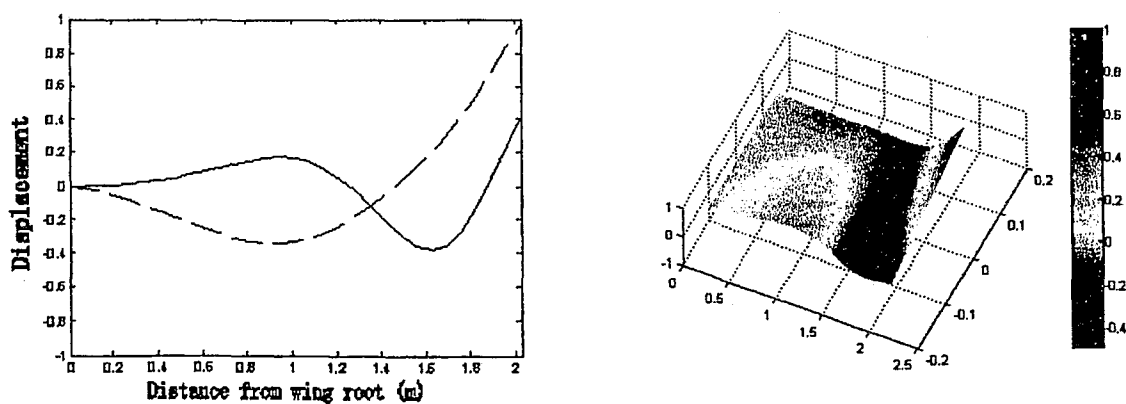


**Figure 6-17: Fifth bending-torsion mode of vibration for a composite graphite/epoxy cubic tapered wing in both 2D and 3-D plots. For the 2-D plot the bending displacement is represented by a solid line (-) and torsion is represented by a dashed line (--).**

## 6.6 Conclusion

The free vibration analysis of thin-walled composite wing-boxes with quadratic and cubic tapers is presented. By implementing the CAS configuration and non-coincident mass and shear axes, the wing exhibits dually coupled vibration. The natural frequencies and modes of deformation have been extracted using the three methods, conventional FEM, DFE, and the *refined DFE* (DFE with deviators). These deviators take into account the variable geometric and/or material parameters of the wing model over each DFE. The convergence of the refined DFE (RDFE) is validated in comparison with the FEM method for multiple tapered geometries and ply orientations. The RDFE method provides a much higher convergence rate than classical finite elements. The corresponding natural modes of vibration were also evaluated and plotted using the advanced plotting features in MATLAB<sup>®</sup>. The programs coded in MATLAB<sup>®</sup> are discussed in the Appendix.

## Chapter 7 Conclusion

### 7.1 *Concluding Remarks*

The free vibration analysis of structures is a crucial part in the design of mechanical and aerospace structures. If the vibration of structures is neglected, this could lead to catastrophic failure of both static and dynamic systems. To prevent such failures an accurate investigation into the vibration response of a system must be carried out. Three of the most appealing techniques now available are the finite element method (FEM), dynamic stiffness matrix (DSM) method and the dynamic finite element (DFE) method. The methods each provide different advantages and disadvantages depending on the model considered and the output desired.

For the free vibration of wings, the FEM provides a quick solution for the natural frequencies and corresponding modes of deformation. The systematic procedure used to formulate the element mass and stiffness matrices, with a Galerkin weighted residual method, shows a clear advantage over other weighted residual and variational methods. Also, the generality of the FEM step-by-step procedure allows for easy implementation to more complex elements.

The application of the DSM for the free vibration analysis of metallic and composite beam structures is well established. The formulation is based on a single frequency dependent stiffness matrix possessing both mass and stiffness properties. The implementation of the exact member theory, for uniform beams, gives this method the capability to converge on any fundamental frequency using only one element. The accuracy and CPU time associated with the post-processing of the DSM is a particularly attractive for the analysis of uniform beams. Although from the observed results in Chapter 5, the accuracy of the technique is less efficient for complex non-uniform elements.

The DFE has also been established for homogenous metallic beams. The goal of the present research was to apply the DFE formulation to the free vibrations of laminated composite wing-beams. The technique combines the advantages of both the DSM and

FEM by providing a viable method for determining the natural frequencies of a structure. Based on the finite element method the DFE provides the same systematic step by step procedure to formulate the element stiffness matrix. The frequency dependent stiffness matrix adopted from the dynamic stiffness matrix method is produced by implementing dynamic trigonometric shape functions (DTFS). These DTFS's are based on the solution to the governing uncoupled differential equations and also differentiate the DFE from the FEM.

From the observed results the DFE provides the fastest convergence to the exact solution for complex elements. The method provides such accurate results for non-uniform beams by implementing a deviator matrix, which differentiates the DFE from the DSM and FEM. From the results pertaining to taper configurations for both the solid rectangular cross-section in Chapter 5 and the thin-walled wing box-section in Chapter 6 the deviators provide a much more accurate solution to the resonant frequencies based on the coarsest mesh. Although the deviators are designed to increase convergence, certain limitations do exist and must be acknowledged (outlined in section 5.5.2). These limitations only exist for small taper ratios where uniform elements are sufficient to achieve an accurate solution to the structure. For highly complex tapers, such as quadratic or cubic, the DFE's observed results present a clear advantage over the other methods considered. Therefore the DFE is valid for elements which exhibit high complexity.

Generally, a finite element based model incorporates numerical integrations to integrate the integrand in the weak form of the governing differential equations of motion. Numerical (e.g., Gauss quadrature) integration could be avoided if a closed form solution to these integrals can be reached. The incentive of producing element matrices based purely on algebraic equations is in the reduced CPU time required to execute a finite element based program. In the conventional FEM this is easily achieved using polynomial shape functions. In the present DFE formulation, due to the frequency dependent shape functions, extensive symbolic integrations have been undertaken using MAPLE<sup>®</sup> to produce an element dynamic stiffness matrix based completely on algebraic expressions. Symbolic expressions have been achieved for both uniform and tapered formulations in Chapter 4 and Chapter 5, respectively. Unfortunately a symbolic element matrix for the composite wing-box configuration prepared in Chapter 6 could not be

achieved due to the complexity of the formulation. A Gauss quadrature technique, using 16 integration points was then used to evaluate the integral expressions numerically.

The graphical user interface (GUI) prepared in the Appendix was coded in MATLAB<sup>®</sup>. Although a more efficient code execution could have been achieved using a programming language such as *FORTRAN*, MATLAB<sup>®</sup> was chosen since it provides an advanced graphical user interface. The extensive plotting features in MATLAB<sup>®</sup> give the user the capability to visualize the modes of deformation in two and three dimensions. The 3-D modes display a more visual representation of the bending and torsion deformations over the 2D plots.

It is an advantage to incorporate 3-D plots as it is easier to distinguish the natural modes of vibration as bending, torsion or bending-torsion. In addition, MATLAB<sup>®</sup> has the capability to convert an m-file function into a stand-alone program based on C++ code generation. Although the stand-alone feature in MATLAB<sup>®</sup> has not been utilized to its fullest extent, however, it presents an attractive factor in the decision of which program to use.

In a glance, by implementing a progressive technique in the development of a complete composite wing model, errors in the formulation and results are prevented. The DFE is formulated for composite aircraft wings and is validated in comparison with other attractive methods such as the DSM and FEM. Advantages and disadvantages are discussed for wings of various geometries and stacking sequences. It is also demonstrated that the DFE can be more advantageously applied to vibrating beam-like periodic structures constructed from complex elements and where higher modes of vibration are desired.

In summary, the proposed DFE provides design engineers with a powerful tool for the preliminary design stage where a huge FEM mesh is not preferred. Once the preliminary design is formalized, an elaborated refined FEM model can then be created for detailed analysis and fine tuning of the model.

## **7.2 Future Work**

The Dynamic finite element method will be extended to Timoshenko beam theory where the inclusion of shear deformation and rotary inertia are considered. The current formulation presented in Chapter 6 for a composite wing-box can also be extended to rotor blade design by addition of an axial force in the governing differential equations of motion. A composite rotor blade design would lead to analysis of aircraft propellers, helicopter blades and rotor and wind turbine stators in new generation of jet engines equipped with axial compressors. From the observed results for complex geometries published by Hashemi and Richard (1999), Hashemi (1998), Hashemi and Borneman (2003), and Hashemi and Borneman (2004), the DFE produces the highest convergence rates compared with conventional FEM and DSM methods. With the added complexity of the axial force produced by blade rotation, the deviators associated with the DFE formulation would result in even higher convergence rates compared to other existing methods.

## **Appendix A: MATLAB<sup>®</sup> Dynamic Finite Element Wing Analysis.**

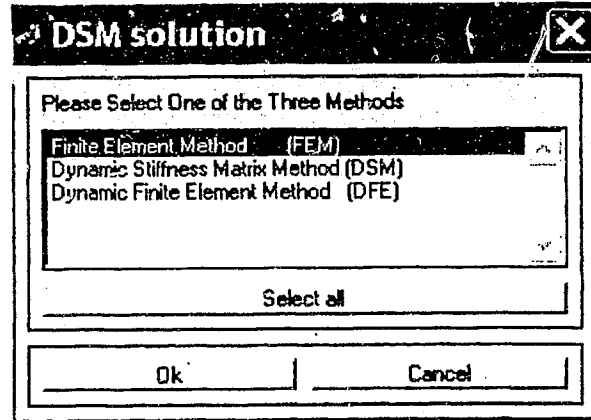
### ***A.1 Introduction***

A MATLAB<sup>®</sup> based program was developed to calculate the natural frequencies of the free vibration of a laminated composite wing. The graphical user interface (GUI) has been exploited to give the user a simple method for displaying the natural frequencies and modes of coupled free vibration. Two programs are explained in detail in this chapter so that any user can use these programs proficiently. The first program is the flat composite cantilevered beam program which is designed to find the natural frequencies and corresponding modes for any solid rectangular cross-section composite. This beam program is extended to models that are tapered by chord if desired. The second program is designed for complex geometric cross-sections, specifically closed section wing-box configurations.

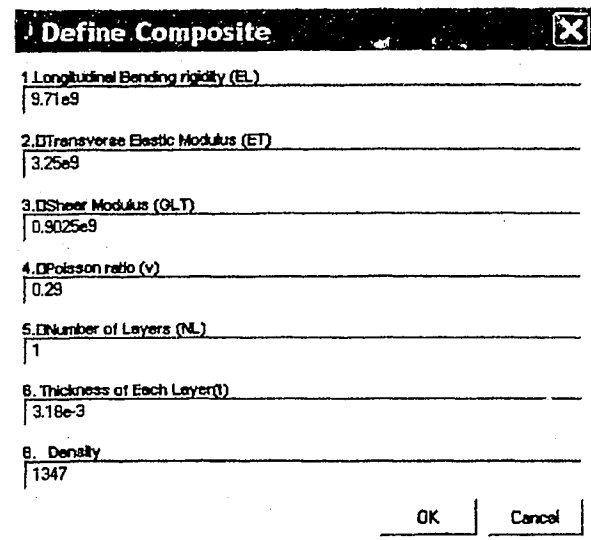
The wing-box configuration has the capability to account for mass distributions in the wing structure (e.g., engine) leading to an offset of the mass axis from the elastic axis. This offset produces a second coupling due to the mass distribution and geometry of the wing. Both programs incorporate a pre-processor to evaluate the effective stiffness of the composite lay-up. The first program utilizes the classical laminate theory to calculate the effective rigidities of the system. The second program incorporates the circumferentially asymmetric stiffness (CAS) configuration to evaluate the effective stiffness for a composite closed section wing-box design.

## A.2 DFE Uniform/Tapered Composite Beam Program

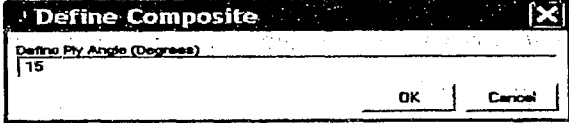
The first step for the analysis of a composite uniform or tapered wing is to select the desired method. Select the method that best fits the desired solution. For example, if multiple frequencies and modes are required, one would choose the finite element method (FEM). For a quick accurate value for a particular frequency of a uniform beam the dynamic stiffness method would be of interest. For more complex geometries such as high tapers angles the dynamic finite element method may be used to achieve an accurate result. To select a method either double click one of the listed methods or highlight the selection and then click 'Ok'



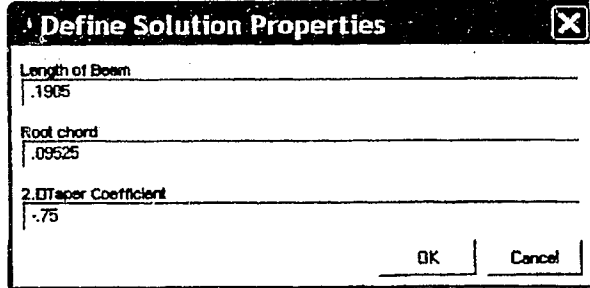
Next, the mechanical properties of the composite must be known. The principal values for longitudinal elastic modulus  $E_L$ , transverse elastic modulus  $E_T$ , shear modulus  $G_{LT}$ , Poisons ratio  $\nu_{LT}$  are required so that the pre-processor can evaluate the effective rigidities of the beam. The program is not limited to only one layer. Multiple layers can be input at different fibre angles.



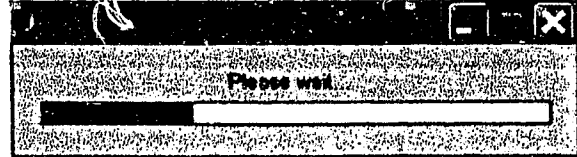
The fibre angles are measured from the fibre direction to the span wise direction of the model. The fibre angles are input one at a time from top of laminate to bottom. The stacking sequence is at the user's discretion, but user should be aware that the program is designed for symmetric stacking only. This type of stacking will produce the coupled bending-torsion composite behaviour.



The geometry of the solid rectangular cross-section beam must be defined. The corresponding boxes for beam length, root chord, and taper coefficient are required. If a uniform beam is desired than the user may set the taper coefficient to zero. The taper is limited to span-wise reducing chord only.



A simple and convenient wait bar has been implemented to give the user a sense of when the program will terminate.



The solution properties are needed to define what type of solution output is required. The range of elements is needed and range of natural frequencies is input to define mesh refinement and number of modes desired. The upper and lower bound frequencies are input for the initial frequency. The accuracy of the natural frequencies can be set to any desired decimal greater than double precision. The accuracy is based on the bisection method in conjunction with the Wittrick-Williams algorithm.

**Define Solution Properties**

1. Initial Element Range  
1

2. Final Element Range  
5

3. Initial Range of Frequencies  
1

4. Final Range of Frequencies  
5

5. Upper Bound Frequency  
1100

6. Lower Bound Frequency  
0

7. Accuracy (Input Number of Decimals; Eg 1=>0.1, 2=>.01)  
5

8. Output Modes 1=yes and 0=no  
0

OK Cancel

The solution is output in a list box. The output natural frequencies are based on the largest number of elements selected in the solution properties, to ensure the results are based on the most refined mesh.

**DFE solution**

Natural frequencies

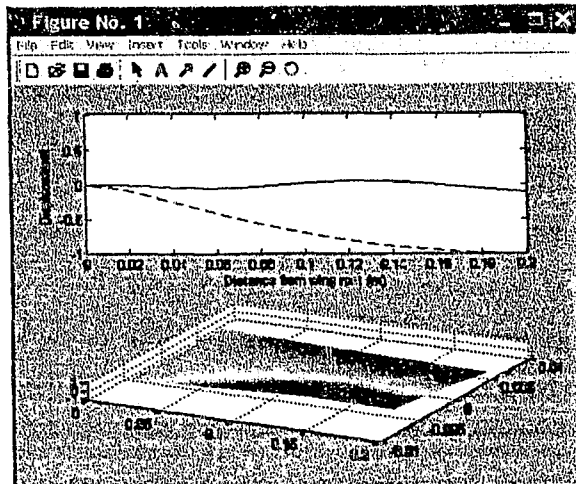
30.8185  
192.864  
538.395  
648.732  
1053.42

Select all

Ok Cancel

To display the modes the user can double click on the values in the list box, then the corresponding mode will pop-up. The modes are displayed in both 2D and 3-D. The 3-D mode was added to give a visual representation of the actual deformation shape of the beam. For tapered beam configurations the 3-D modes will still be displayed in a rectangular plane.

An extra output is performed which corresponds to the frequency data for each element in the element range. This data is output in a 2D array of natural frequencies, columns being the frequency number and rows being the number of elements. A lotus 123 file is written which can be opened by any database. This feature is particularly of interest for convergence analysis.

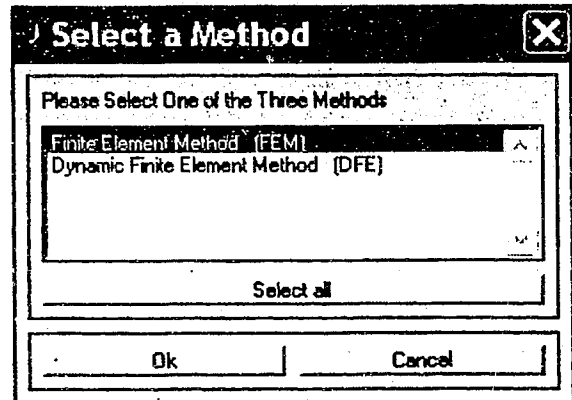


### ***A.3 DFE Wing Analysis for Composite Wing-Box Sections***

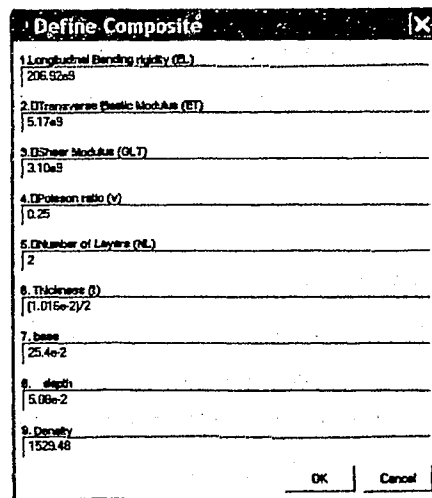
DFE Wing Analysis is designed for determining the free vibration response of composite thin-walled wing-box. The response of the wing can be solved using either the finite element method (FEM) or the dynamic finite element (DFE) method. The wing is modeled as beam assemblies with 3 degrees of freedom per node. The circumferentially asymmetric stiffness (CAS) configuration is employed to ensure the response is only coupled between bending and torsion.

The initial pop-up menu is 'Select a Method' list box. This is where the user decides which method to use for the free dually coupled vibration of a composite wing. The finite element should be selected if the user desires a quick calculation of multiple frequencies. For more complex geometries such as tapers (e.g., Linear, quadratic, cubic) then the DFE should be selected.

Unfortunately the DFE will run slower for tapered wings compared to the previous program for solid rectangular cross-sections. This runtime is slower due to the unavailability a closed form symbolic integration for the deviator terms. The deviator terms rely on a numerical 16 point gauss quadrature integration.



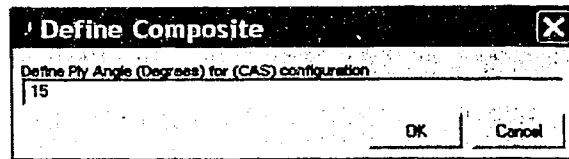
The mechanical properties of the composite are input in the corresponding boxes to the right similar to the previous described program. The difference in this program is that the layers are limited to multiples of 2 since they must correspond to the circumferentially asymmetric stiffness (CAS) configuration used in the pre-processor to evaluate the effective rigidities of a composite box type section.



The composite fibre angle is measured from span wise direction of the wing. The angle is only needed to be entered once, since the pre-processor automatically sets up the CAS configuration of  $[\theta]_2$ ,  $[-\theta]_2$ , for the top and bottom skins respectively and  $[\theta/-\theta]$  for the sides.

Then, the composite wing geometry must be entered. The root width and depth must be input and the corresponding taper coefficients as well. The centre offset is defined based on the mass distribution of the wing and must be pre-calculated prior to program execution. This mass axis offset from the elastic axis produces a second bend-twist coupling.

Similar to the previously described solution properties, they are needed to define what type of solution output is required. The range of elements is needed and range of natural frequencies is input to define mesh refinement and number of modes desired. The upper and lower bound frequencies are input for the initial frequency. The accuracy of the natural frequencies can be set to any desired decimal greater than double precision. The accuracy is based on the bisection method in conjunction with the Wittrick-Williams algorithm.

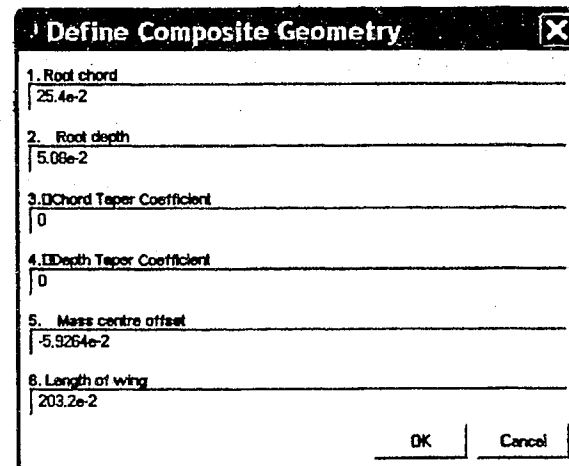


**Define Composite**

Define Ply Angle (Degrees) for (CAS) configuration

15

OK Cancel



**Define Composite Geometry**

1. Root chord  
25.4e-2

2. Root depth  
5.08e-2

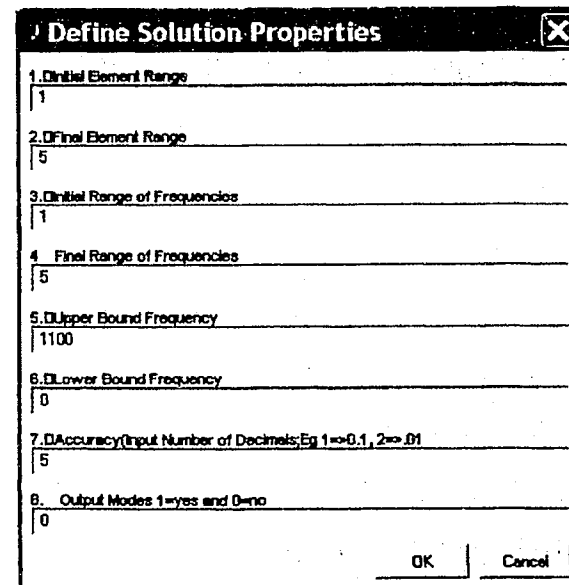
3. DChord Taper Coefficient  
0

4. DDepth Taper Coefficient  
0

5. Mass centre offset  
-5.9264e-2

6. Length of wing  
203.2e-2

OK Cancel



**Define Solution Properties**

1. DInitial Element Range  
1

2. DFinal Element Range  
5

3. DInitial Range of Frequencies  
1

4. DFinal Range of Frequencies  
5

5. DUpper Bound Frequency  
1100

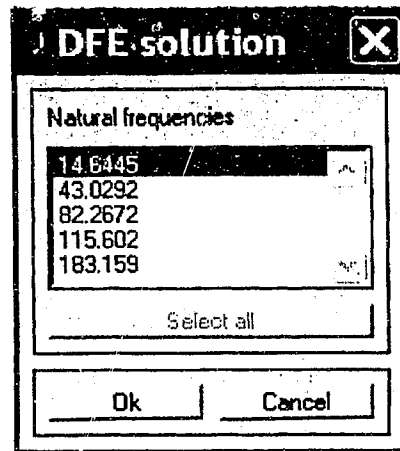
6. DLower Bound Frequency  
0

7. DAccuracy (Input Number of Decimals; Eg 1=>0.1, 2=>.01)  
5

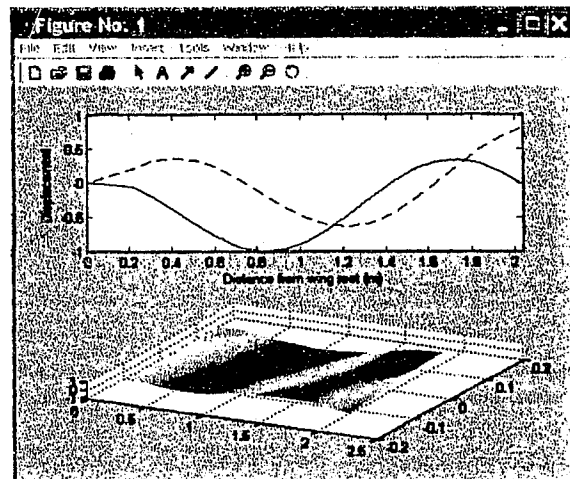
8. Output Modes 1=yes and 0=no  
0

OK Cancel

The solution is output in a list box. The output natural frequencies are based on the largest number of elements selected in the solution properties, to ensure the results are based on the most refined mesh.



To display the modes the user can double click on the values in the list box, then the corresponding mode will pop-up. The modes are displayed in both 2D and 3-D. The 3-D mode was added to give a visual representation of the actual deformation shape of the beam. For tapered beam configurations the 3-D modes will still be displayed in a rectangular plane.

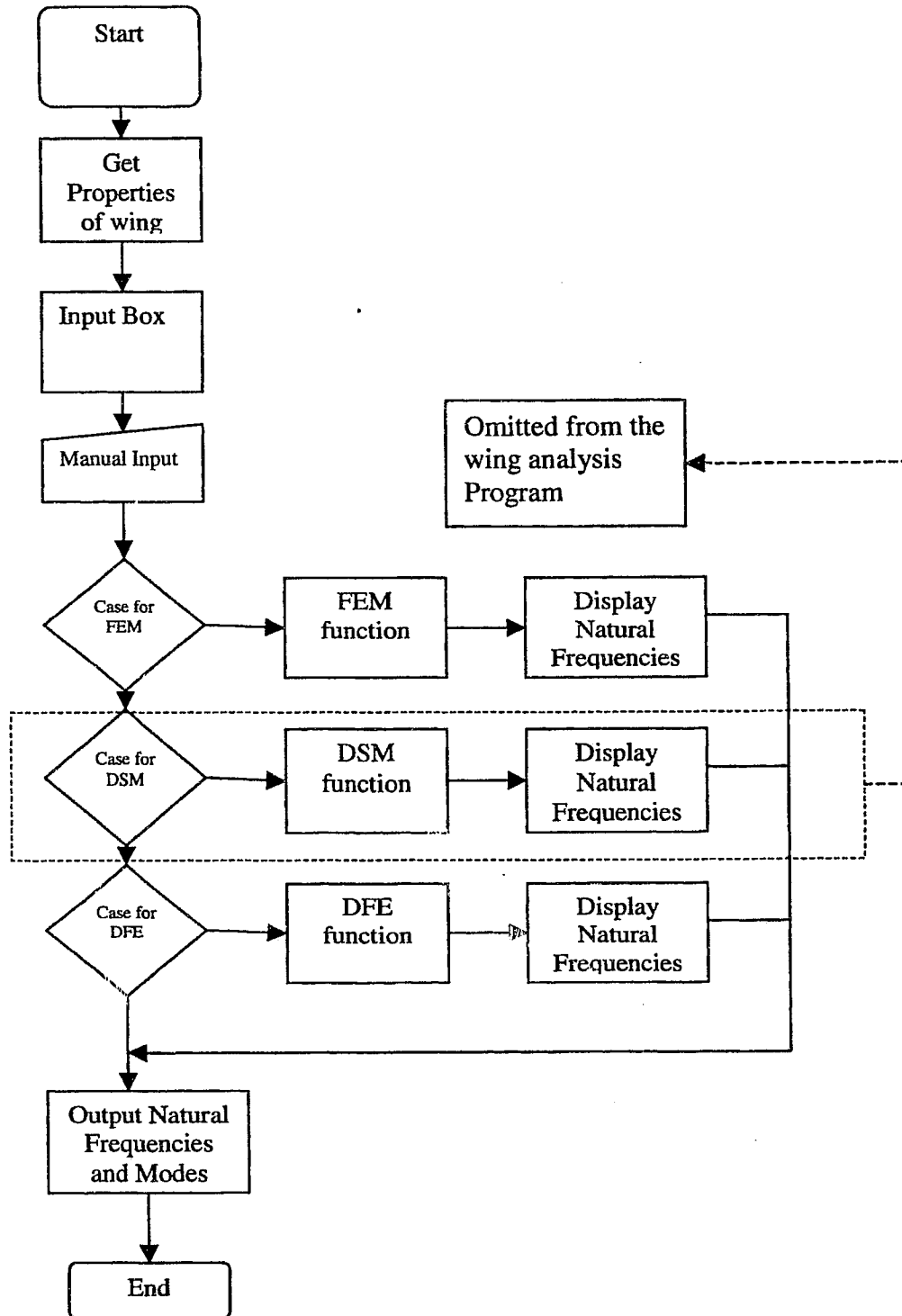


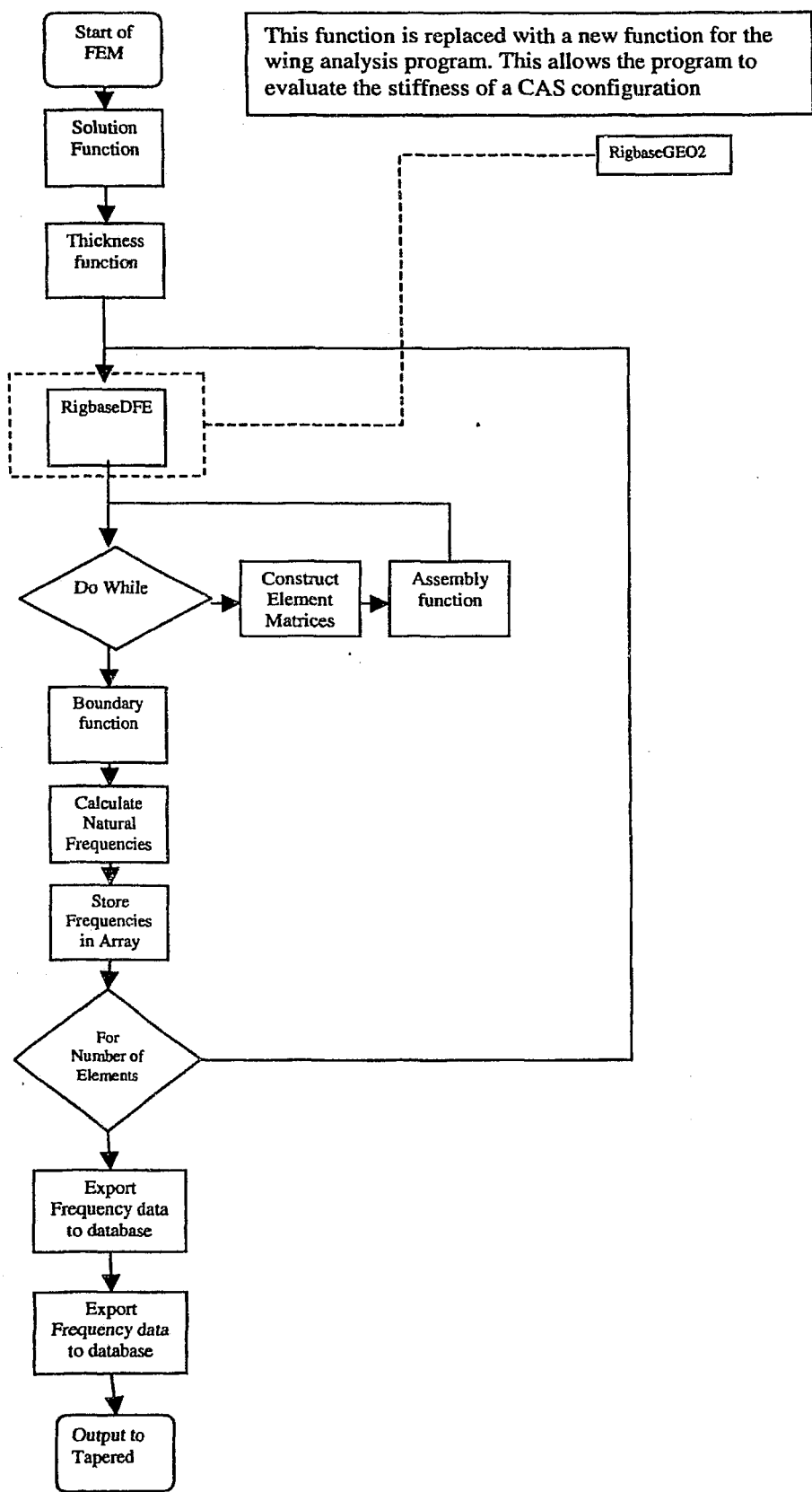
An extra output is performed which corresponds to the frequency data for each element in the element range. This data is output in a 2D array of natural frequencies, columns being the frequency number and rows being the number of elements. A lotus 123 file is written which can be opened by any database. This feature is particularly of interest for convergence analysis.

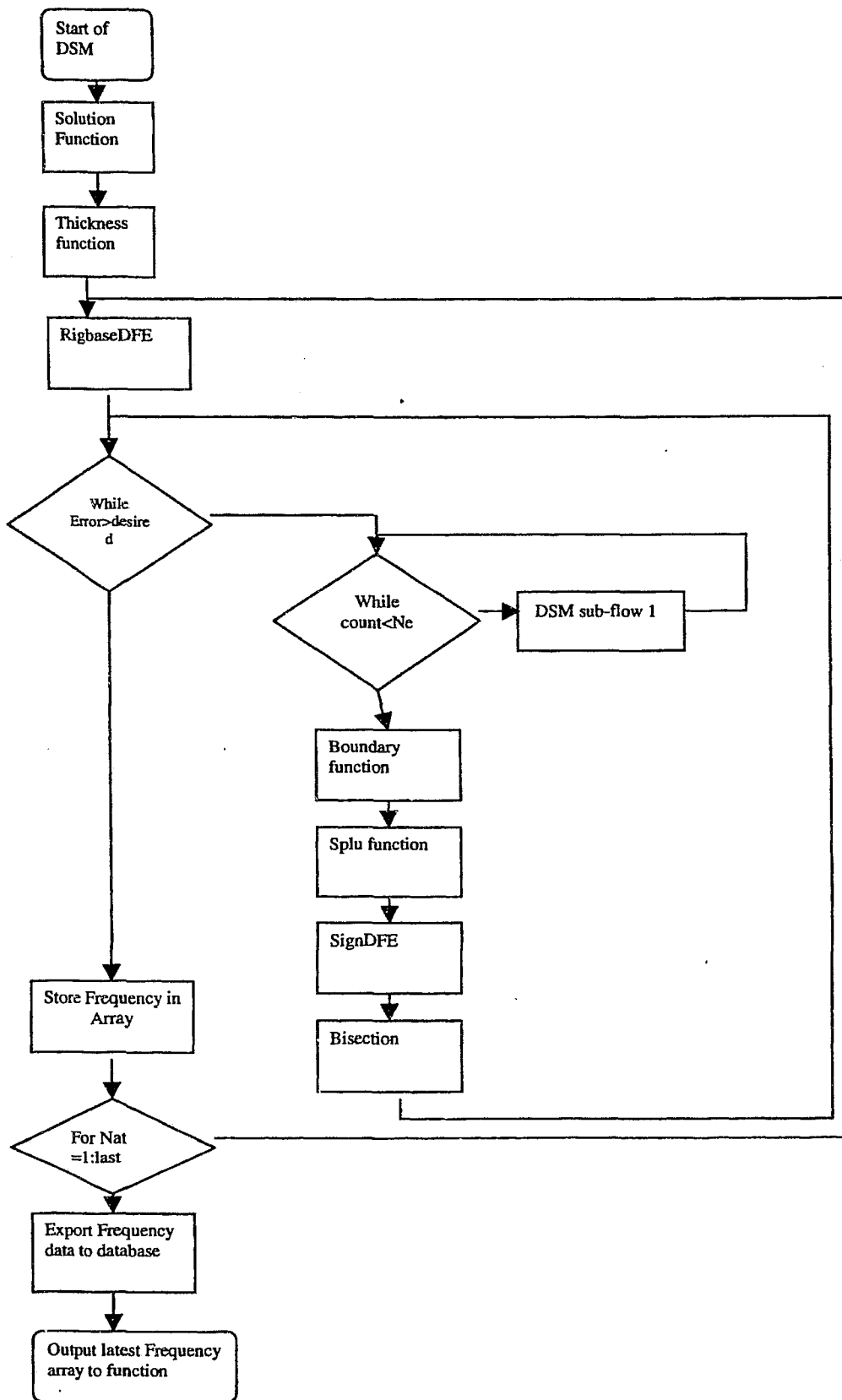
## **Appendix B: Flow Charts**

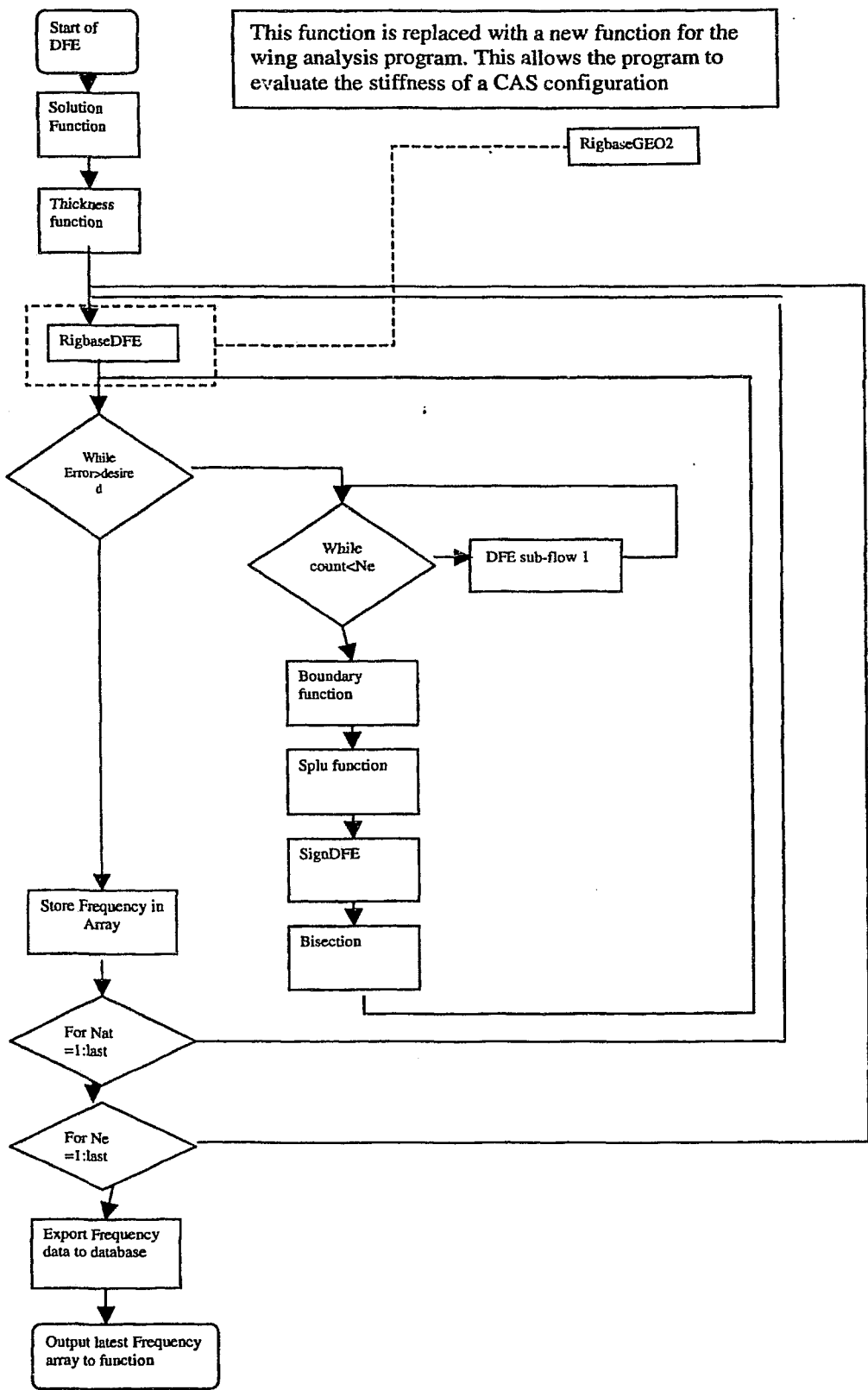
### **Uniform/Tapered Beam & Dually Coupled Wing Analysis Program**

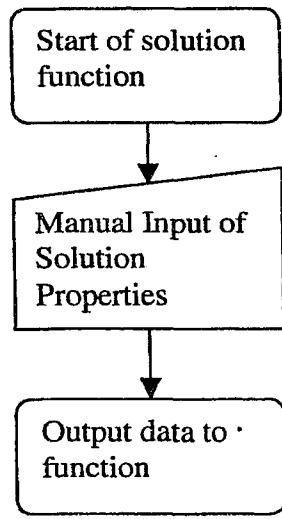
# Uniform/Tapered Beam Program

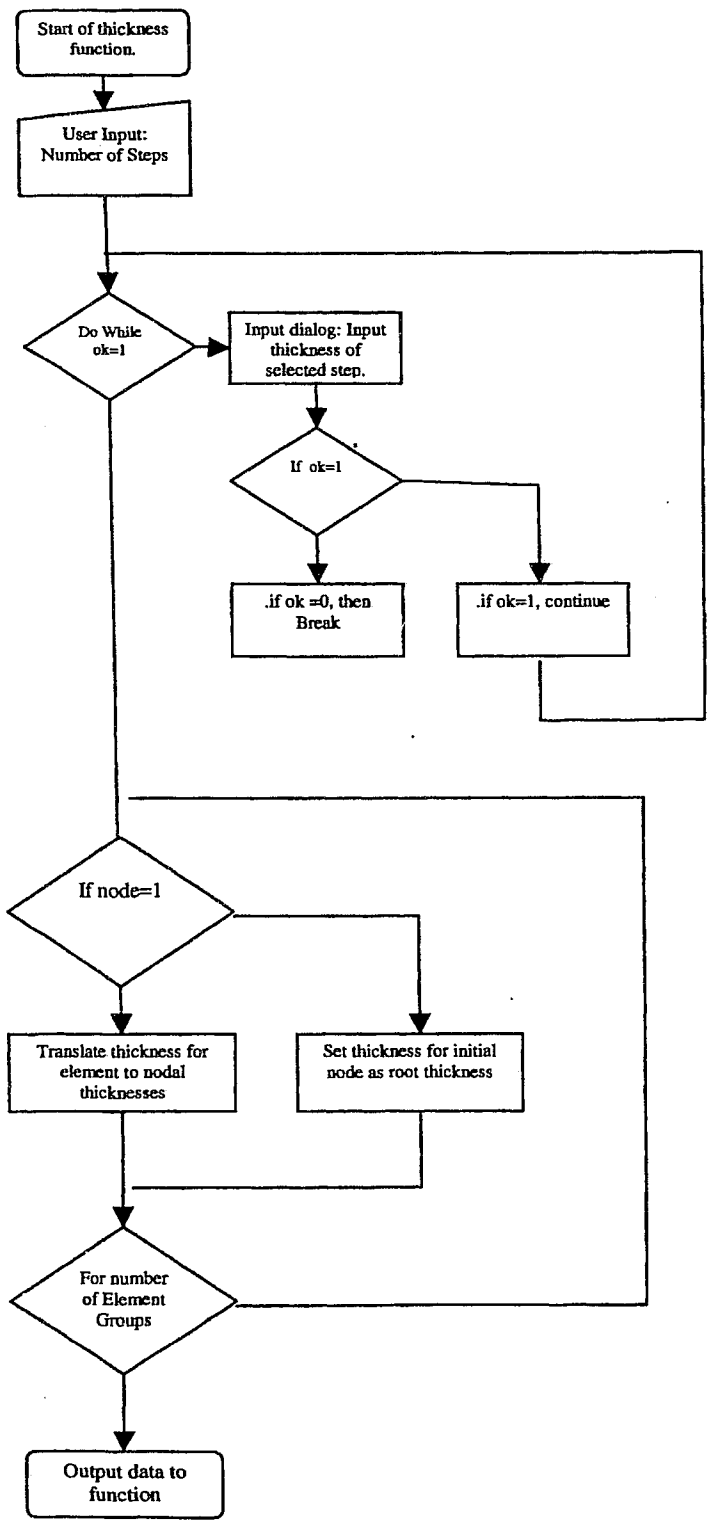


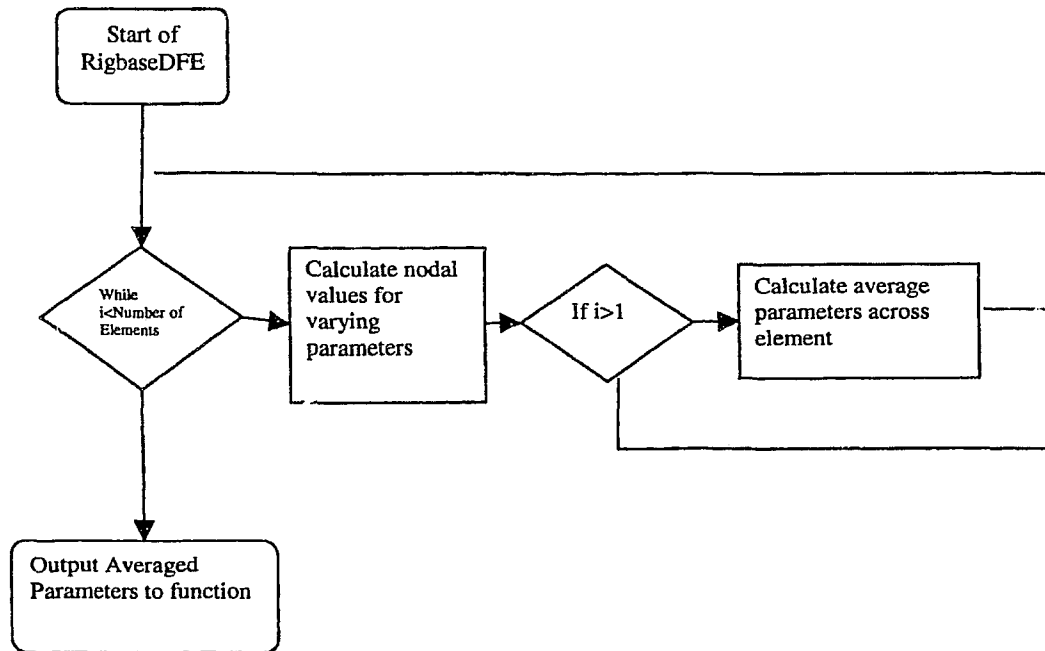
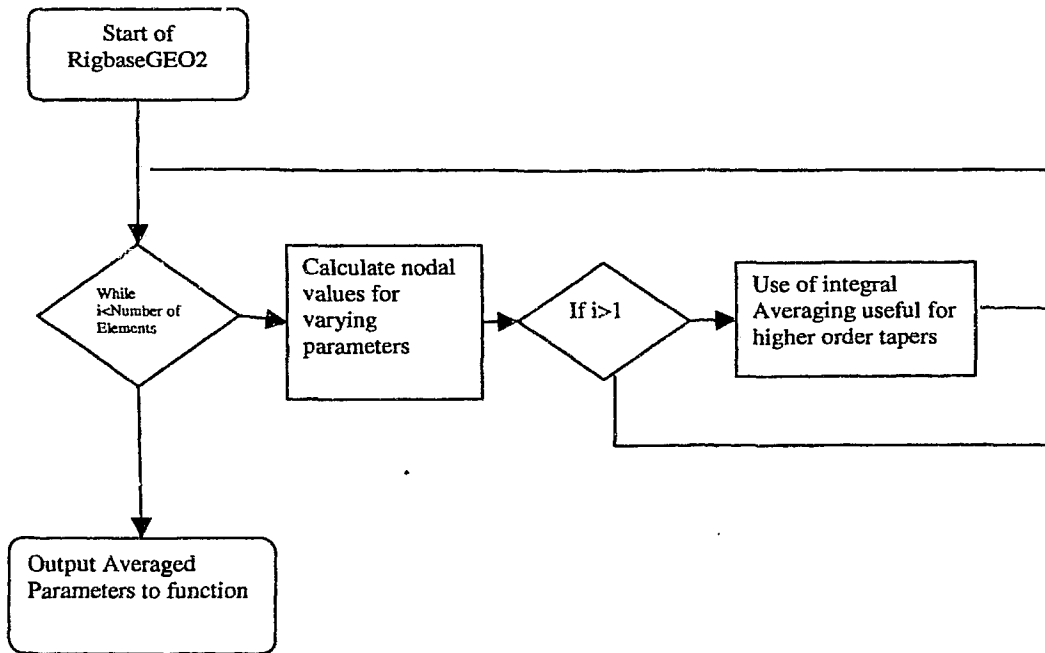


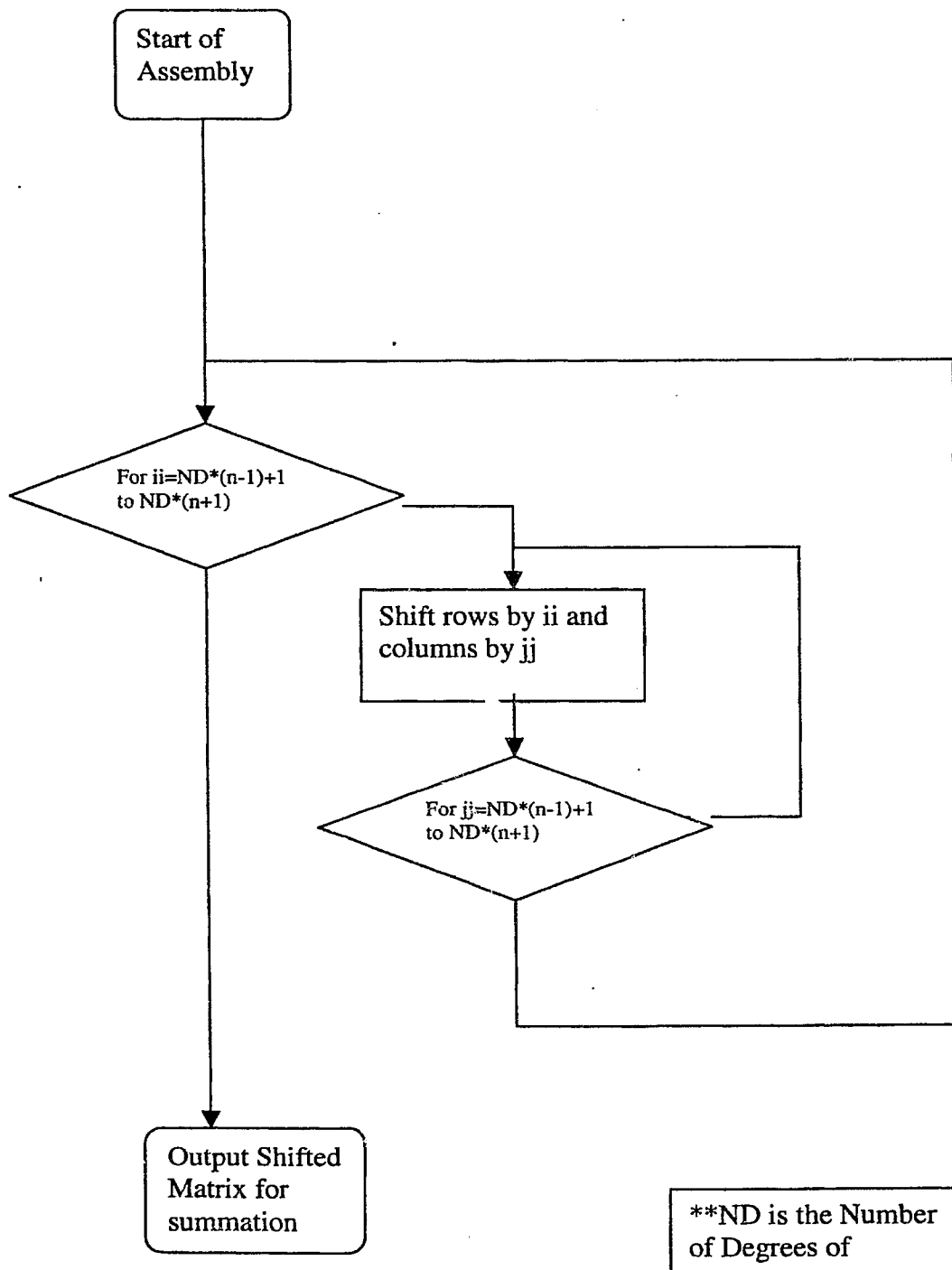


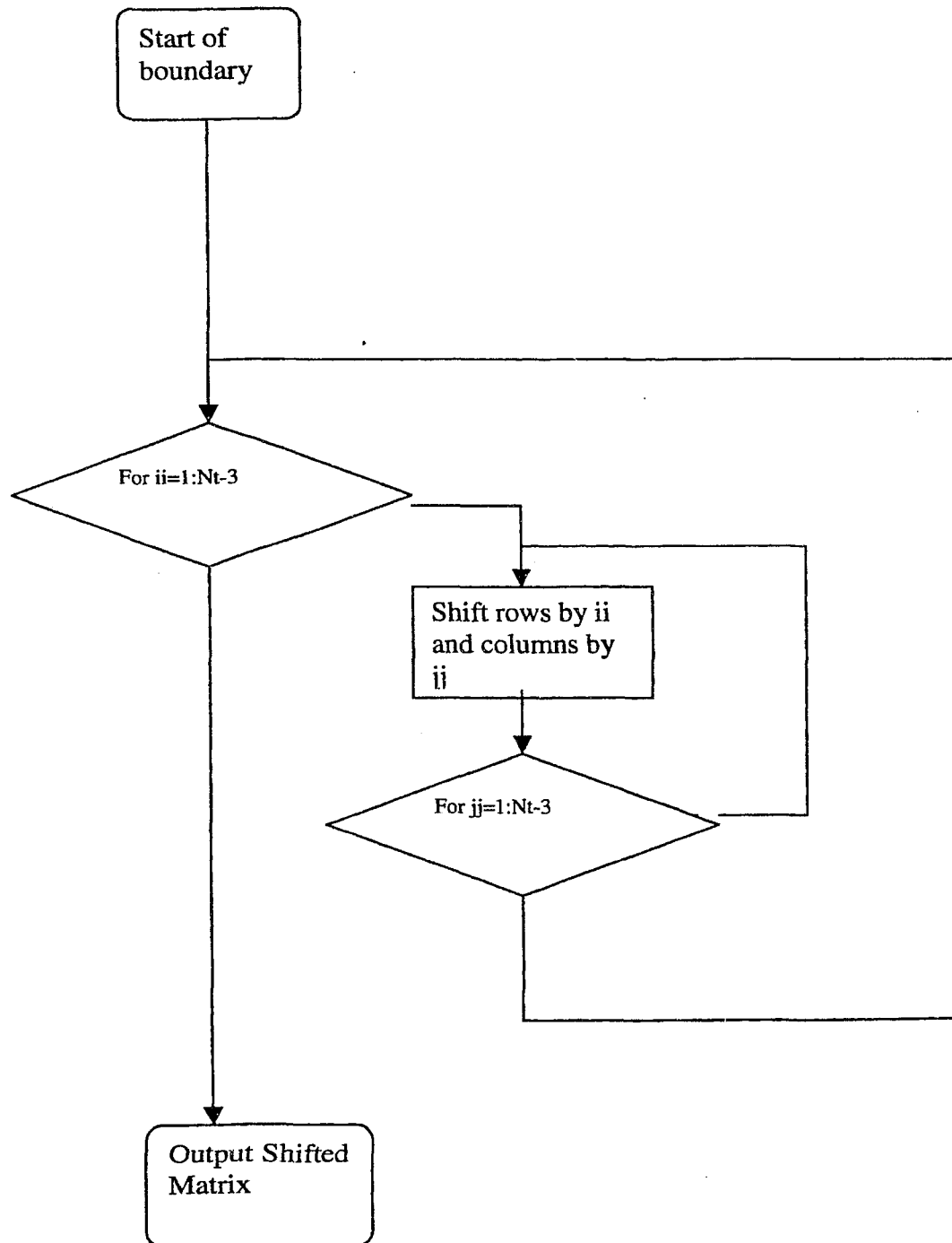


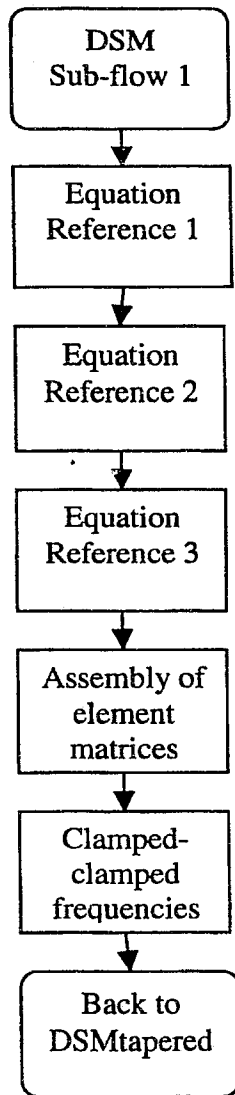


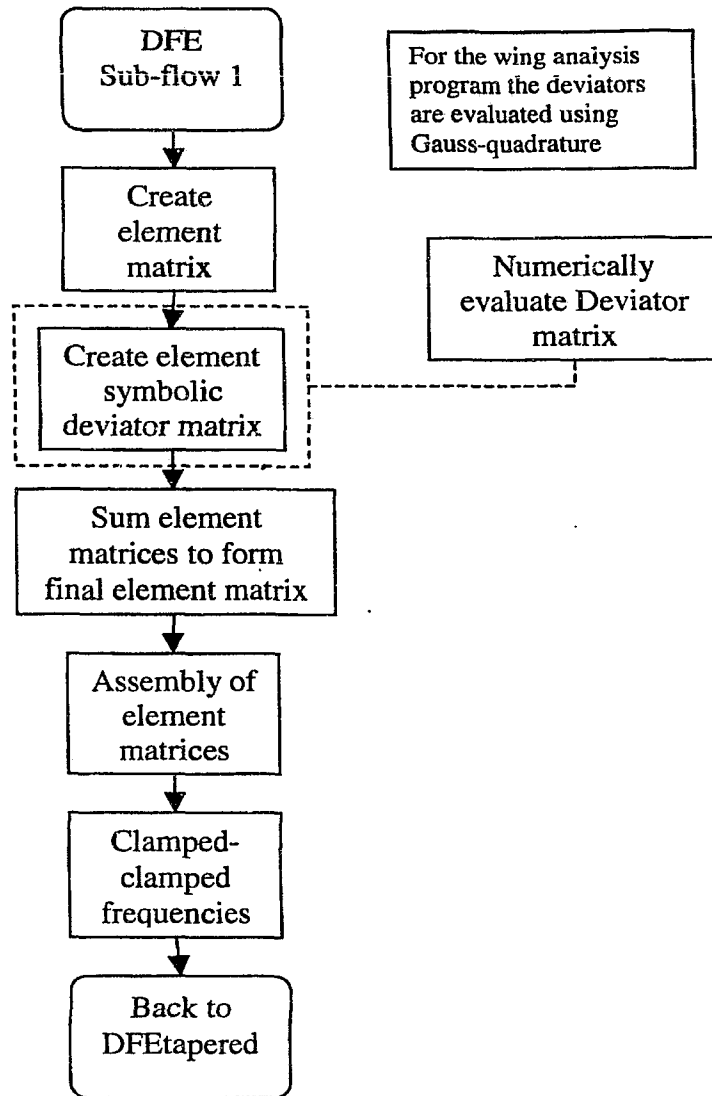


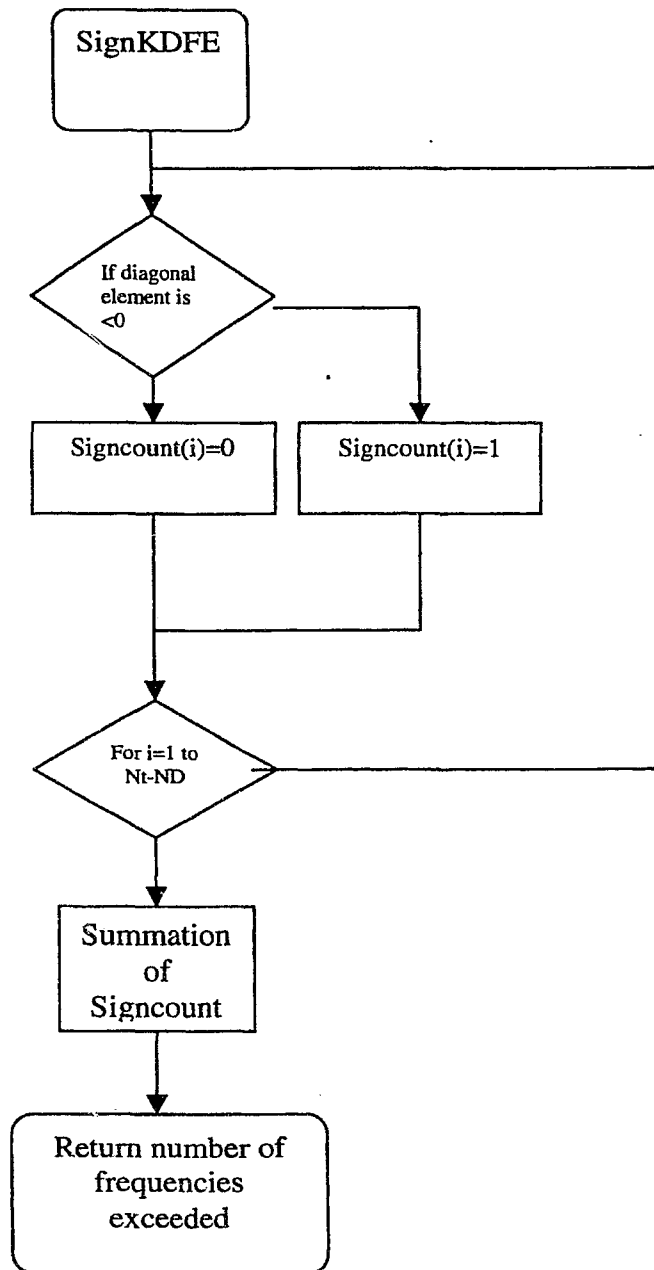


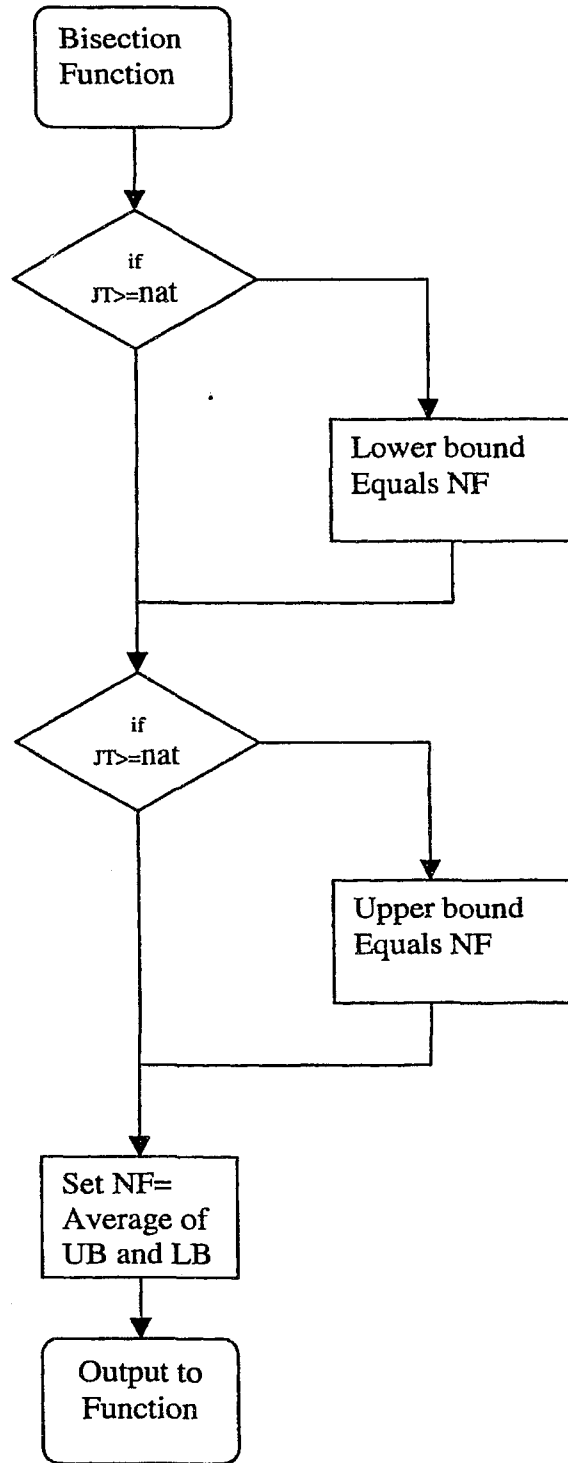


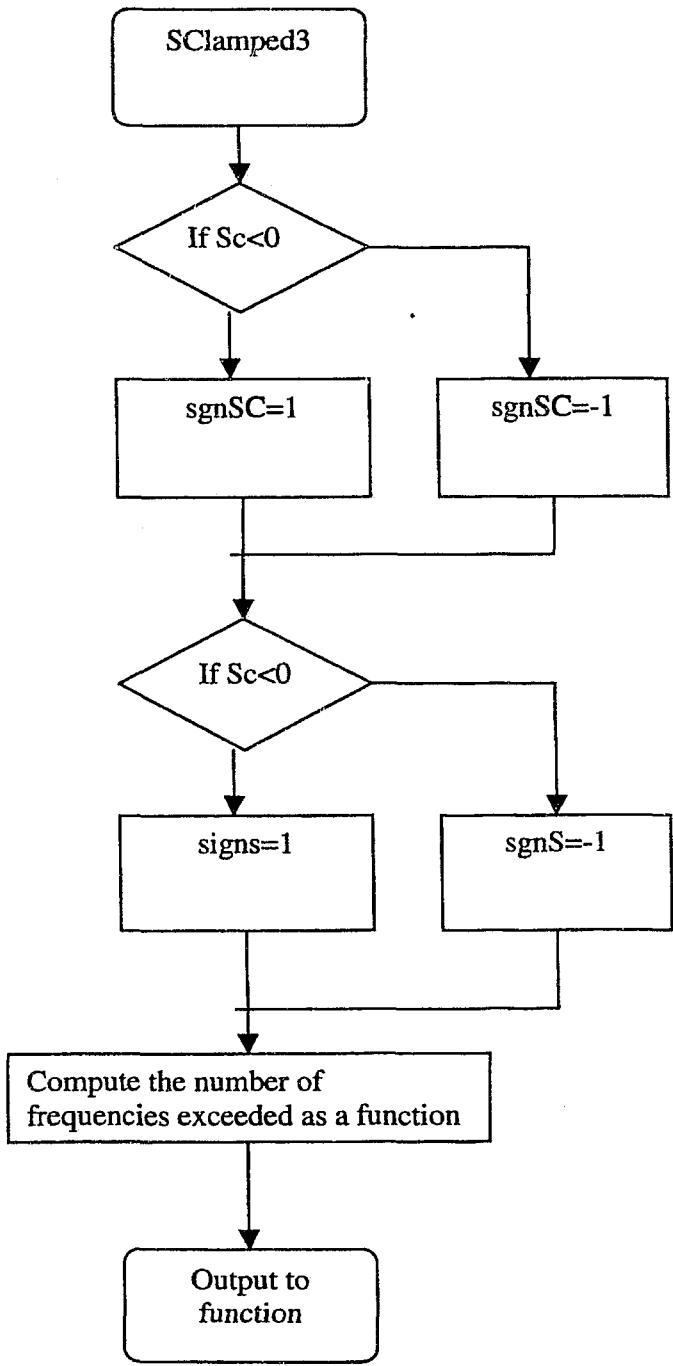












## References

- Abramovich, H. and Livshits, A. (1994). Free Vibration of Non-Symmetric Cross-Ply Laminated Composite Beams. *Journal of Sound and Vibration*, 176(5), pp.597-612.
- Armanios, E. A. and Badir, A. M. (1995). Free Vibration Analysis of Anisotropic Thin-Walled Closed-Section Beams. *AIAA Journal*, 33(10), pp.1905-1910.
- Banerjee, J. R. (1998). Free Vibration of Axially Loaded Composite Timoshenko Beams Using the Dynamic Stiffness Matrix Method. *Computer and Structures*, 69, pp.197-208.
- Banerjee, J. R. and Williams, F. W. (1985). Exact Bernoulli-Euler Dynamic Stiffness Matrix for a Range of Tapered Beams. *International Journal for Numerical Methods in Engineering*, 21, pp.2289-2302.
- Banerjee, J. R. and Williams, F. W. (1996). Exact Dynamic Stiffness Matrix for Composite Timoshenko Beams With Applications. *Journal of Sound and Vibration*, 194(4), pp. 573-585.
- Banerjee, J. R. and Williams, F. W. (1995). Free Vibration of Composite Beams- An Exact Method Using Symbolic Computation. *Journal of Aircraft*, 32(3), pp.636-642.
- Bathe, K. J. (1982). *Finite Element Procedures in Engineering Analysis*. Prentice-Hall , Inc., Englewood Cliffs, New Jersey 07632.
- Berdichevsky, V., Armanios, E. and Badir, A. (1992). Theory of Anisotropic Thin-Walled Closed-Section Beams. *Composite Engineering*, 2(5-7), pp.411-432.
- Berthelot, J. M. (1999). *Composite Materials Mechanical Behaviour and Structural Analysis*. Springer-Verlag New York Inc.
- Borneman, S. and Hashemi, S. M. (2003). Free Vibration Analysis of Laminated Composite Wings: A New Dynamic Finite Element (DFE) Formulation. *Proceeding International Conference for Upcoming Engineers (ICUE), Maxwell session*. Toronto, May 2003.
- Chandra, R., Stemple, A. D. and Chopra, I. (1990). Thin-Walled Composite Beams Under Bending, Torsional, Extensional Loads. *Journal of Aircraft*, 27(7), pp.619-626.

- Chen, X. L., Liu, G. R., Lim, S. P. (2003). An Element Free Galerkin Method for the Free Vibration Analysis of Composite Laminates of Complicated Shape. *Composite Structures*, 59, pp. 279-289.
- Cook, R. D., Malkus, D. S., Plesha, M. E., Witt, R. J. (2001). *Concepts and Applications of Finite Element Analysis, Fourth Edition*. John Wiley & Sons. Inc.
- Eslimy-Isfahany, S. H. R. and Banerjee, J. R. (1997). Dynamic Response of Composite Beams with Application to Aircraft Wings. *Journal of Aircraft*, 34(6), pp.785-791.
- Evrard, T., Butler, R., Hughes, S. W., Banerjee, J. R. (2000). Ply Angle Optimisation of Nonuniform Composite Beams Subject to Aeroelastic Constraints. *AIAA Journal*, 38(10), pp.1992-1994.
- Georghiades, G. A. and Banerjee, J. R. (1997). Flutter Prediction for Composite Wings Using Parametric Studies. *AIAA Journal*, 35(4), pp.746-748.
- Hashemi, S. M. and Borneman, S. (2003). Application of Frequency Dependent Trigonometric Shape Functions in the Vibration Analysis of Laminated Composite Beams. *The Fourth Canadian-International Composites Conference (cancom), proceedings*. August 19-22, Ottawa congress centre, Ottawa, Canada.
- Hashemi, S. M. and Borneman, S., (2004). Vibration Analysis of Composite Wings Undergoing Material and Geometrical Couplings: A Dynamic Finite Element Formulation, Submitted to the 2004 ASME International Mechanical Engineering Congress (ICMECE2004), Aerospace Division, November 13-19, 2004, Anaheim, California, Paper#: IMECE2004-60090.
- Hashemi, Seyed Mohammed, (1998). "Free Vibrational Analysis of Rotating Beam-like Structures: A Dynamic Finite Element Approach", Ph.D. Thesis, Department of Mechanical Engineering, Laval University, Quebec, Canada.
- Hashemi, S. M. and Richard, M. J. (1999). A New Dynamic Finite Element (DFE) Formulation on Lateral Free Vibrations of Euler-Bernoulli Spinning Beams Using Trigonometric Shape Functions. *Journal of Sound and Vibration*, 220(4), pp. 601-624.
- Hashemi, S. M. (2002). The Use of Frequency Dependent Trigonometric Shape Functions in Vibration Analysis of Beam Structures- Bridging Gap Between FEM and Exact DSM Formulations. *Asian Journal of Civil Engineering*. 3(3 & 4), pp. 33-56.
- Hopper, C. T. and Williams, F. W. (1977). Mode Finding in Nonlinear Structural Eigenvalue Calculation. *Journal of Structural Mechanics*. 5(3), pp. 255-278.

Hoorpah, W., Henchi, K. and Dhatt, G. (1994). Calcul Exact des Frequences de Vibration des Structures a Poutres par les Matrices de Rigidite Dynamique Application aux Ponts Mixtes Bipoutres. *Contruction Metalique*, 4, pp. 19-41.

Jaehong, L., Kim, S. (2002). Flexural-Torsional Coupled Composite Beams with Channel Sections. *Computer and Structures*, 80, pp. 133-144.

Jones, R. M. (1998). *Mechanics of Composite Materials Second Edition*. Taylor and Francis Inc.

Jung, S. N., Nagaraj, V. T. and Chopra, I. (2001). Refined Structural Dynamics Model for Composite Rotor Blades. *AIAA Journal*, 39(2), pp.339-348.

Lillico, M. and Butler, R. (1998). Finite Element and Dynamic Stiffness Methods Compared for Modal Analysis of Composite Wings. *AIAA Journal*, 36(11), pp.2148-2151.

Lillico, M., Butler, R., Guo, S., Banerjee, J. R. (1997) Aeroelastic Optimisation of Composite Wings Using the Dynamic Stiffness Method. *The Aeronautical Journal*, pp.77-86.

Roach, A., Hashemi, S. M. (2003). The Use of Dynamic Trigonometric Shape Functions in Coupled Torsion-Axial Vibration of Structural Elements- Bridging the Gap Between FEM And Exact Formulations", Proceeding of the 2nd International Conference for Upcoming Engineers (ICUE 2003). 1-2 May 2003, Ryerson University, Toronto, Canada.

Simpson, A. (1984). On the Solution of  $s(w)x = 0$  By a Newtonian Procedure. *Journal of Sound and Vibration*. 97(1), pp. 153-164.

Smith, E. C. and Chopra, I. (1990). Formulation and Evaluation of an Analytical Model for Composite Box-Beams. 31<sup>st</sup> AIAA/AHS/ASME/ASCE/ASC Structures. Structural Dynamics and Materials Conference. Long Beach. Calif. April 2-4.

Suresh, J. K. and Venkatesan, C. (1990). Structural Dynamic Analysis of Composite Beams. *Journal of Sound and Vibration*, 143(3), 503-519.

Taylor, J. M. and Butler, R. (1997). Optimum Design and Validation of Flat Composite Beams Subject to Frequency Constraints. *AIAA Journal*, 35(3), pp.540-545.

Teh, K. K. and Huang, C. C. (1980). The Effects of Fibre Orientations on Free Vibrations of Composite Beams. *Journal of Sound and Vibration*, 69(2), pp.327-337.

Teh, K. K. and Huang, C. C. (1979). The Vibrations of Generally Orthotropic Beams. A Finite Element Approach. *Journal of Sound and Vibration*, 62(2), pp. 195-206.

Teoh, L. S and Huang, C. C. (1977). The Free Vibration of Beams of Fibre Reinforced Material. *Journal of Sound and Vibration*, 51(4), pp. 467-473.

Volovoi, V. V. and Hodges, D. H. (2002). Single- and Multi- Celled Composite Thin-Walled Beams. *AIAA Journal*, 40(5), pp.960-966.

Weisshaar, T. A. (1980) Divergence of Forward Swept Composite Wings, *Journal of Aircraft*, 17(6), pp. 442.

Williams, F.W. and Kennedy, D. (1988). Reliable Use of Determinants to Solve Nonlinear Structural Eigenvalue Problems Efficiently. *International Journal for Numerical Methods in Engineering*. 26, pp. 1825-1841.

Wittrick, W. H. and Williams, F. W. (1971). A General Algorithm for Computing the Natural Frequencies of Elastic Structures. *Quart. Journ. Mech. and Applied Math.*, Vol. XXIV, Pt. 3, pp.263-284.

Wittrick, W. H. and Williams, F. W. (1983). Exact Buckling and Frequency Calculations Surveyed. *J. Struct. Eng. ASCE*, 109, pp. 169-187.

Wittrick, W. H. and Williams, F. W., (1982). On The Free Vibration Analysis of Spinning Structures by Using Discrete or Distributed Mass Models. *Journal of Sound and Vibration*, 82(1), pp 1-15.

Wu, X. X. and Sun, C. T. (1991). Vibration Analysis of Laminated Composite Thin-Walled Beams Using Finite Elements. *AIAA Journal*, 29(5), pp.736-742.

<http://www.ketchum.org/bridgecollapsepix/tacoprior-297x400.jpg>